INVESTIGATIONS IN FAST NEUTRON SPECTROMETRY

Thesis

submitted by

DAVID G. VASS, B.Sc.

for the degree of

DOCTOR OF PHILOSOPHY

University of Edinburgh,

MAY, 1966.

C O N T E N T S

C O N T E N T S (Contd.)

C O N T E N T S (Contd.)

C O N T E N T S (Contd.)

CHAPTER 1

1.1. Concerning a Proposal for the Formation of a Level near 2.8 MeV in B^{10} by the $Be^9(d,n)B^{10}$ Reaction.

The B^{10} nucleus has been studied extensively, and its known properties have been summarized by Ajzenberg-Selove and Lauritsen (1955 and 1959)[1]. Since then, further investigations of the B^{10} energy levels under 4 MeV have been made through the energy spectra of the particles emitted in the following reactions:- $Li^6(Li^6,d)B^{10}$ (3), $Li^7(Li^6,t)B^{10}$ (3), $Li^7(\alpha,n)B^{10}$ (4), $Be^9(d,n)B^{10}$, $Be^9(He^3,d)B^{10}$ (5), $B^{10}(p,p')B^{10*}$ (6), $B^{10}(d,d')B^{10*}$ (6), $B^{11}(d,t)B^{10}$ (7), $B^{11}(He^3,\alpha)B^{10}$ (8), $C^{12}(d,\alpha)B^{10}$ (9). It is now well established that energy levels exist at 0.72, 1.74, 2.15, and 3.58 MeV in B^{10}, but many contradictory reports have been published concerning the possible existence of a level near 2.9 MeV. All of the evidence for such a level has been obtained from the $Be^9(d,n)B^{10}$ reaction and therefore it is of interest to examine the evidence from this reaction more closely.

1.2. The Neutrons from the $Be^9(d,n)B^{10}$ Reaction.

The first investigations of the neutrons from the $Be^9(d,n)B^{10}$ reaction were made using cloud chambers. Bonner and Brubaker (1936)[10], using 0.9 MeV deuterons, and Staub and Stephens (1939)[11], using deuterons with

energies of 0.6 MeV and 0.88 MeV, found neutron groups corresponding to levels at 0.72, 2.2 and 3.6 MeV in B^{10}. The existence of these levels was confirmed by the nuclear emulsion measurements of Powell (1943)[12], using 0.5 MeV deuterons, and of Whitehead and Mandeville (1950)[13], using 1.62 MeV deuterons. Ajzenberg (1951)[14], using nuclear emulsions and 3.4 MeV deuterons, found these levels together with a new level at 1.79 MeV. Later Pruit, Swartz and Hanna (1953)[15] confirmed the existence of all four levels using 0.95 MeV deuterons. These authors determined the excitation energies in B^{10} as 0.74 ± 0.11, 1.77 ± 0.10, 2.20 ± 0.10 and 3.67 ± 0.09 MeV.

Dyer and Bird (1953)[16], after investigating the neutrons emitted when 600 keV deuterons struck a thick Be^9 target, found the four known levels and submitted evidence for another level at 2.85 MeV in B^{10}. They used nuclear emulsions to obtain the energy spectrum of the neutrons. Support for this additional level came from spectra obtained by Reid (1954)[17], using a neutron counter telescope and 750 keV deuterons, and by Genin (1958)[18], using nuclear emulsions and 570 keV deuterons. However, Karadeniz (1956)[19], also using nuclear emulsions, found evidence for two levels in B^{10} at 2.7 and 3.2 MeV from the energy spectra of the $Be^9(d,n)B^{10}$ neutrons produced by 600 keV deuterons.

More recently, Hjalmar and Slätis (1960)[20], using 7 MeV deuterons to bombard a Be^9 target, reported evidence

for a level near 3.1 MeV from their nuclear emulsion measurements. Also, Coombe and Walker (1962)[21], after using a diffusion cloud chamber to investigate the neutrons from the reaction for 80 keV deuterons, interpreted their measurements as supporting the existence of a single level near 2.9 MeV in B^{10}, although they pointed out that their observations would be consistent with the existence of a pair of levels at 2.7 and 3.1 MeV.

While the above experiments provide evidence for level structure near 2.9 MeV, other workers failed to observe such structure. The nuclear emulsion measurements made by Green, Scanlon and Wilmott (1955)[22], using 850 keV deuterons, and by Shpetnyi (1957)[23], using 0.5, 1.0 and 1.6 MeV deuterons, did not support the existence of level structure at 2.9 MeV.

Recently the $Be^{9}(d,n)B^{10}$ neutron energy spectrum has been investigated using time-of-flight techniques. The investigations made by Juna, Horvath and Konecny (1960)[24] using 0.8 MeV deuterons, and by Garg, Gale and Calvert (1962)[25], using 2.8 MeV deuterons were inconclusive concerning the possible existence of a level near 2.85 MeV in B^{10} due to inadequate energy resolution in the region of interest. No mention was made of the 2.85 MeV level problem in either report. However, spectra with high energy resolution have been obtained by Morrison, Ferguson and Evans (1961)[26] for deuterons with energies of 2, 3 and 4 MeV, by Riley, Braben and Neilson (1963)[27], using

1.9 MeV deuterons, and by Siemssen, Cosack and Felst (1965)[28] at various deuteron energies between 1.1 and 3.2 MeV. No indication of the formation of a level near 2.85 MeV in B^{10} was found in any of these experiments.

$Be^{9}(d,n)B^{10}$ neutron energy spectra produced by 1.85 MeV deuterons were published by Good (1960)[29] and by Neilson, Dawson and Johnson (1959)[30] to illustrate the performance of their time-of-flight spectrometers. In the spectrum obtained by Good, there is an unidentified peak which could be attributed to a level near 2.8 MeV in B^{10}. However, this peak (of doubtful statistical significance) may be due to an instrumental effect, and therefore no emphasis should be placed on this evidence. No indication of such a peak occurs in the spectrum of Neilson et al.

1.3. The γ-rays Produced in the $Be^{9}(d,n)B^{10}$ Reaction.

Simple measurements of the energies of the B^{10} γ-rays fail to yield information about the existence (or non-existence) of a 2.85 MeV level. If such a level exists, the energies of the γ-rays emitted in its decay would be the same as those emitted in the decay of the four already well established levels at 0.72, 1.74, 2.15 and 3.58 MeV. It is therefore necessary to search for evidence using γ-ray coincidence spectrometers. Shafroth and Hanna (1954)[31], using deuterons with energies less than 0.7 MeV, succeeded in determining the γ-ray

transitions which occur between the various established energy levels in B^{10} (Fig. 1). However, their results could also be interpreted in terms of a decay scheme with a level at 2.86 MeV, and thus their experiment was inconclusive regarding the existence of such a level. Another γ-ray coincidence experiment by Meyerhof and Chase (1958)[32] using 2.8 MeV deuterons was primarily concerned with the levels in B^{10} near 5 MeV, and could not provide conclusive evidence about a level near 2.86 MeV.

Galloway and Sillitto (1961)[33] however, not only interpreted the results of their γ-ray coincidence experiments as providing evidence for a level at 2.86 MeV in B^{10} but also deduced the branching ratio for the decay of this level; the 2.86 MeV level decays directly to the ground state and to the 0.72 MeV level with a branching ratio of about 10:1. These authors used 600 keV deuterons to populate the B^{10} levels.

The relative intensities of the B^{10} γ-rays have been measured under similar experimental conditions by Bradford (1962)[34]. He concluded that his measurements, taken in conjunction with the measurement of the branching ratio of the 2.15 MeV level by Sprenkel and Daughtry[35], provided evidence for a level at 2.86 MeV in B^{10}.

1.4. The Internal Conversion Electrons from the $Be^9(d,n)B^{10}$ Reaction.

Warburton, Alburger and Wilkinson (1963)[39] have investigated the internal conversion electrons from B^{10} using 2.0 and 2.7 MeV deuterons, but they do not mention the possible existence of a level near 2.86 MeV. However, as in the case of Meyerhof and Chase, Warburton et al. were primarily interested in the higher energy levels.

1.5. A Discussion of the Evidence about the Possible Existence of a level near 2.86 MeV in B^{10}.

The earlier neutron spectra have been examined critically in the recent papers of Hjalmar and Slätis (1960)[20] and Coombe and Walker (1962)[21]. Hjalmar and Slätis have suggested that there are indications of the formation of a weak 2.86 MeV level in B^{10} in the spectra of Bonner and Brubaker (1936), Staub and Stephens (1939), Powell (1943), Ajzenberg (1951) and Whitehead and Mandeville (1950). Dyer and Bird (1953) had previously drawn attention to this evidence in the work of Staub and Stephens, and Powell. Coombe and Walker have been more cautious in their comments, but they point out that any neutron group corresponding to level structure near 2.86 MeV in B^{10} could have been masked by fluctuations in the background or by poor energy resolution in most of the spectra previously published (1962). However, their own

spectra also suffer from relatively poor statistical accuracy due to the inefficient method of detecting neutrons in their experiment. These comments emphasize the inconclusive nature of the evidence about the postulated 2.86 MeV level.

Galloway and Sillitto (1961)[33], after examining the previous work on B^{10}, concluded that the 2.86 MeV level appears to be formed with appreciable intensity only in the $Be^{9}(d,n)B^{10}$ reaction for deuteron energies less than about 800 keV. Up to date, the only exception to this classification of the evidence is the observation of a level near 3.1 MeV in B^{10} for 7 MeV deuterons by Hjalmar and Slätis. The recent time-of-flight investigations, which do not reveal level structure near 2.86 MeV, were all made with deuteron energies above 1 MeV.

1.6. The B^{10} γ-ray Decay Scheme.

The generally accepted decay scheme for B^{10} is that published by Ajzenberg-Selove and Lauritsen (1955, 1959 and 1962)[1,2] (see Figure 1(a)). The γ-ray transition assignments are those determined by Shafroth and Hanna (1954)[31], and the branching ratios of the 2.15 and 3.58 MeV levels appear to be estimated from the relative intensities of the B^{10} γ-rays measured by Ramussen, Hornyak and Lauritsen (1949)[36]; some assumption was made about the distribution of the 1.43 MeV γ-rays between the 3.58 → 2.15 MeV and the 2.15 → 0.72 MeV transitions.

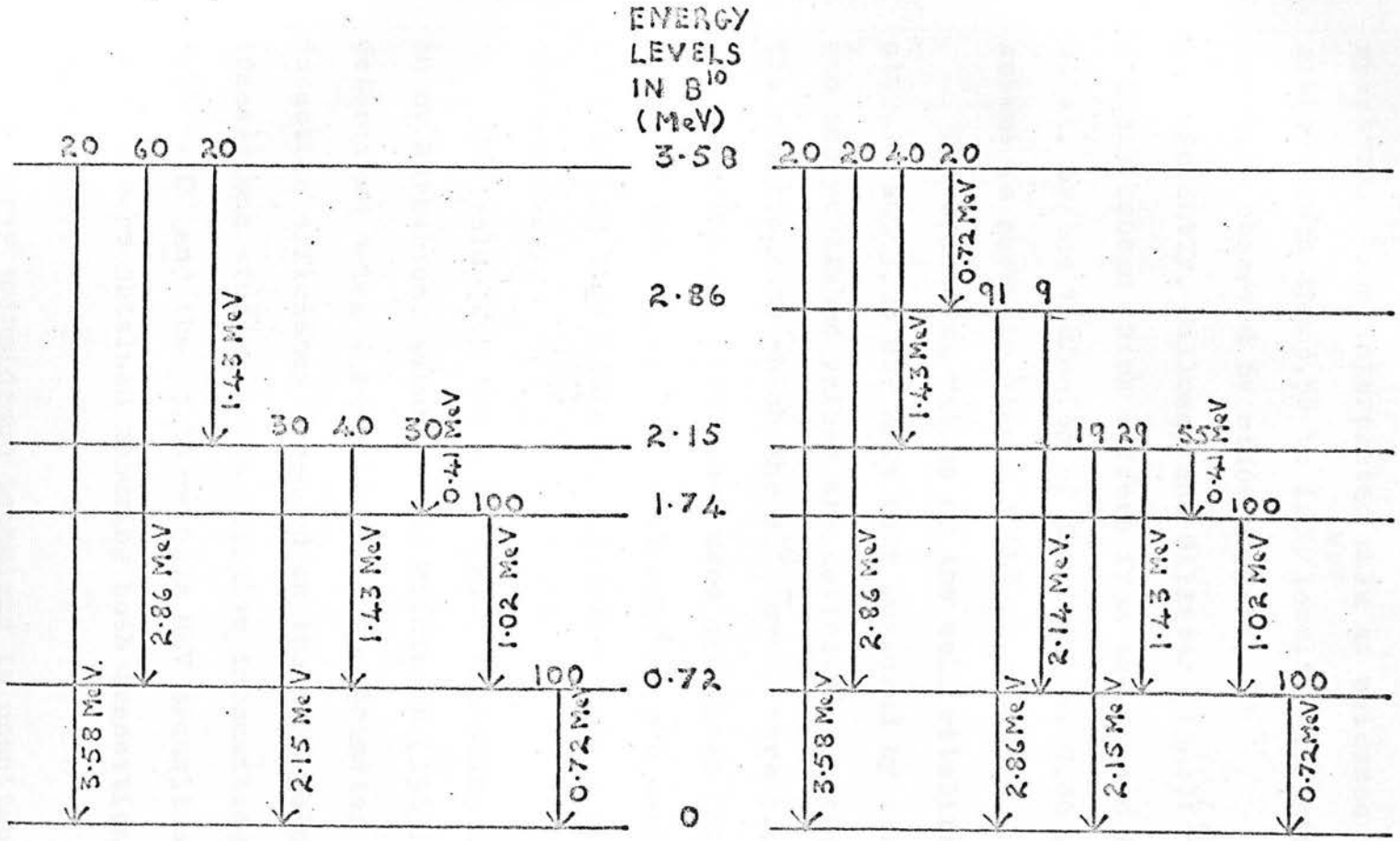

FIG. 1(a)

FIG. 1(b)

FIG.1. ENERGY LEVEL SCHEME AND γRAY TRANSITION ASSIGNMENTS FOR B^{10}.

(a) AJZENBERG-SELOVE AND LAURITSEN (1959)

(b) GALLOWAY AND SILLITTO (1961)

(THE BRANCHING RATIOS OF THE LEVELS ARE INDICATED FOR BOTH SCHEMES.)

Singh (1959)[37] and later Hornyak, Ludemann and Roush (1964)[38] have observed 1.84 MeV γ-rays in the B^{10} spectrum. They interpreted this as evidence for transitions from the 3.58 to 1.74 MeV levels, but this γ-ray has not been observed by other workers.

Recently, Galloway and Sillitto (1961)[33] proposed a decay scheme which differs from the scheme of Ajzenberg et al. by the inclusion of the level at 2.86 MeV. This scheme is shown in Figure 1 (b).

The branching ratios of the well established levels at 2.15 and 3.58 MeV have been measured by various workers and the published values are collected together in Table 1. The reactions by which the B^{10} levels were populated and the experimental techniques used are given in columns 3 and 4 of the table. The measurements are easily compared by studying this table and therefore only a few comments are necessary.

The value for the 3.58 : 2.86 branching ratio obtained by Warburton, Alburger and Wilkinson (1963)[39] was determined using a magnetic pair spectrometer whose detection efficiency depended on the multipolarity of the transitions studied. The relative intensities of the $3.58 \rightarrow 0$ and the $3.58 \rightarrow 0.72$ MeV transitions given in Table 1 were obtained assuming both transitions to be of the M1 type.

A γ-ray coincidence technique is unsuitable for the study of the 3.58 MeV level since there is only a weak

	Ref.	Reaction	Technique	2.15 MeV Branching ratios			3.58 MeV Branching ratios				
				2.15	1.43	0.41	3.58	2.86	1.84	1.43	0.72
Ajzenberg-Selove & Lauritsen (1955,59,62)	(1,2)	Review (see text)		30	40	30	20	60	-	20	-
Galloway & Sillitto (1961)	(33)	$Be^9(d,n)B^{10}$	γ-ray coincidence expt.	19	25	56	20	20	-	40	20
Sprenkel & Daughtry (1961)	(35)	$Be^9(p,\gamma)B^{10}$	"	16	29	55	-	-	-	-	-
Hornyak, Laudemann & Roush (1964)	(38)	$Be^9(p,\gamma)B^{10}$	"	27	26	47	18	54	10	18	-
Segel, Singh, Hanna & Grace (1966)	(40)	$B^{10}(p,p')B^{10}$	"	24	23	53	12	76	-	12	-
Singh (1959)	(37)	$Be^9(p,\gamma)B^{10}$	γ-ray intensities	-	-	-	-	-	10%	-	-
Meyerhof & Chase (1958)	(32)	$Be^9(d,n)B^{10}$	"	-	-	-	25	75	-	-	-
Warburton, Alburger & Wilkinson (1963)	(39)	$Be^9(d,n)B^{10}$	Magnetic pair spectrometry	-	-	-	20	80	(see text)		

Table 1. Summary of Branching Ratio Measurements for the 2.15 and 3.58 MeV Levels in B^{10}.

γ-ray feed to this level from the higher energy levels in B^{10}. Therefore, it is difficult to measure the branching ratio of the 3.58 MeV level reliably because of the difficulty in selecting the γ-rays from its decay. Moreover, the interpretation of measurements of the relative intensities of the γ-rays from the decay of the 3.58 MeV level depends on whether a level exists at 2.86 MeV or not. In deducing values for the branching ratio of the 3.58 MeV level in B^{10} the authors mentioned in Table 1, with the exception of Galloway and Sillitto, assumed that there is no level structure near 2.86 MeV.

1.7 The Proposed Investigation.

As most of the evidence for level structure near 2.86 MeV has been obtained from neutron and γ-ray studies of the $Be^{9}(d,n)B^{10}$ reaction at low energies, it was decided to investigate the neutrons emitted from this reaction for 600 keV deuterons using a n-γ coincidence time-of-flight technique. This technique enables neutron spectra with high energy resolution and good statistical accuracy to be obtained. Also, if a neutron group associated with the formation of a level near 2.86 MeV were to be observed, then an analysis of the energy spectrum of those γ-rays in coincidence with this group should yield information about the decay of the level.

It was also decided to measure the branching ratio of the 3.58 MeV level in view of the discrepancies in the values obtained by earlier workers for this ratio.

CHAPTER 2

THE BASIC EQUIPMENT FOR THE NEUTRON TIME-OF-FLIGHT SPECTROMETER

2.1. An Outline of the n-Y Time-of-Flight Technique.

The time T (nsecs) taken by a neutron of energy E (MeV) to travel a distance D (m) is $T = \frac{72.3D}{\sqrt{E}}$. The angular distributions of the flight times per metre flight path (D = 1) of the $Be^9(d,n)B^{10}$ neutron groups for various deuteron energies may be calculated from the reaction kinematics (Appendix I). Such angular distributions for the neutrons associated with the 0.72, 1.74 2.15, 3.58 and the proposed 2.86 MeV levels in B^{10} produced by 600 keV deuterons are shown in Fig. 2.

Before considering the n-Y coincidence spectrometer in detail, it is, perhaps, helpful to outline the operation of the spectrometer. The measurement of the flight-time of a neutron emitted in the $Be^9(d,nY)B^{10}$ reaction requires the determination of (1) the precise instant at which the neutron is emitted from the target (i.e. the instant at which the reaction occurs) and (2) the instant at which the neutron arrives at the end of its flight path. The instant of emission of a neutron was determined by detecting an associated B^{10} Y-ray in a scintillation counter placed very close to the target and the arrival of the neutron at the end of its flight path was determined

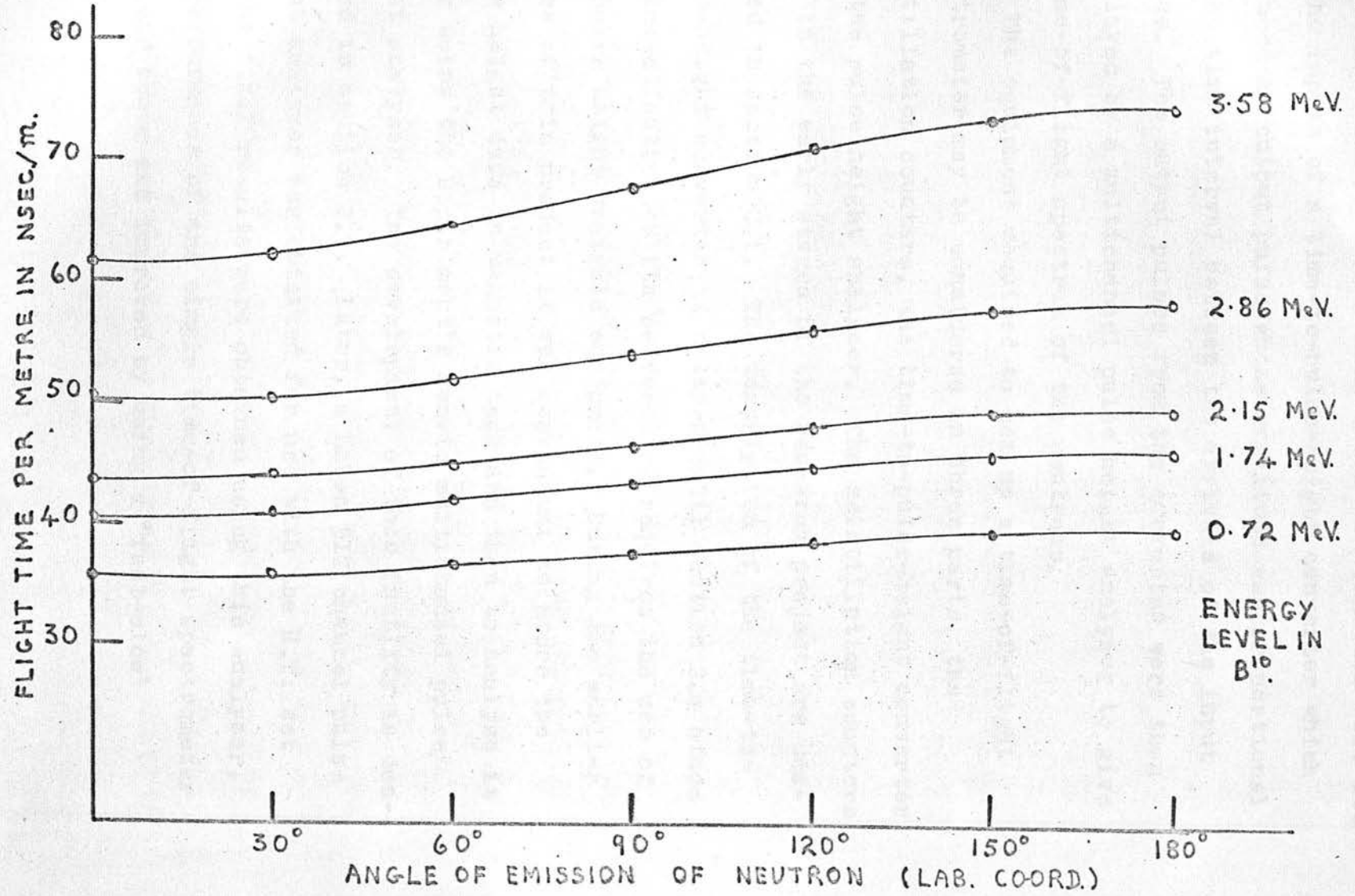

FIG. 2. ANGULAR DISTRIBUTIONS OF THE FLIGHT TIMES PER METRE OF THE NEUTRON GROUPS EMITTED FROM THE $Be^{9}(d,n\gamma)B^{10}$ REACTION FOR 600 KeV DEUTERONS.

by detecting the neutron in another scintillation counter. Timing pulses from the two scintillation counters were fed to the inputs of a time-to-pulse-height converter which produced an output pulse whose amplitude was proportional to the time interval between the arrivals of the input pulses. The output pulses from the converter were then displayed by a multichannel pulse height analyser to give a time-of-flight spectrum of the neutrons.

The equipment required to set up a time-of-flight spectrometer may be considered in three parts, the scintillation counters, the time-to-pulse-height converter and the pulse height analyser. The scintillation counters used in the early stages of the research project are described in section 2.2. The description of the time-to-pulse-height converter is delayed until section 2.4 since the investigation of its performance requires the use of the pulse height analysis equipment. During the earlier stages of this project it was convenient to store the pulse height data on magnetic tape and then to analyse it later using the Department's Sunvic multichannel pulse height analyser. The development of this facility is described in section 2.3. Later, a Laben 512 channel pulse height analyser was obtained for use with the H.T. set and the final results were obtained using this analyser. The performance of the simple time-of-flight spectrometer outlined above was improved by using a "fast-slow"

coincidence technique which is described in the final section of this chapter, 2.5.

2.2. The Υ-ray and Neutron Scintillation Counters.

The Υ-ray and neutron scintillation counters used in time-of-flight spectrometry should obviously be capable of producing sharply rising pulses with precise timing of the interactions between the radiations and the scintillators. Also the scintillators should have high detection efficiencies for their respective radiations with, however, low sensitivities to background radiations.

The Υ-ray scintillation counter

The Υ-ray detector used in the early stages of this research project consisted of a NaI(Tℓ) crystal, $1\frac{1}{4}$" diameter by 1" long, mounted directly to the cathode of a photomultiplier, E.M.I. type 6262B. Silicone grease was used to ensure a good optical contact between the crystal and photocathode. The resistor dynode chain, mounted on paxolin wafers, was attached to the base of the photomultiplier, and the whole assembly was enclosed in a light-tight container. The detector had already been used in a "fast-slow" coincidence experiment and it is described elsewhere[41], but for completeness the details of the construction of the container and the circuit diagram of the carbon resistor chain are given in Figs. 3 and 4(a), respectively.

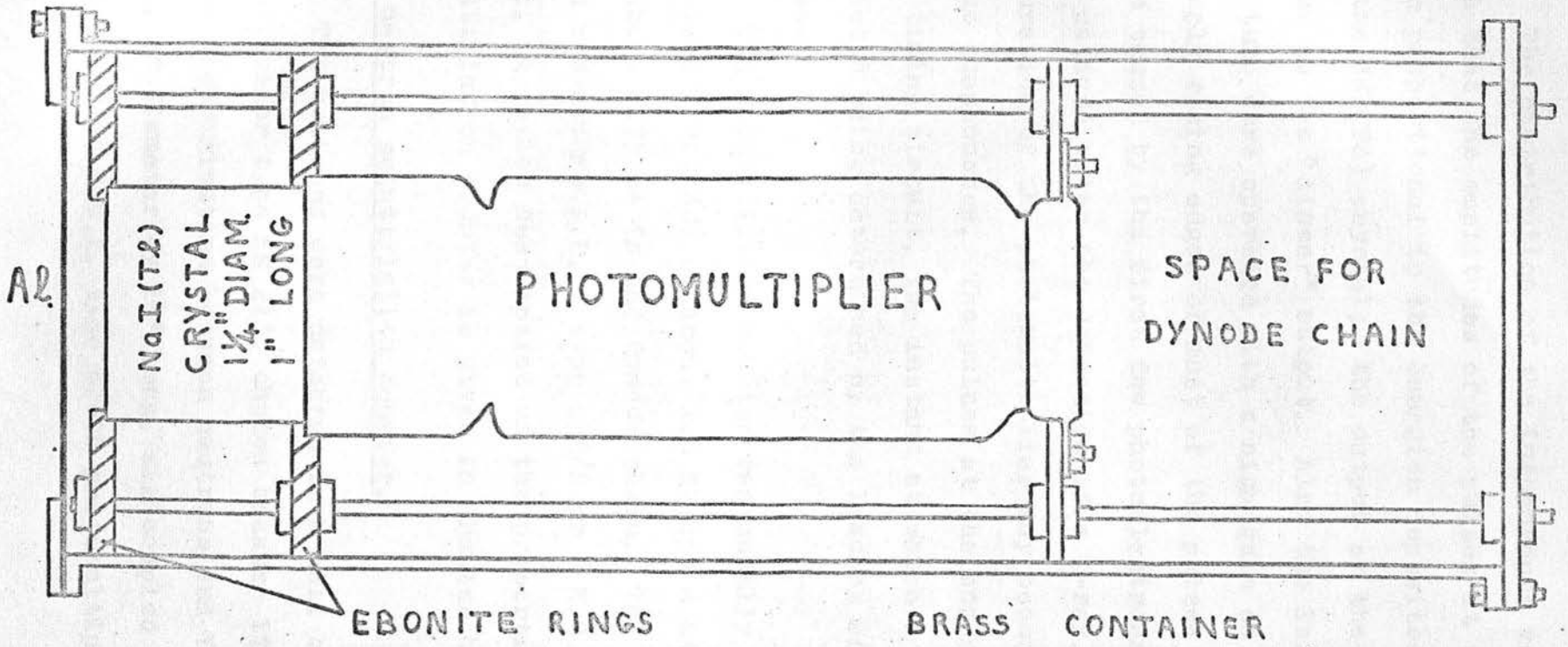

FIG. 3. THE γRAY SCINTILLATION DETECTOR

The distribution of the interdynode voltages was such that the amplitudes of the pulses at the 9th dynode were proportional to the energies deposited by the γ-rays in the NaI(Tℓ) crystal; the output at the 9th dynode is known as the "linear" output. Also the later stages of the tube were operated with a high gain so that the sharply rising edges of most of the pulses at the anode were caused by the first few photoelectrons emitted from the cathode after the detection of a γ-ray. Current saturation of the photomultiplier may occur, but this is of no consequence. The pulses at the anode were fed to the timing circuit, the instant at which a γ-ray was detected being determined by the leading edge of the pulse.

The scintillation counter was usually operated with an overall voltage of about 1.5 kV and a standing current of about 0.75 mA in the dynode chain. The power supply used was either an I.D.L. type 532/B or a N.E. 5302 E.H.T. unit. A fuller description of the properties of this scintillation counter is given in Chapter 4.

<u>The neutron scintillation counter</u>.

The neutrons were detected in a cell of liquid scintillator type NE 213, chosen because it exhibits pulse shape discrimination between neutrons and γ-rays. The cell, 5" diameter by 1½" long, was coupled to the photocathode of an E.M.I. type 6262B photomultiplier by a

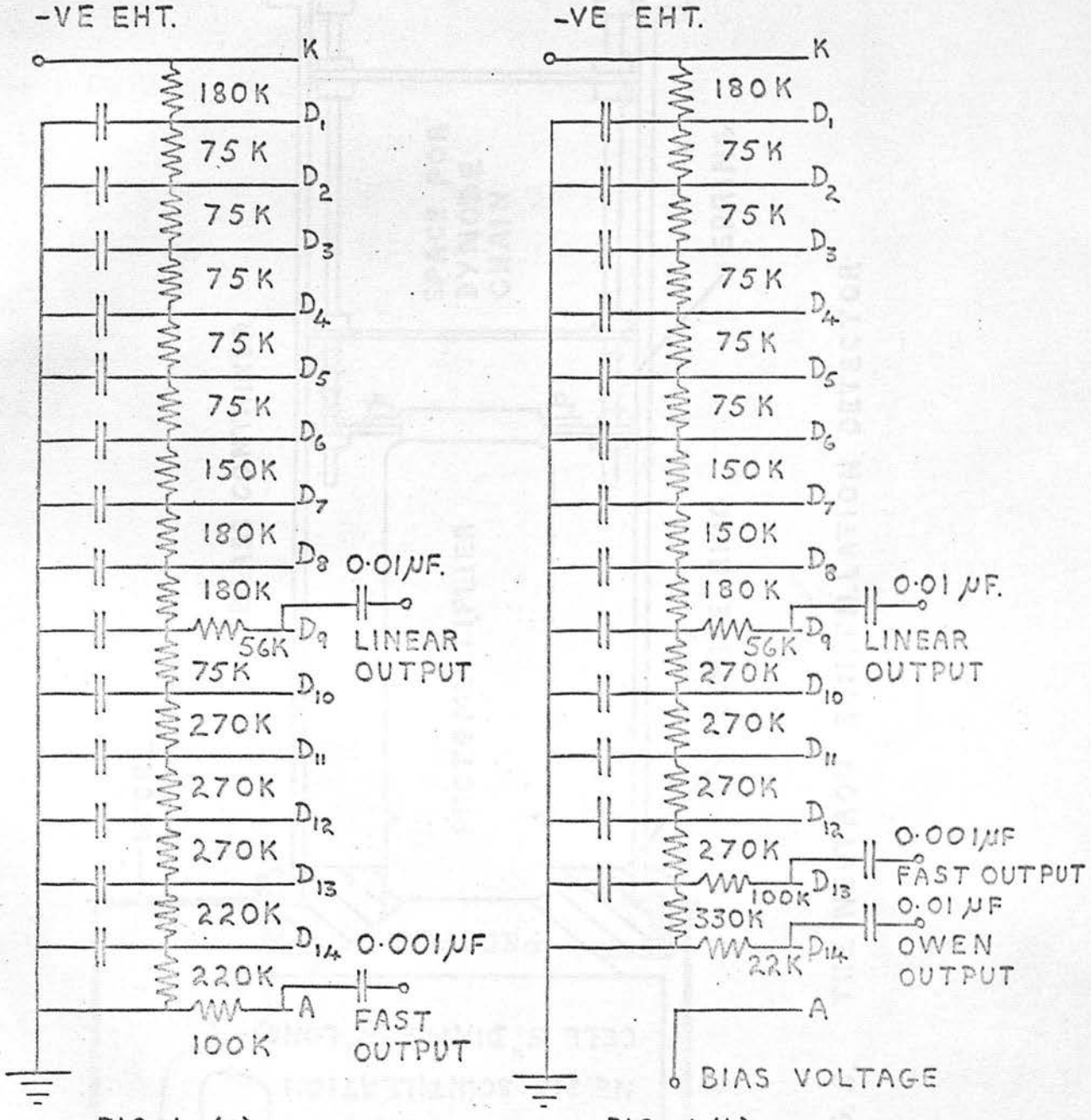

FIG. 4 (a)

FIG. 4(b)

FIG 4 THE CARBON RESISTOR DYNODE CHAINS
(a) γRAY DETECTOR.
(b) NEUTRON DETECTOR.
(ALL DECOUPLING CAPACITORS ARE 0·01μF.)

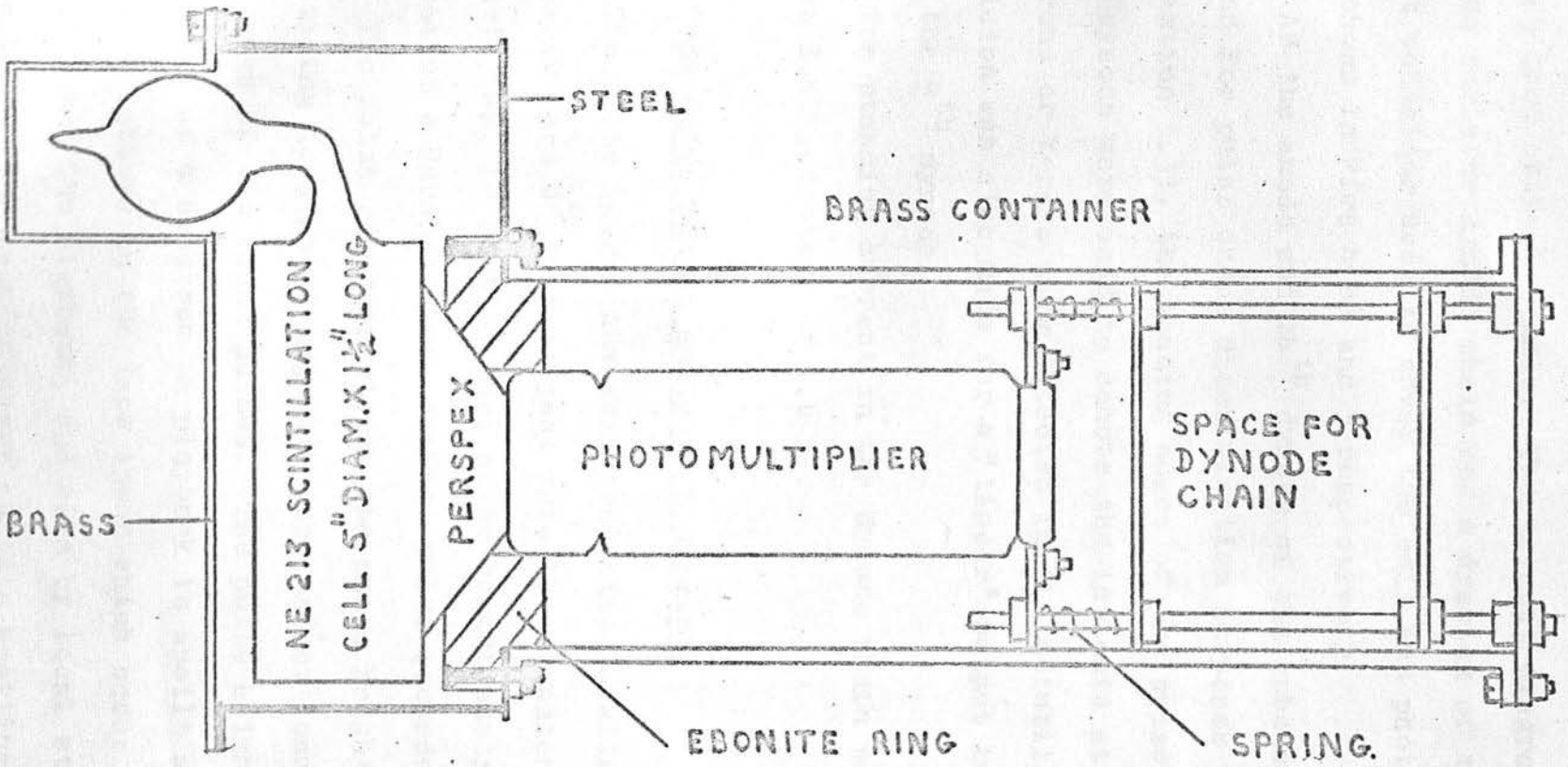

FIG. 5. THE NEUTRON SCINTILLATION DETECTOR

conical light guide 1" thick using siliconegrease to ensure good optical joints. The circuit diagram of the carbon resistor dynode chain and a drawing of the light-tight container used to cover the cell and photomultiplier are shown in Figs 4(b) and 5 respectively.

As the anode and 14th dynode of the tube were required for pulse shape discrimination purposes (described in section 3.3), the leading edges of the pulses at the 13th dynode were used to denote the instants at which neutrons or γ-rays were detected in the scintillator. Provision was also made for a "linear" output to be taken from the 9th dynode.

The standing current in the dynode chain was 0.7 mA for an E.H.T. voltage of 1.6 kV.

2.3. The Pulse Height Analysis Equipment.

The pulse height analysis facilities available during the early part of this project were the occasional use of a Sunvic (Mk. I) multichannel pulse height analyser and the use of a Marshall twin channel pulse recorder, type 203. The pulse recorder stores the pulse height data by magnetising lengths of magnetic tape proportional to the amplitudes of the input pulses. The pulse height resolution of a spectrum on playback is spoilt slightly by the variations in the tape speed which occur during the recording and the playback, and also by local stretching of the tape. The manufacturers quote a spoiling of pulse height resolution of about 1 - 2%.

However, despite the slight spoiling of resolution it was decided to record pulse height spectra and then to analyse the recorded data whenever the pulse height analyser was available.

Unfortunately the pulse recorder was found to be incompatible with the electronic equipment used in the laboratory, and it was necessary to build a shaping circuit to link the recorder to the existing amplifiers, A.E.R.E. type 1008, so that pulse height distributions from these amplifiers could be recorded. The specifications of typical pulses from an amplifier and the input pulses required for the recorder are compared in Table 2.

	Marshall recorder type 203 input pulse specification	Amplifier AERE type 1008 output pulse specification
Polarity of pulses	-ve	+ve
Amplitude range of pulses	150 mV - 15V	0 - 60 V
Rise time of pulses	1.5 - 5μsec	$< \frac{3}{4}$ μsec.

Table 2. Pulse Specifications.

The pulse shaping circuit.

A circuit was designed which accepted pulses from an amplifier and shaped them to give negative pulses between 0 and 15 volts in amplitude with rise times of about

2 μsecs and durations of 4-5 μsec. The circuit diagram is shown in Figure 6.

Pulses between 0 and 60 volts in amplitude at the input are attenuated by the resistor chain R before passing through the cathode follower based on the double triode V1 (E88CC), the attenuation being chosen so that the range of pulse amplitudes at "A" is 0 to 25 volts. The pulses are then lengthened at the grid of the valve V3 (M 8100) which is a linear amplifier with a gain of about 0.75. In the quiescent state the fast pentode V2 (E180F) is non-conducting, so that pulses from the cathode follower charge the capacitance C1 and the grid of V3 through the low forward resistance of the OA10 diode, D1. After C1 is charged, it can only discharge through R2, R3 and the back resistances of diodes D1 and D2 with a time constant of a few msec. Thus the potential change at the grid of V3 is negligible for times of the order of a few μsecs, and a negative voltage step with a rise time of about 2 μsec is produced at "B". This negative voltage step is applied to the grid of a sharp cut-off pentode V4 (E180F), which is normally conducting, thus switching off the anode current and producing a positive voltage step at "F". After passing through a 4 μsec delay line the positive voltage step causes the valve V2 to conduct, thereby discharging in about 1 μsec the capacitance C1 and any stray capacitance at this point in the circuit. The

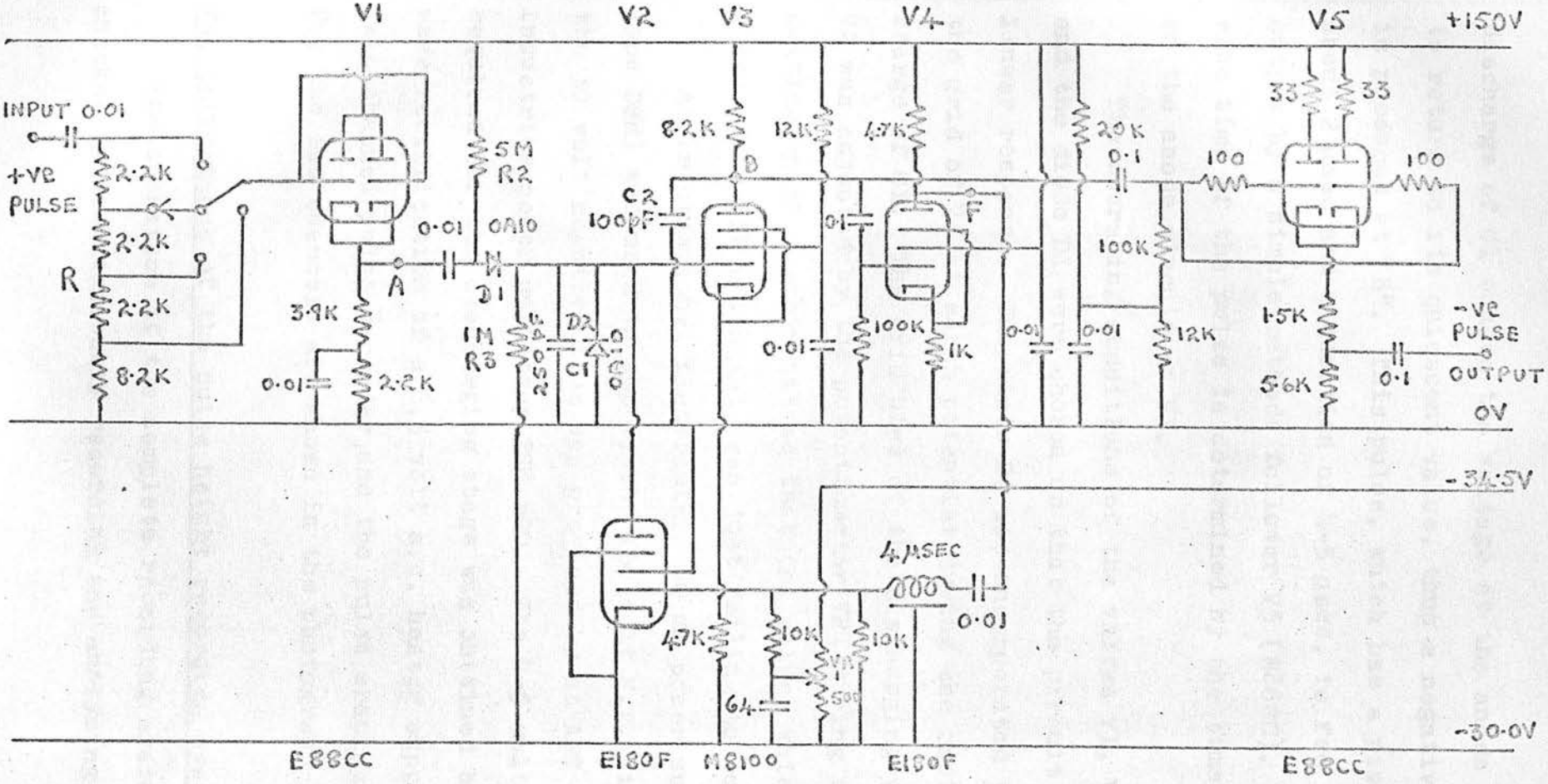

FIG 6. THE PULSE SHAPING CIRCUIT.

discharge of C1 causes the voltage at the anode of V3 to return to its quiescent value, thus a negative pulse is produced at "B". This pulse, which has a rise time of about 2 μsec and a duration of 4-5 μsec, is fed to the output by a simple cathode follower V5 (E88CC). The rise time of the pulse is determined by the time constant of the anode circuit of V3.

The operating conditions of the valves V1, V3 and V5 and the diode D1 were chosen so that the circuit has a linear response. The diode D2 was incorporated to clamp the grid of V3 at earth potential during the rapid discharge of C1. The grid bias of the discharging valve V2 was adjusted by the potentiometer VR1 during the setting up of the circuit so that the valve, which has a sharp cut-off potential, was just failing to conduct.

An International Electronics 100 mA power supply type DSM1 was used to supply the 150 volt H.T. line, while the 30 volt negative line was provided by an APT Electronic Industries power unit type TSU 500. The 4-5 volt bias required for the discharging stage was obtained by full wave rectification of a 6.3 volt a.c. heater supply. The twin channel pulse recorder and the pulse shaping circuits for the two channels are shown in the photograph in Fig. 7.

The performance of the pulse height recording system.

The operation of the complete recording system was checked by simultaneously recording and analysing the same

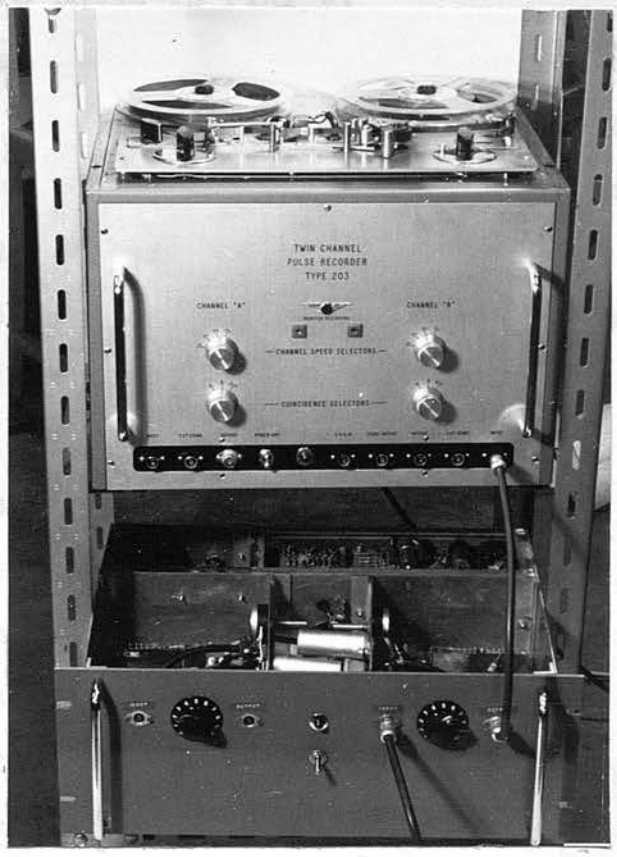

FIGURE 7 : The Pulse Shaping Circuits and the Marshall Twin Channel Pulse Recorder.

pulse height spectrum from an amplifier and then comparing the "direct" spectrum with the spectrum obtained when the recorded one was replayed into the multichannel pulse height analyser. A block diagram of the apparatus used in this test is shown in Fig. 8.

Test pulses from a Solatron pulse generator, type GO 1005, were attenuated and fed through an AERE type 1008 Amplifier. The pulses at the output of the amplifier were then fed simultaneously to the pulse recorder by way of the shaping circuit and to the multichannel pulse height analyser. As the analyser was situated about 150 yards from the H.T. Laboratory, a method devised by Galloway[41] for sending pulses without distortion along a coaxial cable to the analyser was used. The positive pulses from amplifier I were first attenuated by a 2.2 KΩ resistor in series with the 69Ω cable, and then passed through the cable to a cathode follower and amplifier. The pulses from amplifier II (type 1008) were then presented at the input of the multichannel analyser. A similar arrangement was used to send the negative pulses from the pulse recorder to the analyser during the playback of the tape, the amplifier beingadjusted to accept pulses of the opposite polarity in this case (Fig. 8, b).

Test pulses, 0.8 μsec long and of various amplitudes, were analysed and recorded simultaneously using a tape speed of 15" per sec., and a pulse repetition rate of 10^3 pulses per second. A graph of the channel numbers of the peaks in the "recorded" spectrum against the channel numbers of

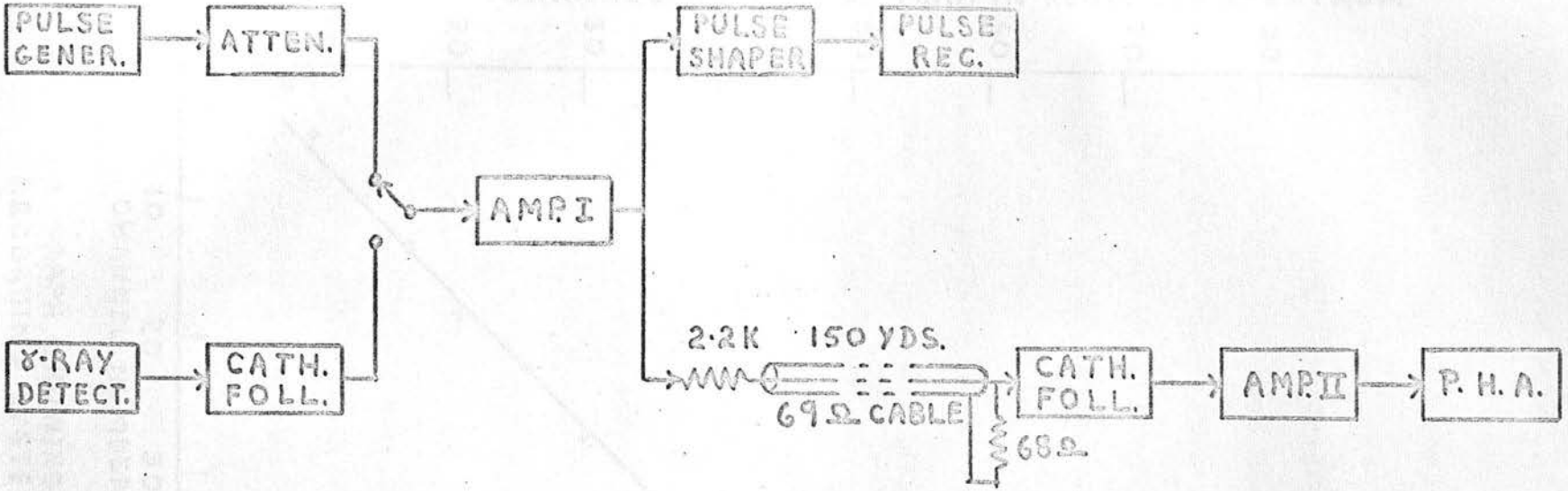

FIG. 8 (a).

FIG. 8 (b).

FIG. 8 (c).

FIG. 8 (a) DIAGRAM OF PULSE HEIGHT RECORDING SYSTEM.
(b) DIAGRAM OF PLAY-BACK SYSTEM.
(c) DIAGRAM OF ALTERNATIVE PLAY-BACK SYSTEM.

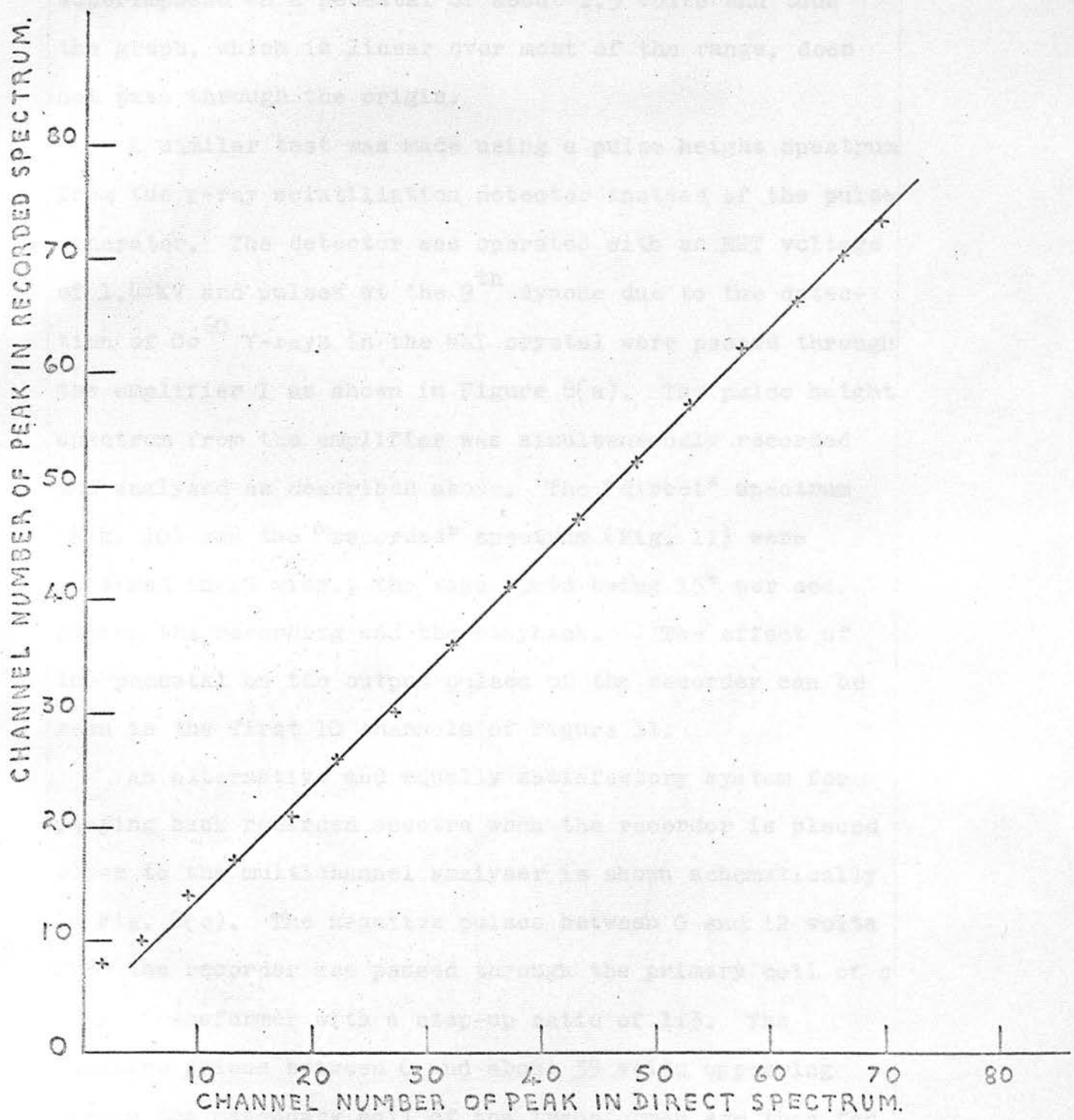

FIG. 9. A GRAPH SHOWING THE LINEARITY OF THE PULSE HEIGHT RECORDING SYSTEM.

the corresponding peaks in the "direct" spectrum was plotted in Fig. 9. The output pulses from the tape recorder are superimposed on a pedestal of about 1.5 volts and thus the graph, which is linear over most of the range, does not pass through the origin.

A similar test was made using a pulse height spectrum from the γ-ray scintillation detector instead of the pulse generator. The detector was operated with an EHT voltage of 1.4 KV and pulses at the 9^{th} dynode due to the detection of Co^{60} γ-rays in the NaI crystal were passed through the amplifier I as shown in Figure 8(a). The pulse height spectrum from the amplifier was simultaneously recorded and analysed as described above. The "direct" spectrum (Fig. 10) and the "recorded" spectrum (Fig. 11) were obtained in 15 mins., the tape speed being 15" per sec. during the recording and the playback. The effect of the pedestal on the output pulses of the recorder can be seen in the first 10 channels of Figure 11.

An alternative and equally satisfactory system for playing back recorded spectra when the recorder is placed close to the multichannel analyser is shown schematically in Fig. 8(c). The negative pulses between 0 and 12 volts from the recorder are passed through the primary coil of a pulse transformer with a step-up ratio of 1:3. The positive pulses between 0 and about 35 volts appearing across the secondary coil of the transformer are then fed to the analyser. This method enables amplifier II to be used for other purposes.

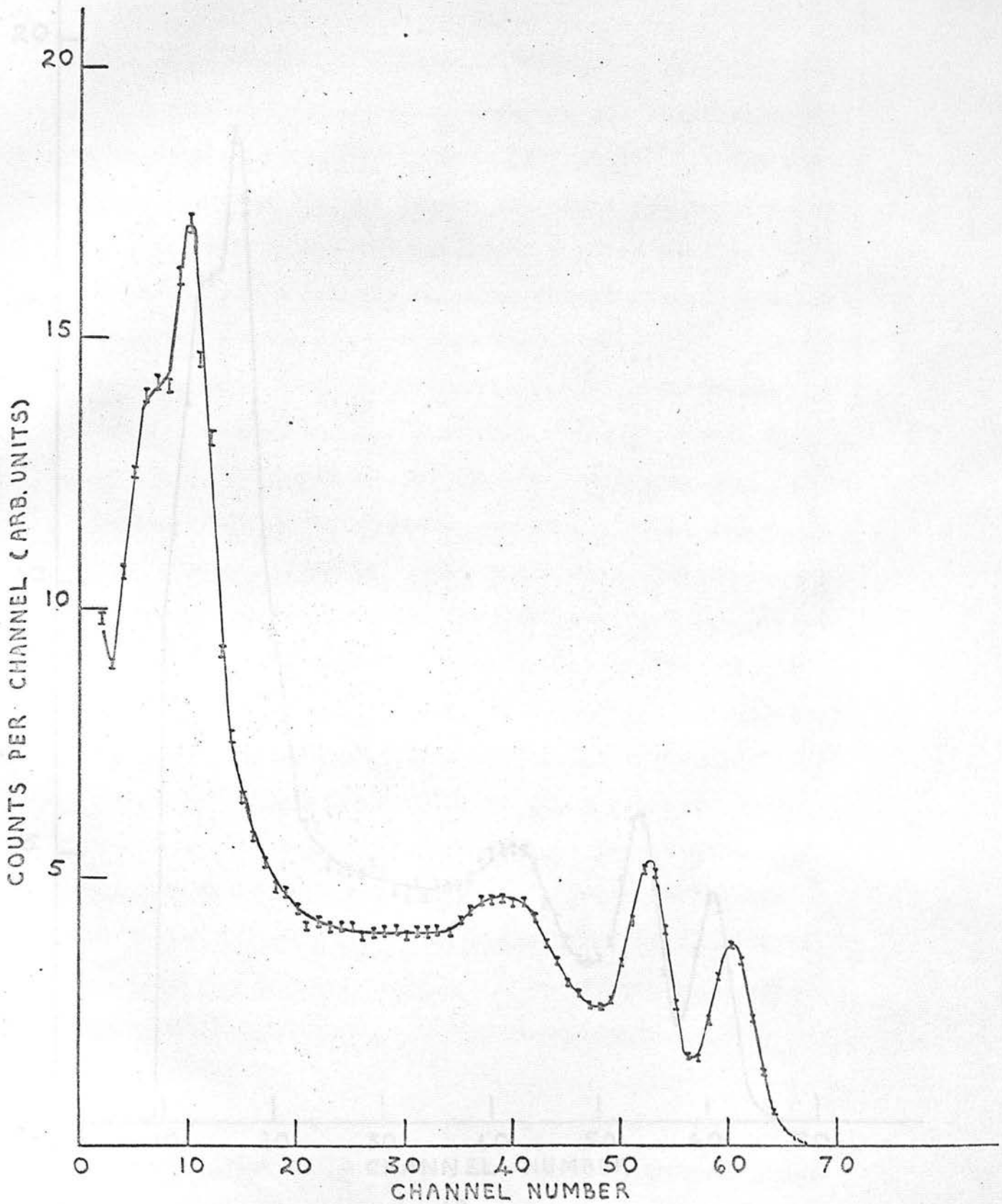

FIG. 10. THE SPECTRUM OF Co^{60} γRAYS ANALYSED DIRECTLY.

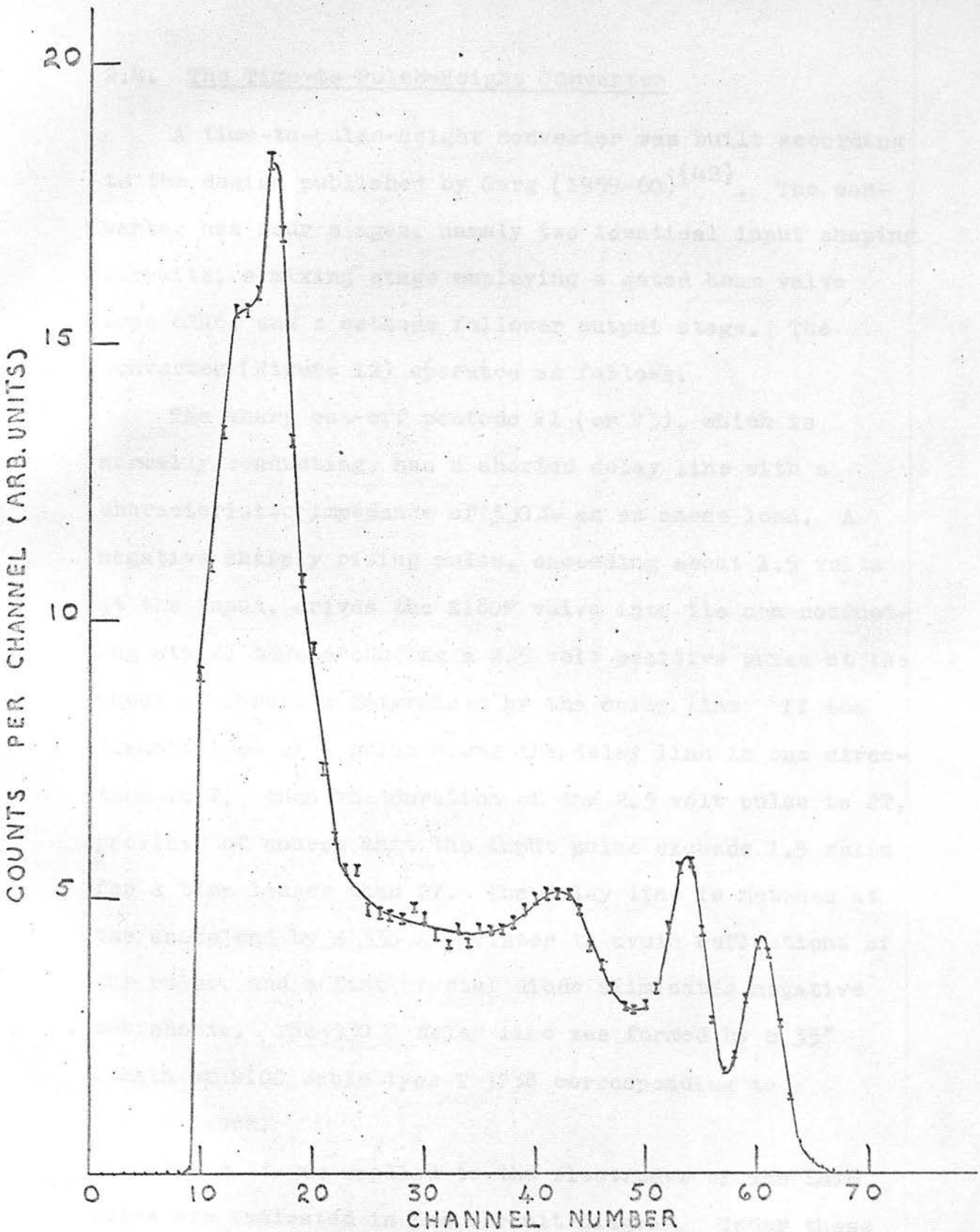

FIG. 11. THE SPECTRUM OF Co^{60} γRAYS RECORDED SIMULTANEOUSLY WITH THE DIRECT SPECTRUM, FIG. 10.

2.4. The Time-to-Pulse-Height Converter

A time-to-pulse-height converter was built according to the design published by Garg (1959-60)[42]. The converter has four stages, namely two identical input shaping circuits, a mixing stage employing a gated beam valve type 6BN6, and a cathode follower output stage. The converter (Figure 12) operates as follows.

The sharp cut-off pentode V1 (or V3), which is normally conducting, has a shorted delay line with a characteristic impedance of 330 Ω as an anode load. A negative sharply rising pulse, exceeding about 1.5 volts at the input, drives the E180F valve into its non-conducting state, thus producing a 2.5 volt positive pulse at the anode of duration determined by the delay line. If the transit time of a pulse along the delay line in one direction is T, then the duration of the 2.5 volt pulse is 2T, provided of course that the input pulse exceeds 1.5 volts for a time longer than 2T. The delay line is matched at the anode end by a 330 Ω resistor to avoid reflections of the pulse, and a fast crystal diode eliminates negative overshoots. The 330 Ω delay line was formed by a 35" length of BICC cable type T 3238 corresponding to T = 50 nsecs.

The voltages applied to the electrodes of the 6BN6 valve are indicated in the circuit diagram. Under these conditions the valve does not conduct unless the potentials

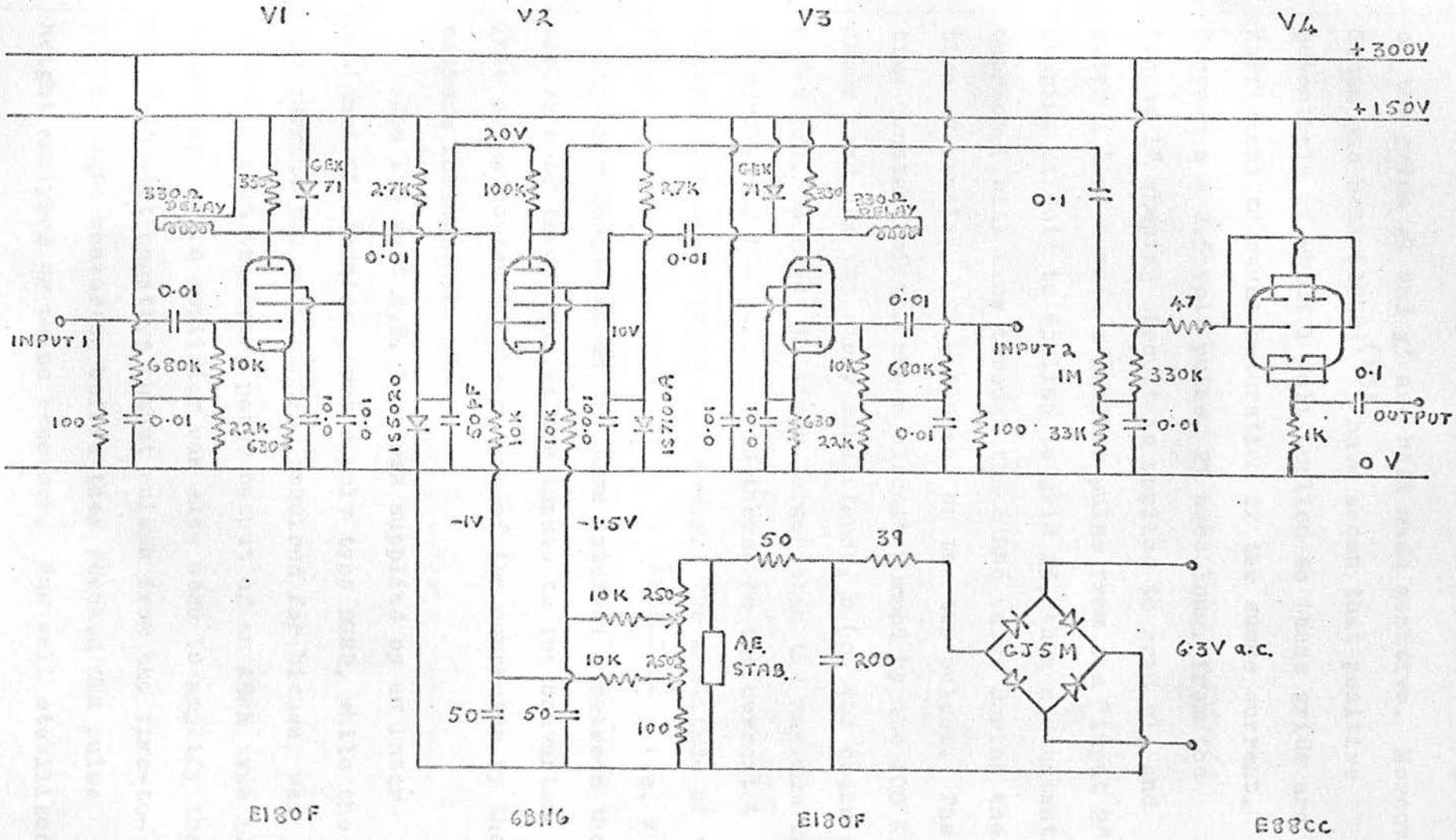

FIG. 12 CIRCUIT DIAGRAM OF THE TIME-TO-PULSE HEIGHT CONVERTER.

of the grids g1 and g3 are both made positive. Moreover Green and Bell (1958)[43] have shown that positive potentials of about 1 volt applied to these grids are sufficient to cause saturation of the anode current. Suppose a + 2.5 volt pulse, 2T nsec long, from the "input 1" shaping circuit is applied to grid g1, and after a time t nsec a similar pulse from the "input 2" shaping circuit is applied to grid g3, then a constant current I will flow through the 6 BN6 valve during the time of overlap, (2T - t)nsec, of the two pulses. The time constant of the anode circuit formed by the 100 KΩ anode load and its stray capacitance, c (of the order of a few pF), is about 10 times larger than the maximum time of overlap of the pulses, and therefore the current I charges the capacitance c linearly. The amplitude of the pulse formed at the anode is $V = \frac{I(2T - t)}{c}$, i.e. V is linearly dependent on the time interval t between the arrivals of the pulses at the inputs to the converter. This pulse is fed to the output of the converter by the cathode follower V4, E88CC.

The 150 volt H.T. line was supplied by an International Electronics power supply type DSM2, while the low current 300 volt supply, required for biases, was obtained from the spare power output of an AERE type 1008 amplifier. This amplifier was also used to amplify the 0 - 0.75 volt negative output pulses from the time-to-pulse-height converter before they reached the pulse height analyser or pulse recorder. The well stabilized

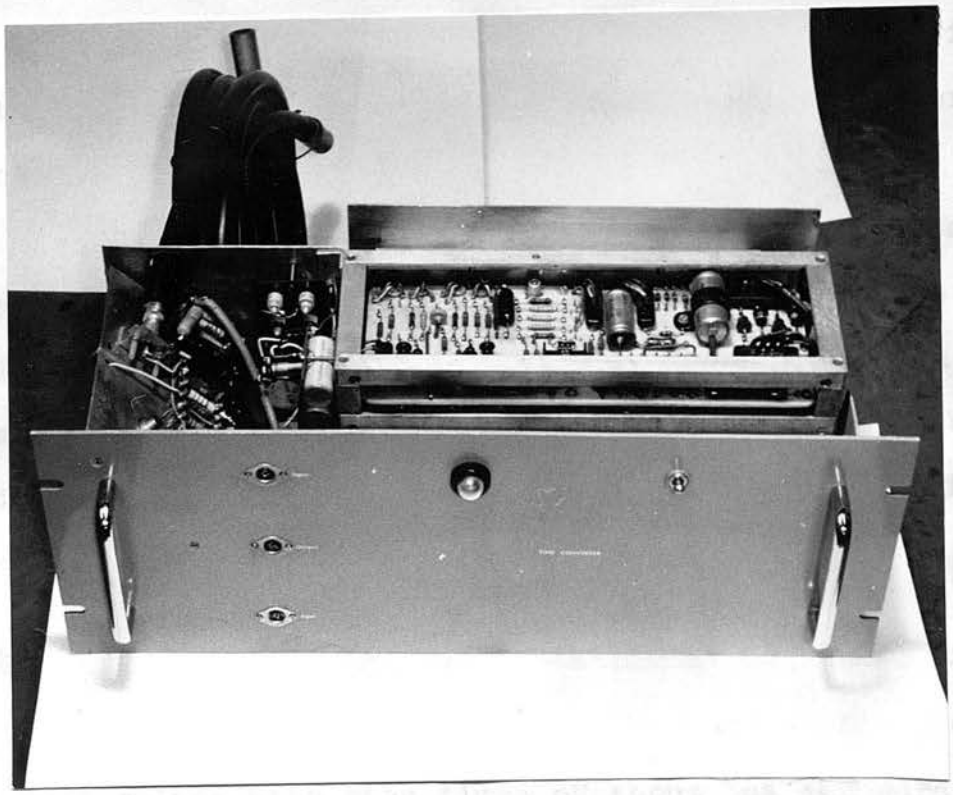

FIGURE 13 : The Time-to-Pulse-Height Converter.

1.5 and 1.0 volt grid biases for the 6BN6 valve were produced by full-wave rectification and smoothing of a 6.3 volt a.c. heater supply as shown in the circuit diagram (Fig. 12).

The circuit was found to be very sensitive to inter-stage pickup and therefore all connections were short and screened where possible.

There is an error in the circuit diagram published by Garg[42]; the GEX 71, or equivalent, diodes are shown with the wrong polarity. This mistake is rectified in a later paper[44] in which a similar circuit is described. Figure 13 is a photograph of the time-to-pulse-height converter unit.

The performance of the time-to-pulse-height converter

A pulse generator, AERE type 1147B, supplied negative 2 volt pulses with rise times of about 3ns and durations of 1 μsec which were fed to the inputs of the time-to-pulse-height converter. The pulses to "input 2" were delayed by time intervals between -100 ns and +100 ns relative to the pulses to "input 1" by inserting appropriate lengths of 330 Ω delay cable between the generator and converter. (A negative time delay corresponds to the arrival of the pulse at "input 2" before that at "input 1"). Pulses at the output of the time-to-pulse-height converter after amplification were displayed by the Sunvic (Mk I) multichannel pulse height analyser, Figure 14. The graph

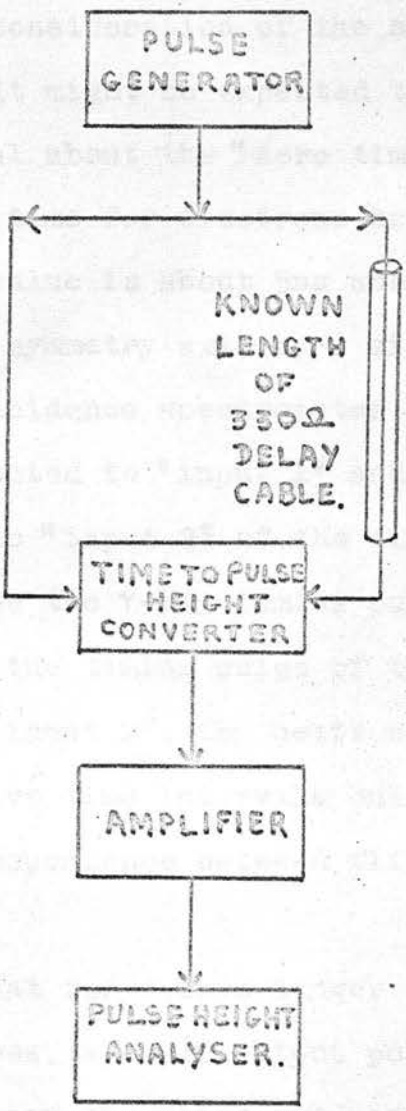

FIG. 14. BLOCK DIAGRAM OF THE SYSTEM FOR TESTING THE TIME-TO-PULSE HEIGHT CONVERTER.

of the channel numbers of the delayed coincidence peaks against the time intervals between the input pulses is shown in Fig. 15.

From a casual consideration of the symmetry of the converter circuit, it might be expected that the graph should be symmetrical about the "zero time interval" axis. However the transit time for electrons between grids g1 and g3 of the 6BN6 value is about 5ns and this causes the displacement of the symmetry axis by a similar amount.

If the n-Υ coincidence spectrometer is set up with the Υ-ray detector connected to "input 1" and the neutron detector connected to "input 2" of the time-to-pulse-height converter, then since the Υ-ray timing pulse always arrives at "input 1" before the timing pulse of the associated neutron arrives at "input 2", the neutron flight-times correspond to positive time intervals only. Therefore there is a 1-1 correspondence between flight-times and channel numbers.

It was found that for delays longer than 100 ns between the input pulses, a small output pulse occurred due to feed through between the third grid and the anode of the 6BN6 valve. In Fig. 15 these pulses were recorded in channel 9, but usually such pulses were eliminated from the spectrum by using the subtractor at the input to the multi-channel pulse height analyser.

The gain of the amplifier following the converter was increased until the coincidence peaks were displayed

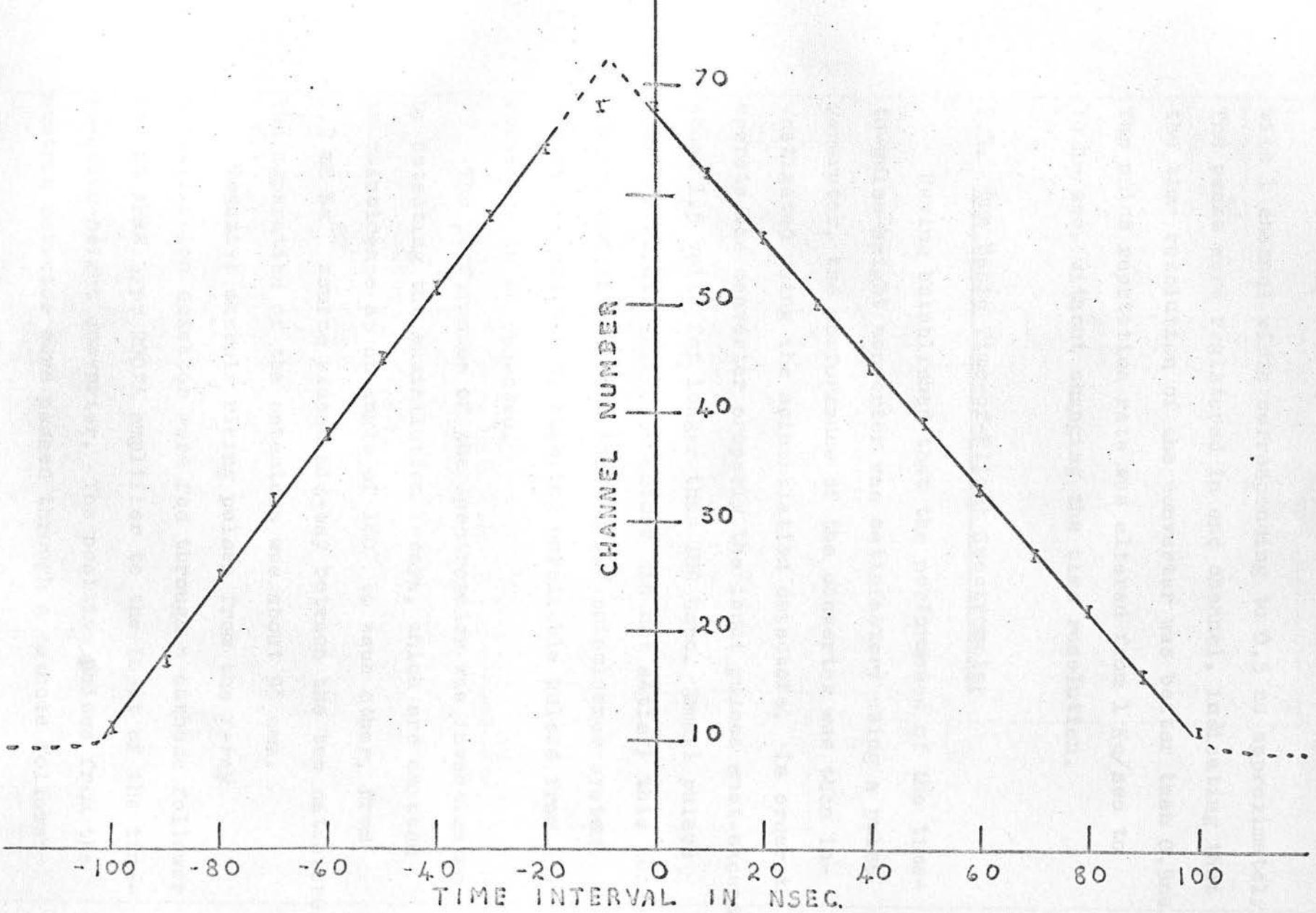

FIG 15. A GRAPH OF THE CHANNEL NUMBERS OF THE DELAYED COINCIDENCE PEAKS VERSUS THE TIME INTERVALS BY WHICH THE PULSES TO INPUT 2 ARE DELAYED RELATIVE TO THE PULSES TO INPUT 1 OF THE CONVERTER.

with 1 channel width corresponding to 0.5 ns approximately. The peaks were registered in one channel, indicating that the time resolution of the converter was better than 0.5ns. The pulse repetition rate was altered from 1 Kc/sec to 10 Kc/sec. without changing the time resolution.

2.5. The Basic Time-of-Flight Spectrometer

Having established that the performance of the time-to-pulse-height converter was satisfactory using a pulse generator, the performance of the converter was then investigated using the scintillation detectors. In order to operate the converter properly the input pulses must exceed about 1.5 volts for longer than 100 nsec. Small pulses from the scintillation detectors did not satisfy this condition, and therefore a "fast-slow" coincidence system, Figure 16, was set up enabling unreliable pulses from the converter to be rejected.

The performance of the spectrometer was investigated by detecting the annihilation γ-rays, which are emitted in coincidence at an angle of 180° to each other, from 0.2 mC Na^{22} source placed mid-way between the two detectors. The separation of the detectors was about 95 cms.

Negative sharply rising pulses from the γ-ray scintillation detector were fed through a cathode follower and an AERE type 2002A amplifier to the input of the time-to-pulse-height converter. The positive pulses from the neutron detector were passed through a cathode follower

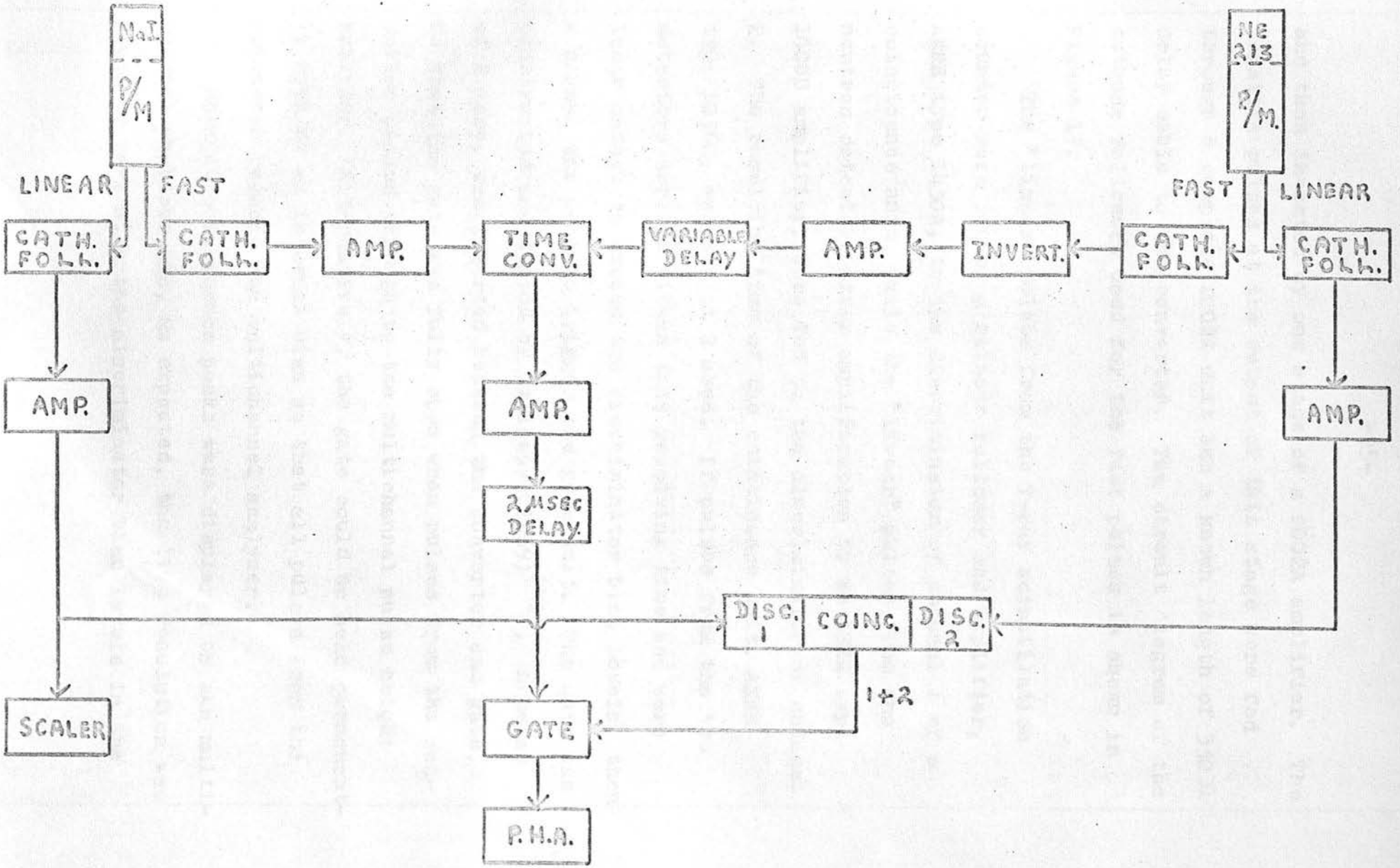

FIG. 16. THE BASIC TIME-OF-FLIGHT SPECTROMETER.

and then inverted by one stage of a 2002A amplifier. The negative pulses at the output of this stage were fed through a complete 2002A unit and a known length of 330 Ω delay cable to the converter. The circuit diagram of the cathode followers used for the fast pulses is shown in Figure 17.

The "linear" pulses from the γ-ray scintillation counter were fed by a cathode follower and amplifier, AERE type 1430A, to the discriminator of channel 1 of a coincidence unit, while the "linear" pulses from the neutron detector, after amplification by an AERE type 1008B amplifier, were fed to the discriminator of channel 2. The resolving time of the coincidence unit, AERE type 1036C, was set at 2 μsec. If pulses from the two detectors arrived within this resolving time and were large enough to exceed the discriminator bias levels, then a signal was sent to trigger the gate unit. The gate was constructed and tested by Galloway (1959)[41]. A delay of 2 μsec. was inserted between the converter and gate, so that the gate was fully open when pulses from the converter passed through to the multichannel pulse height analyser. Alternatively, the gate could be held permanently open by an internal bias so that all pulses from the converter reached the multichannel analyser.

Delayed coincidence peaks were displayed by the multichannel analyser and, as expected, the time resolution was found to vary with the discriminator bias levels in the

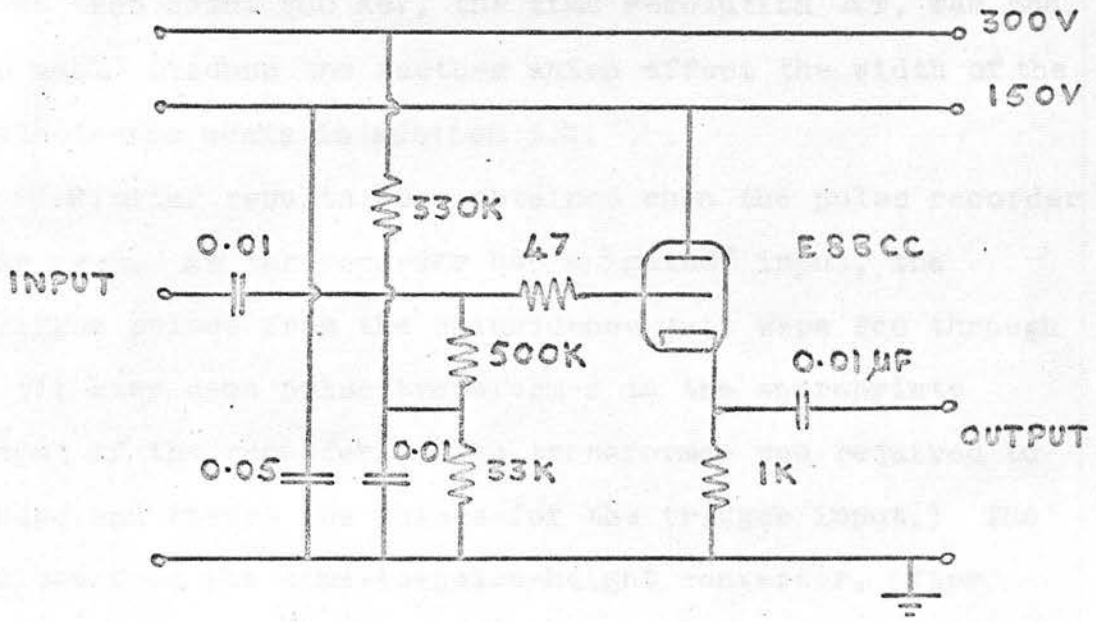

FIG.17. THE CATHODE FOLLOWER FOR THE SHARPLY RISING PULSES FROM THE DETECTORS.

slow channels. Typical coincidence peaks, obtained in 1 min., are shown in Figure 18. The time resolution of the spectrometer with the gate held permanently open was about 10ns. When the bias level in each channel was set to reject pulses corresponding to γ-rays with energies less than about 200 keV, the time resolution ΔT, was 6ns. We shall discuss the factors which affect the width of the coincidence peaks in section 3.4.

Similar results were obtained when the pulse recorder was used. As the recorder had a "gated" input, the trigger pulses from the coincidence unit were fed through a 3:1 step down pulse transformer to the appropriate input of the recorder. (The transformer was required to shape and invert the pulses for the trigger input.) The pulses from the time-to-pulse-height converter, after being delayed by 2 μsec, as before, passed through the shaping circuit to the "gated" input of the recorder. The linearity of the spectrometer and the resolution of the delayed coincidence peaks were the same in the "recorded" and "direct" spectra.

The time range of the time-to-pulse-height converter

The time interval between the neutron groups associated with levels at 2.15 and 2.86 MeV in B^{10} is about 7ns for a 1 metre flight path (Figure 2), and therefore a 2 metre flight path would be required to resolve these groups adequately. Unfortunately the flight time of the slowest neutron group would then be about 135ns, which

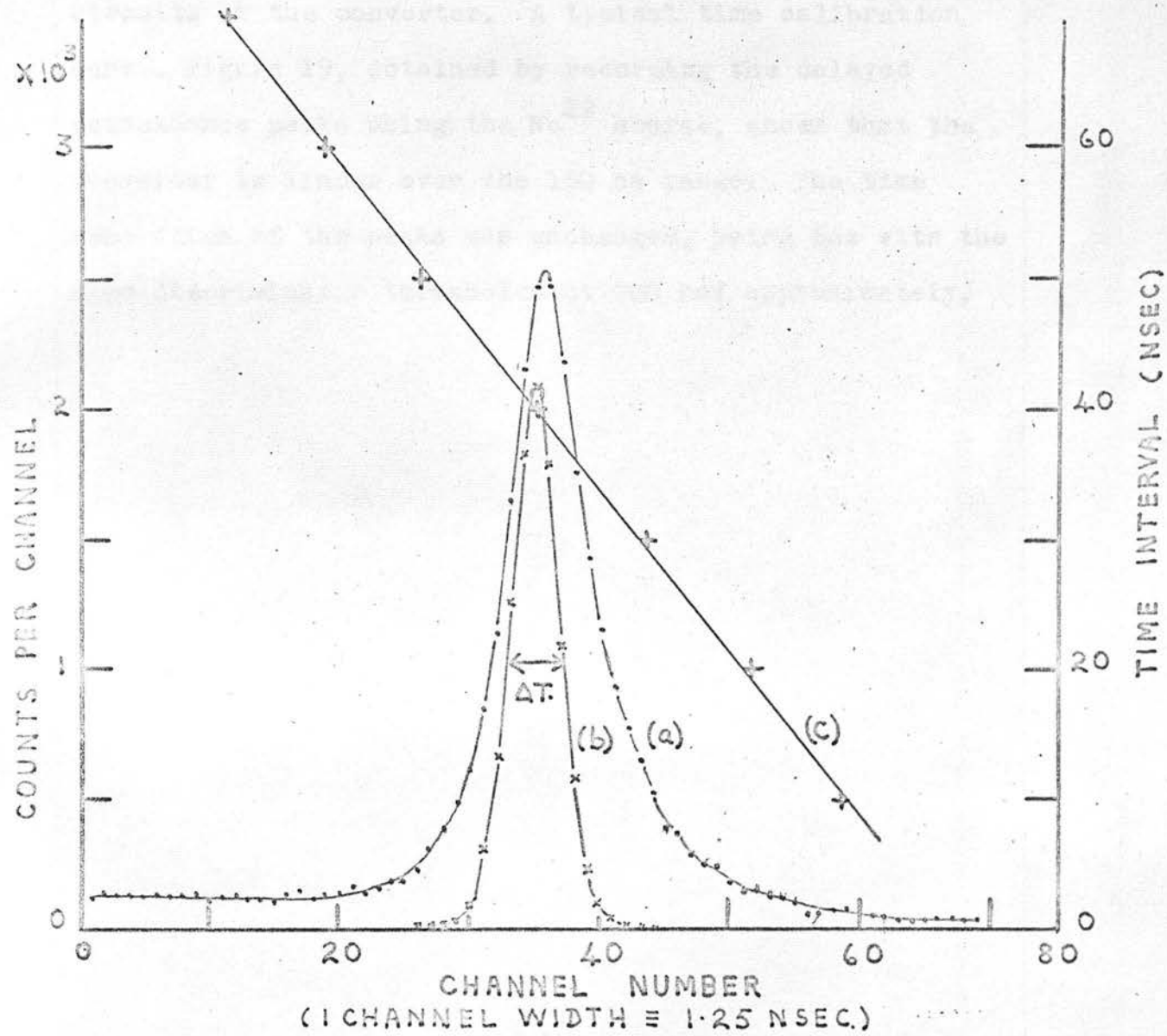

FIG. 18. SPECTRA OF TYPICAL COINCIDENCE PEAKS (a) WITH GATE HELD OPEN AND (b) WITH DISCRIMINATOR THRESHOLDS SET AT 200 keV. (c) THE TIME INTERVAL v CHANNEL NUMBER CALIBRATION CURVE.

lies outside the time range of the converter. Therefore, the range of the converter was increased by using longer delay lines, corresponding to T = 80ns, in the shaping circuits of the converter. A typical time calibration curve, Figure 19, obtained by recording the delayed coincidence peaks using the Na^{22} source, shows that the converter is linear over the 150 ns range. The time resolution of the peaks was unchanged, being 6ns with the slow discriminator thresholds at 200 keV approximately.

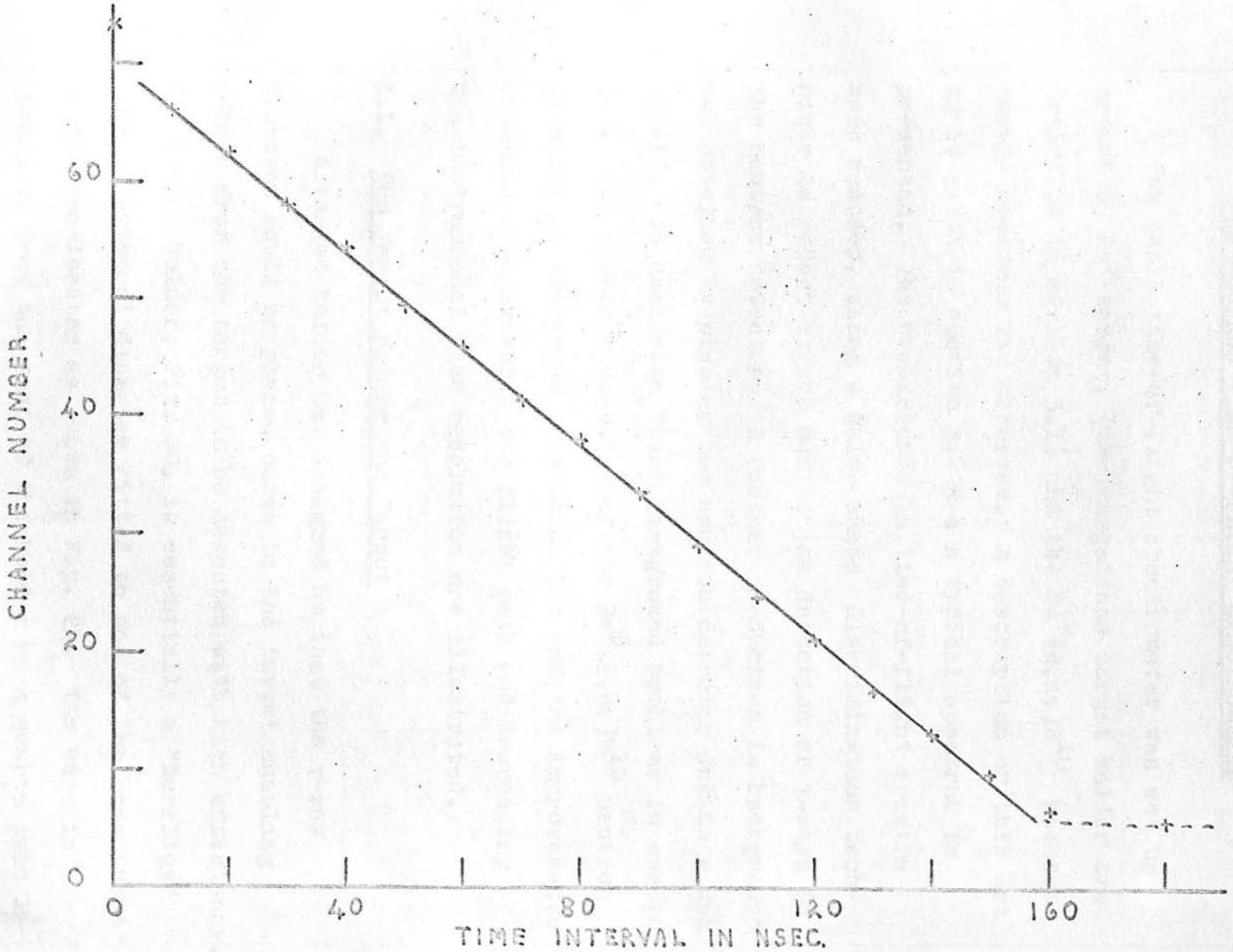

FIG. 19. THE CHANNEL NUMBER v TIME INTERVAL CALIBRATION CURVE.

CHAPTER 3

THE NEUTRON TIME-OF-FLIGHT SPECTROMETER

The basic time-of-flight spectrometer was set up around a Be^9 target, (the target and target holder are described in section 3.1) and the $Be^9(d,n\gamma)B^{10}$ neutron energy spectrum was observed. A description of this set up is given in section 3.2 and a typical spectrum is presented. The backgrounds in time-of-flight spectra were reduced, using a pulse shape discrimination technique to reject events due to the detection of γ-rays in the neutron detector. A further reduction in background was obtained by placing the neutron detector inside a wax shield. We deal with these background problems in section 3.3. The energy resolution of the $Be^9(d,n\gamma)B^{10}$ neutron spectrum is discussed in section 3.4 and the improvements obtained by increasing the flight path and decreasing the instrumental time resolution are illustrated.

3.1. The Target Holder and Target

A target holder was designed so that the γ-ray detector could be placed close to the target enabling γ-rays from the target to be detected with high efficiency. The target holder, Fig. 20, is essentially a "Duralloy" tube 1" external diameter fitted to one of the beam-tubes of the accelerator as shown in Fig. 21. The base is insulated from the rest of the holder by a quartz tube $1\frac{1}{8}$"

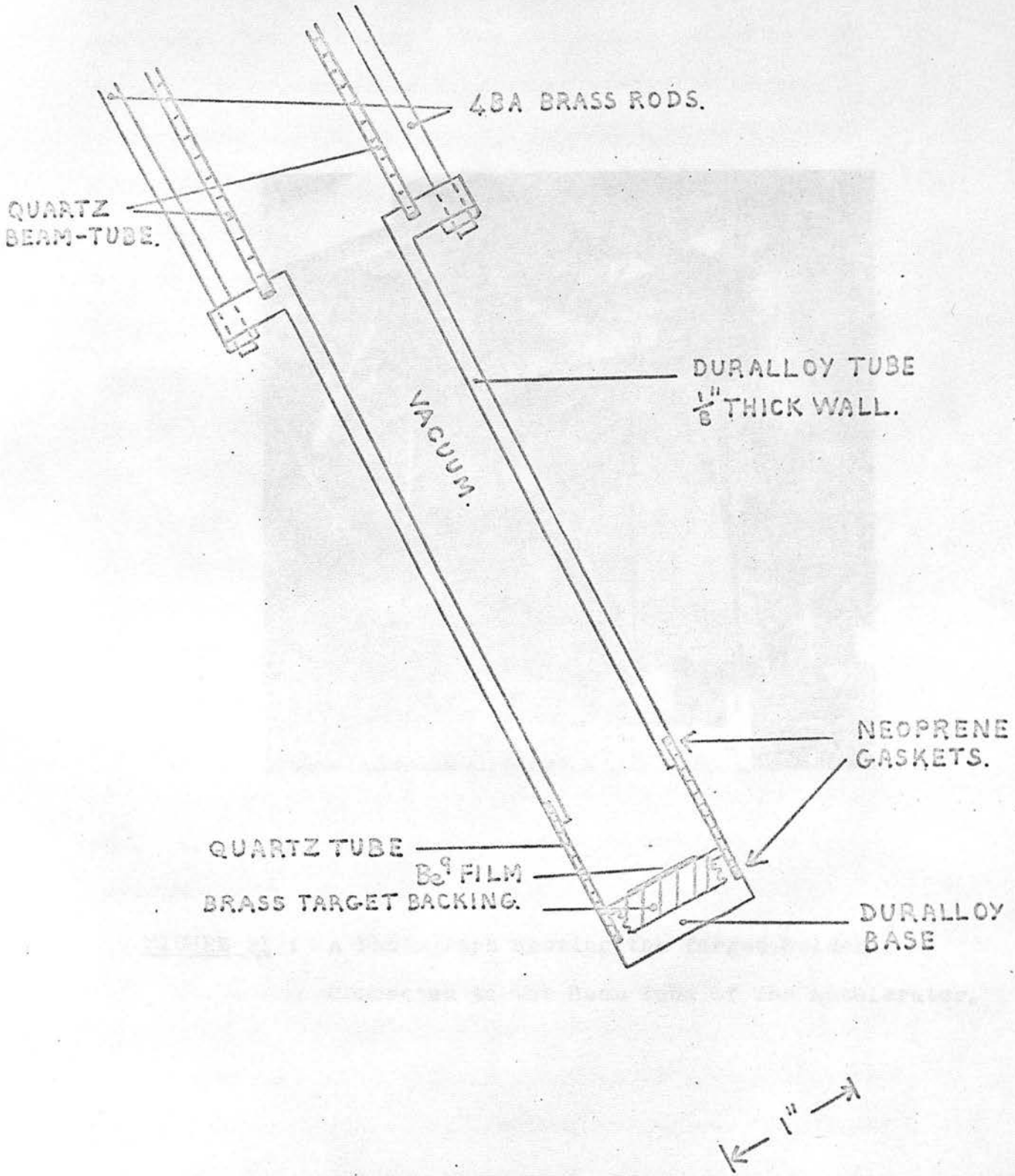

FIG. 20. THE TARGET HOLDER.

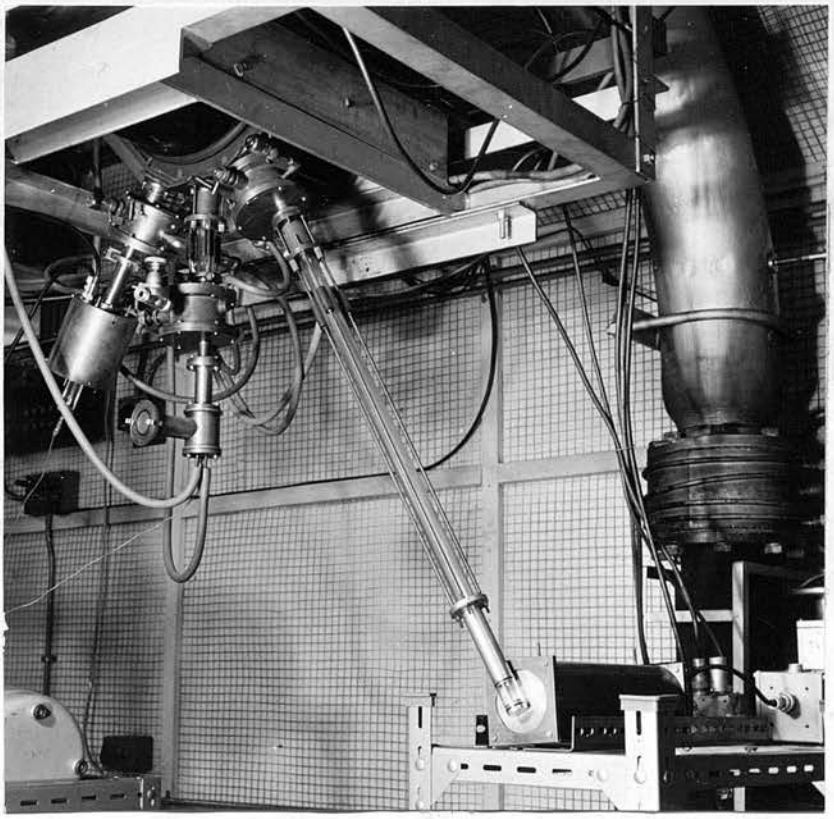

FIGURE 21 : A Photograph Showing the Target Holder Connected to the Beam Tube of the Accelerator.

long so that the beam current striking the target can be measured. The "Duralloy" base and quartz tube are held in position by atmospheric pressure, neoprene gaskets smeared with silicon grease being used to ensure vacuum tight joints. The beam-tube and target holder can be isolated from the main vacuum system of the accelerator by a valve fitted between the beam-tube and the analysing magnet, Fig. 21. Targets can be changed easily since air can be admitted to the target holder and pumped out again without affecting the main vacuum system.

The accelerated ion beam after being deflected through 30° by the field of the analysing magnet passed along the beam-tube to the target. When beam currents greater than 0.5 μA were used, cold air was blown onto the target holder to prevent overheating of the target. The target was a thin film of Be^{9} which had been evaporated onto a brass disc $\frac{3}{16}$" thick. As the film was just optically transparent, its thickness was estimated to be less than 500Å. This corresponds to a surface density of less than 0.01 mg./cm.^{2}.

3.2. $Be^{9}(d,n)B^{10}$ Neutron Time-of-flight Spectra Using the Basic Spectrometer.

The basic time-of-flight spectrometer, Fig. 16, which had been tested using a Na^{22} source was set up around the Be^{9} target. The γ-ray detector was placed with the front face of the NaI(Tℓ) crystal about 2 cm. from the centre of

the target and at an angle of 90° to the deuteron beam direction, Fig. 21. The neutron detector was mounted with the NE213 scintillation cell at 1.3 metres from the target. The flight path was chosen for convenience in the horizontal plane through the target and it was arranged that the neutrons were observed at 60° to the beam direction.

Time-of-flight spectra of the $Be^9(d,n\gamma)B^{10}$ neutrons for 600 keV deuterons were recorded at various deuteron beam currents. The reaction-rate was monitored by measuring the γ-ray counting rate using an A.E.R.E. type 1009 scaler with a 5 volt threshold bias. During each run the γ-ray counting rate was kept constant by adjusting, if necessary, the controls of the H.T. set. It was observed that for beam currents of the order of 4 μA the background in the spectra due to accidental coincidences obliterated the details of the true time-of-flight spectra. However, it was found by a series of trials that spectra with acceptable background levels could be obtained in reasonably short times using beam currents of about 0.2 μA.

A typical time-of-flight spectrum obtained in 4 hours with a deuteron current of $\approx$ 0.1 μA is shown in Figure 27(a). The spectrum is displayed with a channel width corresponding to about 1.75 ns. . The γ-ray timing pulses were delayed by 20ns at the input of the time-to-pulse-height converter in order to displace the prompt γ-ray

coincidence peak from the non-linear region of operation of the time-to-pulse-height converter; the non-linearity would affect the width of the prompt peak. The prominent peaks in the spectrum, Figure 27(a) are identified as the prompt γ-ray coincidence peak and the neutron groups associated with the formation of the well known excited states in B^{10} at 0.72, 1.74, 2.15 and 3.58 MeV. The neutron groups associated with the 1.74 and 2.15 MeV levels are not resolved in the spectrum due to poor energy resolution. The intensity of the "3.58 MeV" neutron group was found to depend strongly on the setting of the threshold bias in the neutron "linear" channel.

The presence of the prompt γ-ray coincidence peak indicated that the neutron counter was sensitive to large numbers of γ-rays which could contribute to the rather high random background in the spectrum. It was decided therefore to use the pulse shape discrimination technique of Owen (1959)[45] to reduce the background due to the detection of γ-rays in the neutron counter.

3.3. The Reduction of Background in Time-of-flight Spectra

Pulse shape discrimination between γ-rays and neutrons

It has been observed by Owen (1959)[45] that after certain phosphors have been excited by γ-rays, neutrons or charged particles, the intensity of the light emitted by the phosphor decays with "fast" and "slow" components having mean values for the decay time constants of about

3 nsec and < 100 nsec respectively. Also the relative intensities of the two components have been found to depend on the type of particle which interacts with the phosphor. The liquid scintillator type NE 213 was chosen as the scintillator for the neutron detector because the ratio of the intensity of the slow component to that of the fast component is larger for neutrons than for γ-rays. The enhancement of the difference in shape of the current pulses through the photomultiplier resulting from the detection of γ-rays and neutrons is achieved by current saturation effects between the last dynode and the anode of the 6262B photomultiplier.

The anode is biased only a few volts positive relative to the 14^{th} dynode, Figure 22, using a Farnell 12 volt power unit type T.B.0., , so that the current between the dynode and the anode is easily saturated. During most of the early portion of any pulse the electron current arriving at the 14^{th} dynode exceeds the saturated current leaving and therefore the potential of the dynode is driven negative by the accumulation of electrons. As the current pulse decays a time is reached when the current arriving equals the current leaving the dynode; the maximum value of the negative potential occurs at this instant. Later the electron current leaving the dynode becomes greater than that arriving due to the secondary emission process and the negatively charged dynode is first discharged and then charged positively. The ratio of the "fast" to "slow" components of the pulses is such

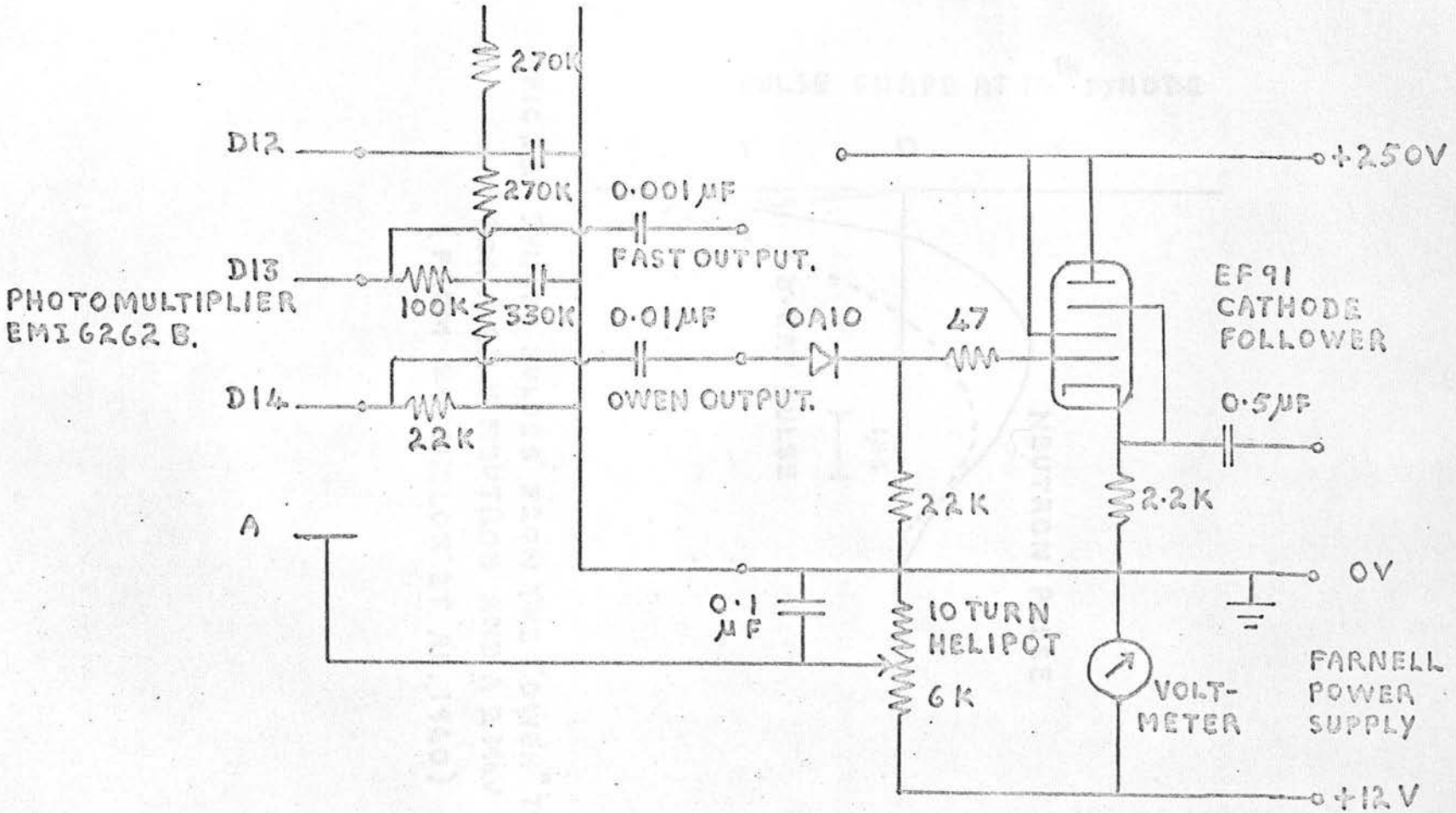

FIG. 22. THE ANODE BIAS AND OWEN OUTPUT CIRCUIT FOR PULSE SHAPE DISCRIMINATION.

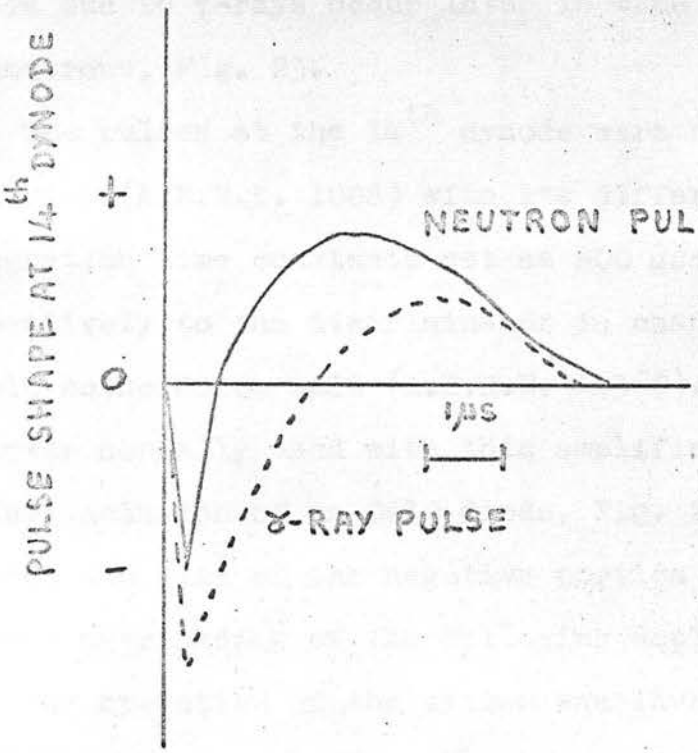

FIG 23. DYNODE PULSES FROM THE "OWEN" TYPE CIRCUIT FOR A 6MeV NEUTRON AND A 2MeV γRAY. (FROM BATCHELOR ET AL., 1960)

that the potential of the dynode is driven only slightly positive for γ-rays and strongly positive for neutrons. Moreover it has been found by Batchelor, Gilboy, Purnell and Towle (1960)[46] that the positive parts of the pulses due to γ-rays occur later in time than those due to neutrons, Fig. 23.

The pulses at the 14th dynode were fed through an amplifier (A.E.R.E. 1008) with its differentiation and integration time constants set at 800 μsec and 0.8 μsec respectively to the discriminator in channel 3 of a triple coincidence unit (A.E.R.E. 1036C). The cathode follower normally used with this amplifier was modified by the inclusion of an OA10 diode, Fig. 22; this diode limited the size of the negative portion of the pulse to prevent overloading of the following amplifier.

The operation of the system was investigated by applying the positive "Owen" pulses and the "linear" pulses from the 9th dynode of the photomultiplier simultaneously to the y- and x-plates of an oscilloscope respectively. The brightness of the trace on the screen of the oscilloscope was controlled by the output pulses from the coincidence unit. The experimental arrangement is shown in Fig. 24.

The gain of the amplifier for the "linear" pulses was chosen to give pulses of a suitable amplitude for the discriminator, and as a result these pulses had to be attenuated by a 100KΩ resistor at the input of the

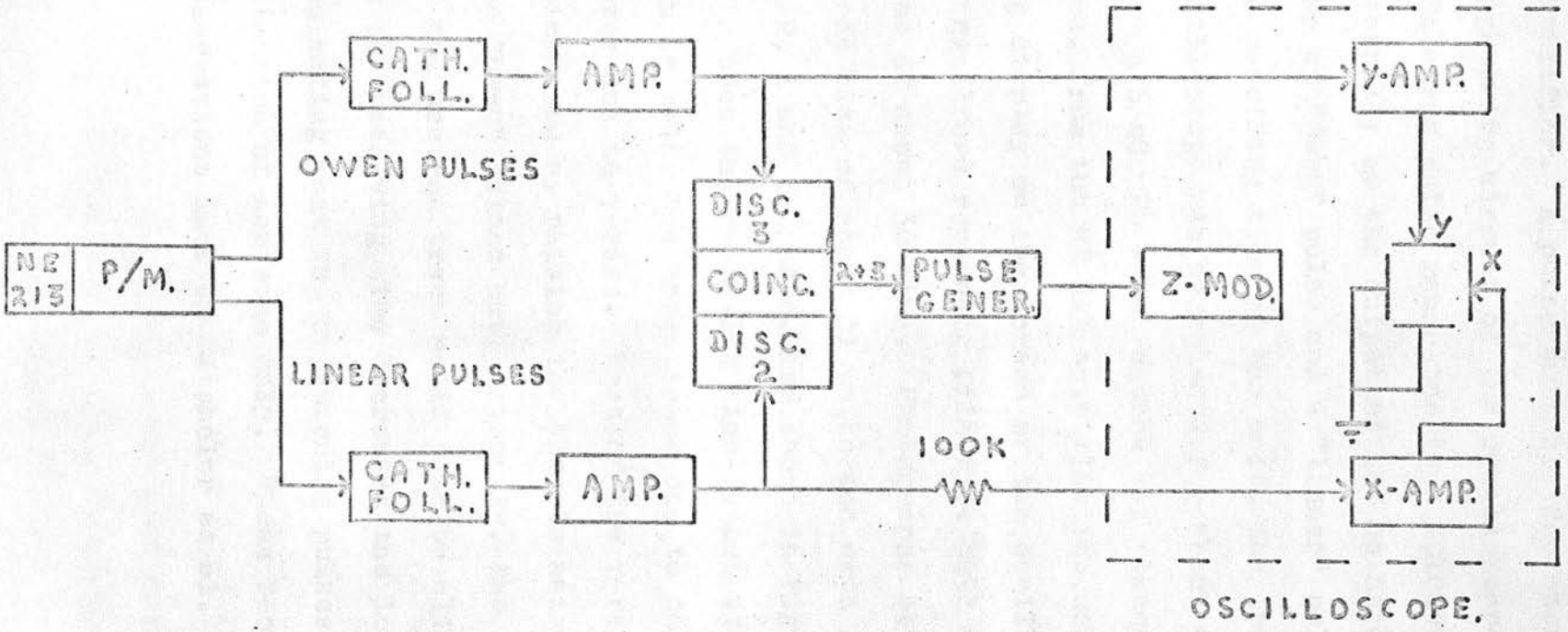

FIG. 24 BLOCK DIAGRAM OF ELECTRONICS USED TO INVESTIGATE THE PULSE SHAPE DISCRIMINATION TECHNIQUE.

Solatron oscilloscope type CD643S to avoid overloading its x-amplifier. A pulse suitable for operating the trace brightening circuit of the oscilloscope was obtained from a Solatron pulse generator type GO1005 when triggered externally by the output of the coincidence unit. Every-time an "Owen" pulse and a "linear" pulse arrived within the resolving time of the unit, the trace of the oscilloscope was brightened for about 0.2 μsec.

A 6 mC Po - Be source was placed centrally about 1 cm. from the NE 213 scintillation cell, and the resulting display on the screen of the oscilloscope photographed using Ilford recording film type 5G91 with an exposure time of about 30 mins. Photographs obtained with an anode bias of about 11 volts and with resolving times of 4, 2, 1 and 0.5 μsec. are shown in Figure 25.

When the resolving time is set at 4 μsec. two traces can be seen, the upper trace due to neutrons and the lower due to γ-rays. Most of the γ-ray trace could be eliminated by raising the discrimination threshold for the "Owen" pulses but, obviously, the low energy region of the neutron trace would also be eliminated. However, as the resolving time decreases the lower trace vanishes indicating that the brightening pulses are due to the detection of neutrons only. These results confirm the observations made by Batchelor et al. (1960)[46].

Figure 25(a)

T_R = 4 μsec.

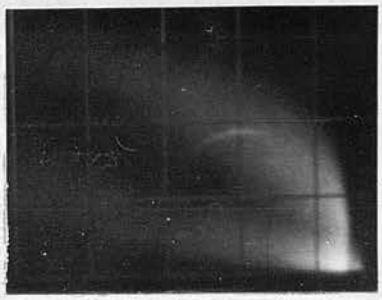

Figure 25(b)

T_R = 2 μsec.

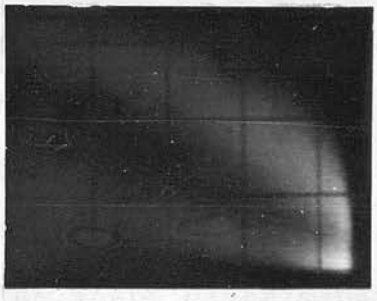

Figure 25(c)

T_R = 1 μsec.

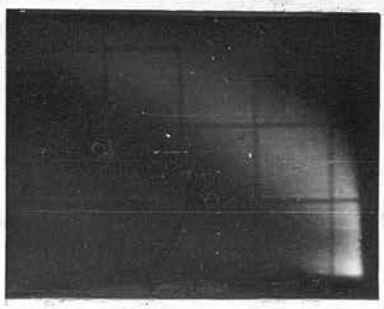

Figure 25(d)

T_R = 0.5 μsec.

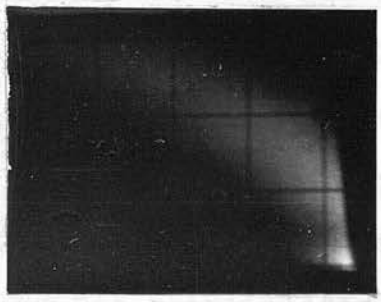

FIGURE 25 : Oscilloscope Photographs of Neutron Events (upper trace) and γ-ray events (lower trace), using a Po - Be source.

The coincidence resolving time, T_R decreases from 4 μsec. in Fig. 25(a) to 0.5 μsec. in Fig. 25(d) as indicated.

The $Be^9(d,n\gamma)B^{10}$ neutron spectrum with pulse shape discrimination

The pulse shape discrimination system was incorporated into the basic time-of-flight spectrometer previously described. A block diagram of the complete spectrometer is shown in Fig. 26. A typical $Be^9(d,n\gamma)B^{10}$ time-of-flight spectrum recorded in about 3 hours under similar conditions to that of Fig. 27(a) is shown in Fig. 27(b). A comparison of these spectra shows that the prompt coincidence γ-ray peak has been eliminated by the pulse shape discrimination system, and that the general level of the background has been reduced by 25%.

The $Be^9(d,n\gamma)B^{10}$ neutron spectrum with shielded neutron detector

The background in the spectrum obtained using pulse shape discrimination, Fig. 27(b), is still quite large and part of it must be due to accidental coincidences between γ-rays in the NaI(Tℓ) crystal and neutrons which have been scattered, mainly from the floor, walls and ceiling of the target room into the NE 213 scintillator. Therefore the neutron detector was placed inside a cylindrical paraffin wax shield $2\frac{1}{4}'$ long with 6" thick walls. (The shield can be seen in Fig. 28.) The 5" diameter NE 213 scintillator was placed about $1\frac{1}{2}'$ from the front face of the shield. A $Be^9(d,n\gamma)B^{10}$ neutron time-of-flight spectrum, Fig. 27(c), was recorded in about 3 hours under similar operating

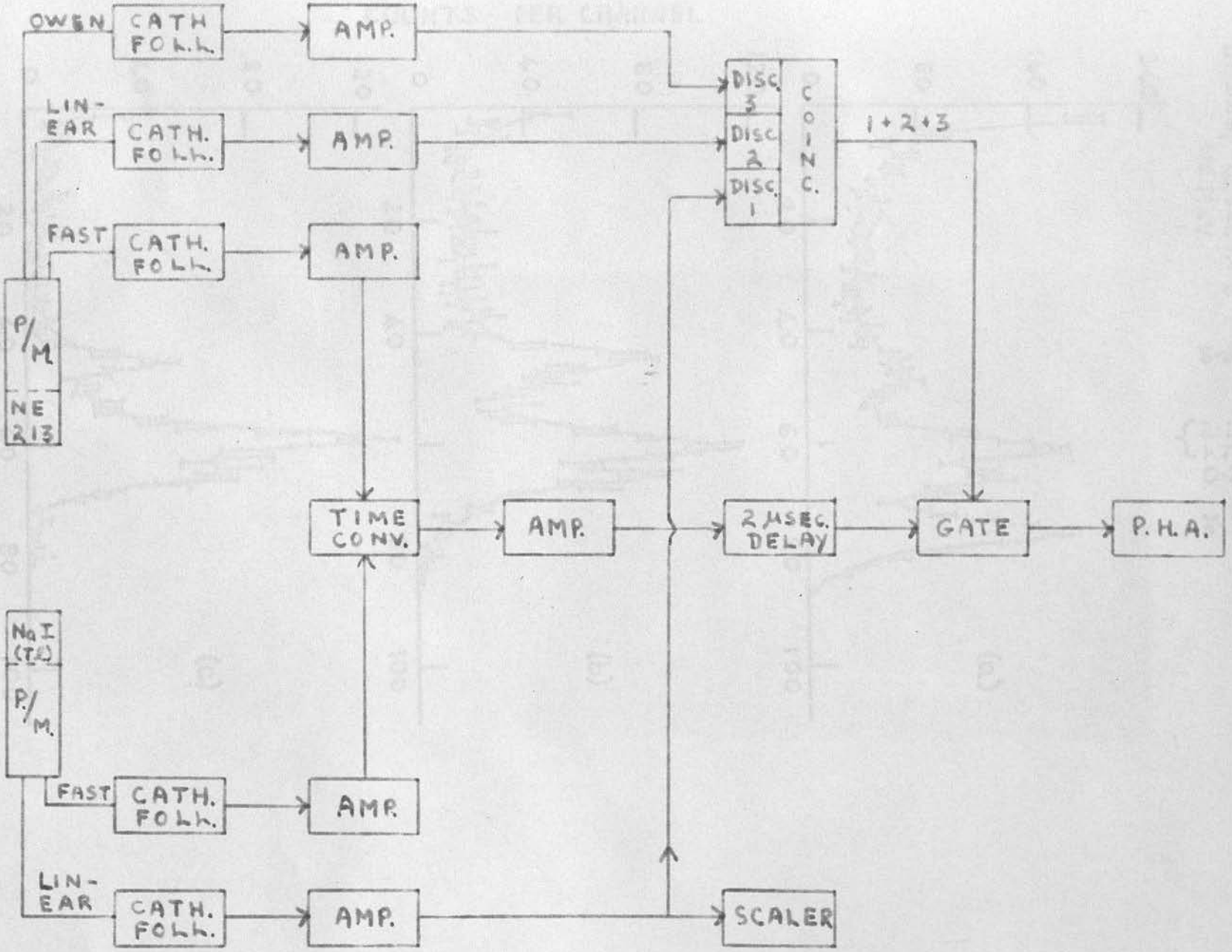

FIG 26 THE NEUTRON TIME-OF-FLIGHT SPECTROMETER.

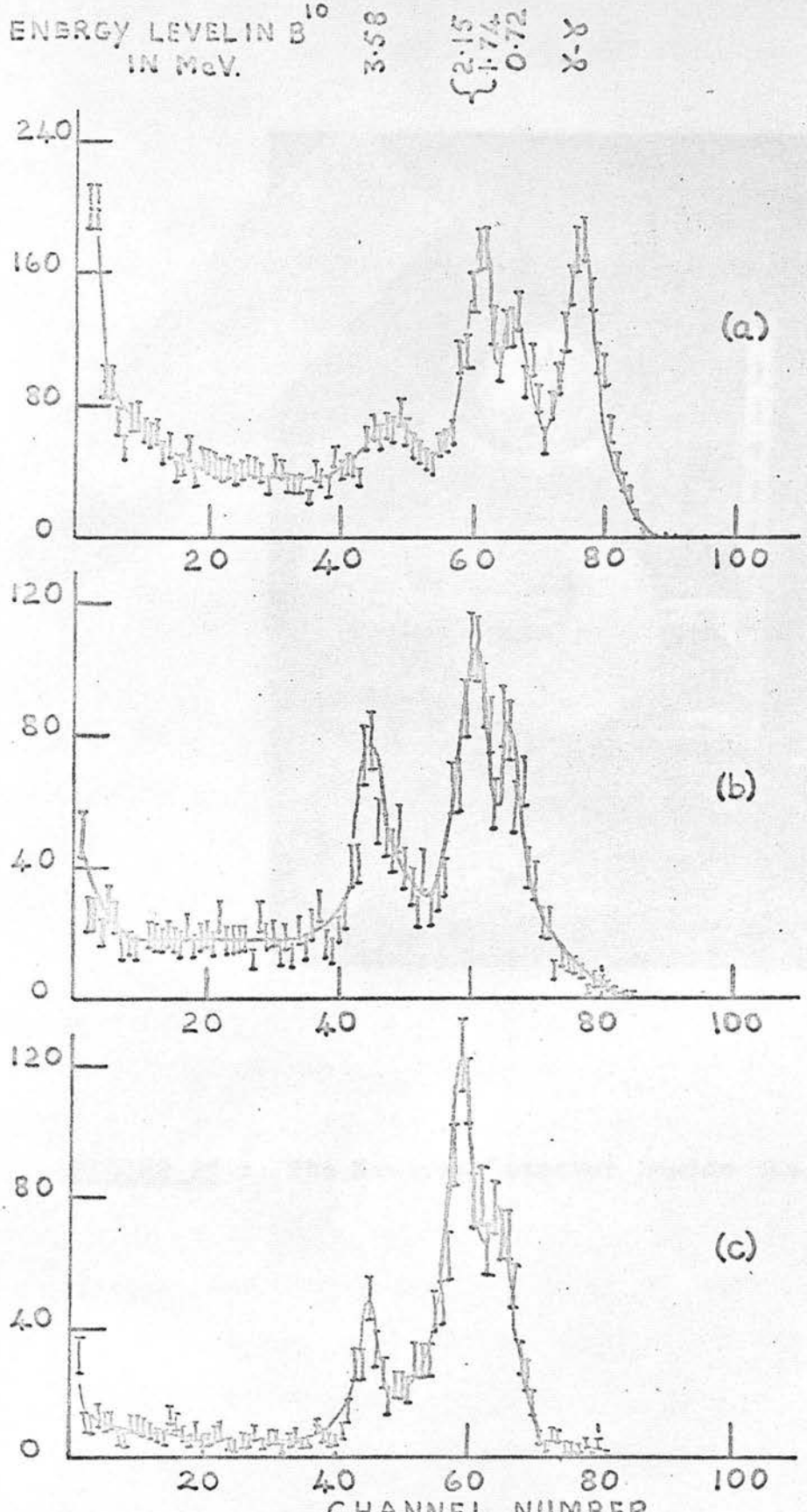

FIG. 27. $Be^9(d,n)B^{10}$ NEUTRON TIME-OF-FLIGHT SPECTRA,
(a) USING BASIC TIME-OF-FLIGHT SPECTROMETER,
(b) WITH PULSE SHAPE DISCRIMATION AGAINST γRAYS ADDED,
(c) AS IN (b) WITH WAX SHIELDING.

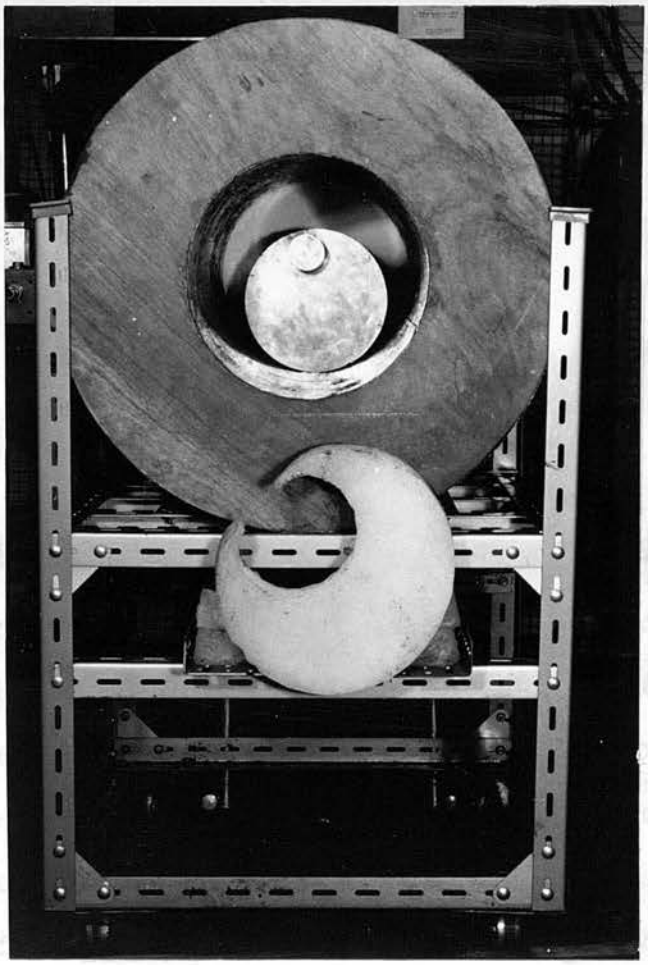

FIGURE 28 : The Neutron Detector inside the Wax Shield.

conditions to that of Fig. 27(b), but with the neutron detector inside the wax shield. The background was reduced by the wax shield to less than 50°/o of its previous level in Fig. 27(b).

The variation of the intensity of the "3.58 MeV" neutron group relative to the other groups in Figs. 27(a), (b) and (c) is attributed to slight changes in the threshold bias presented to the "linear" pulses in the neutron channel of the spectrometer.

3.4. The Energy Resolution in Time-of-flight Spectra

In neutron energy spectra obtained by time-of-flight measurements the energy resolution of a peak, ΔE (defined as the width of the peak at half its maximum height) is given by $\Delta E = \frac{2 \Delta T \, E^{3/2}}{72.3 \, D}$ MeV, where E is the energy of the neutron group in MeV, D is the length of the flight path in metres and ΔT is the time resolution of the spectrometer in nsec. There are two main ways of improving the energy resolution. The simpler way is by increasing the flight path, D, but this of course reduces the n-γ coincidence rate and hence increases the the time required to obtain spectra of a given statistical accuracy. The other, and better way of improving the energy resolution is by decreasing the instrumental time resolution of the spectrometer.

The improvement in energy resolution by increasing the flight path

The time-of-flight T of a neutron group increases with the length of the flight path according to the relationship $T = \frac{72.3D}{\sqrt{E}}$ nsec. If the energy resolution is improved by lengthening the flight path then the flight time of the slowest neutron group in a spectrum may exceed the time range of the time-to-pulse-height converter. This situation is illustrated in Fig. 29(a). The channel numbers of the prompt γ-ray coincidence peak and of the neutron groups may be deduced from the "channel number versus time interval" curve for the time-of-flight spectrometer as shown schematically in Fig. 29(a). (See Fig. 15). The slowest neutron group n_s is not observed because its flight-time is greater than the time range covered by the time-to-pulse-height converter. Usually the prompt γ-ray coincidence peak, γ is not observed due to the pulse shape discrimination against γ-rays in the neutron detector, and therefore about half of the time range covered by the time-to-pulse height converter is not used efficiently for displaying the neutron groups. All of the neutron groups in a spectrum can be displayed by delaying the timing pulses from the γ-ray detector to the time-to-pulse-height converter by T_γ nsec, provided the time interval between the slowest and fastest neutron groups is less than the time range of the converter.

If the flight-time of the slowest neutron group just

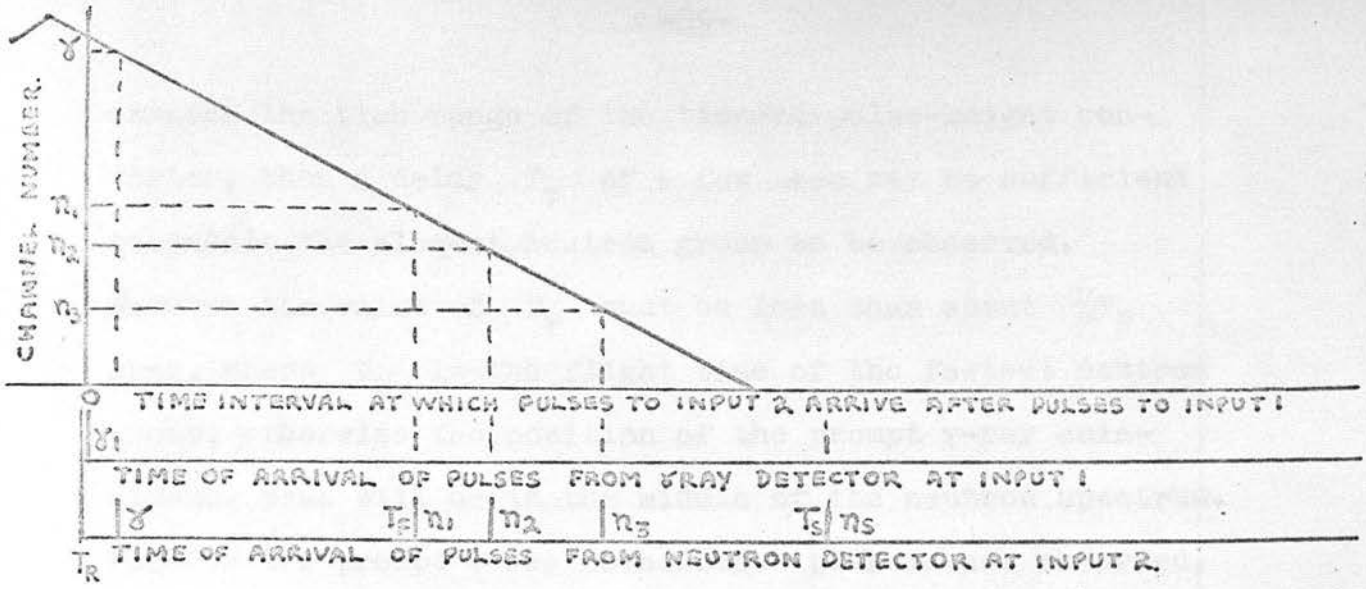

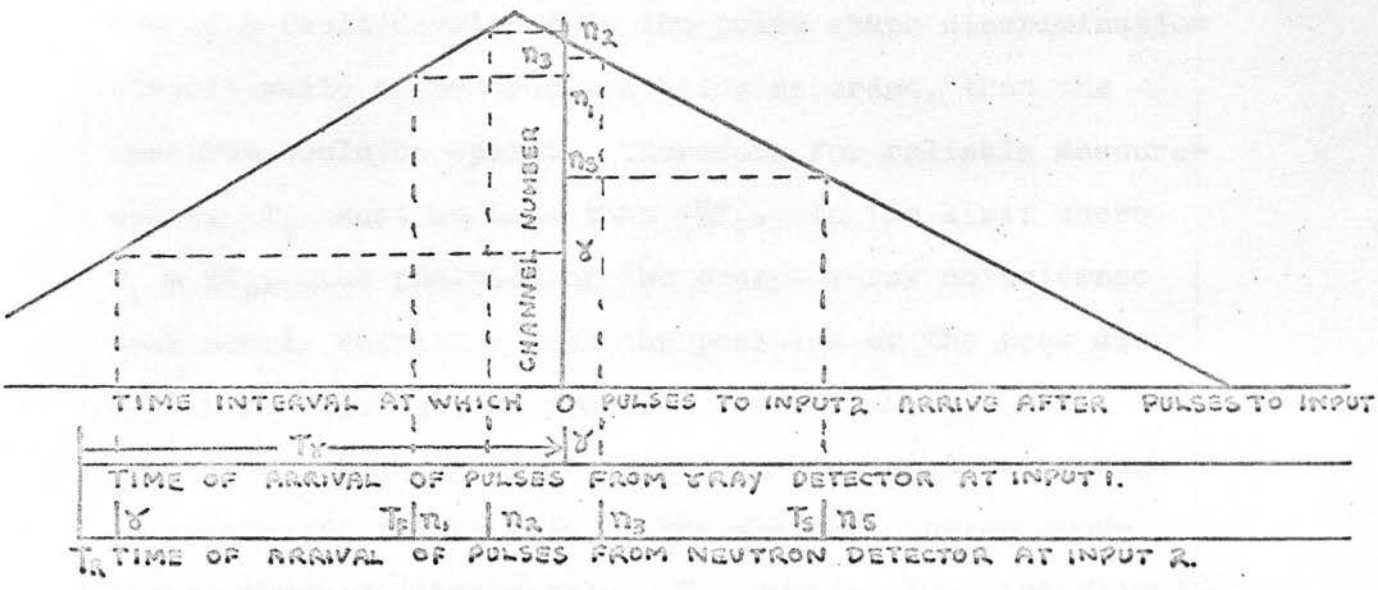

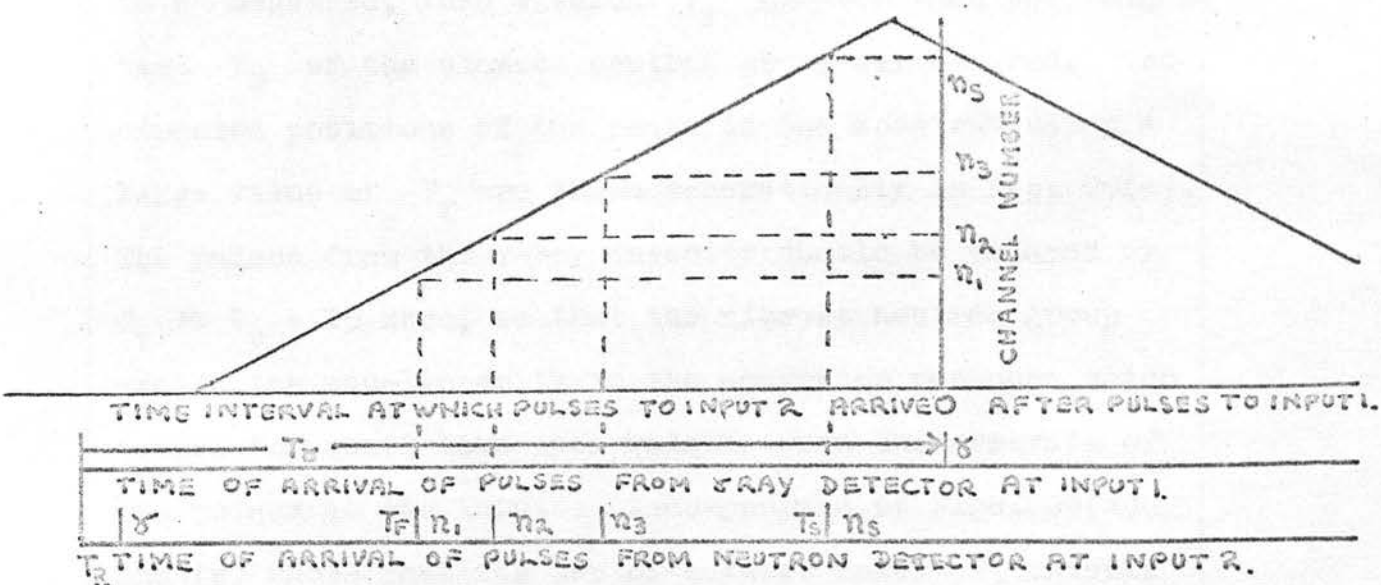

T_R = INSTANT AT WHICH NUCLEAR REACTION OCCURS.

FIG. 29. DIAGRAMS SHOWING THE EFFECT OF DELAYING THE γ RAY TIMING PULSE BY T_γ NSEC.

exceeds the time range of the time-to-pulse-height converter, then a delay T_γ of a few nsec may be sufficient to enable the slowest neutron group to be observed. However the value of T_γ must be less than about $\frac{1}{2}T_F$ nsec, where T_F is the flight time of the fastest neutron group, otherwise the position of the prompt γ-ray coincidence peak will be in the middle of the neutron spectrum. Usually the prompt γ-ray coincidence peak is not observed, but if a fault developed in the pulse shape discrimination circuit while a spectrum was being recorded, then the spectrum would be spoilt. Therefore for reliable measurements, T_γ must be less than $\frac{1}{2}T_F$. In the limit where $T_\gamma = \frac{1}{2}T_F$, the position of the prompt γ-ray coincidence peak nearly coincides with the position of the peak due to the fastest neutron group.

If a value T_γ less than $\frac{1}{2}T_F$ is not large enough to enable the flight time of the slowest neutron group to be measured, then a value T_γ greater than the flight time T_S of the slowest neutron group may be used. The expected positions of the peaks in the spectrum using a large value of T_γ are shown schematically in Fig. 29(c). The pulses from the γ-ray detector should be delayed by $T_\gamma \approx T_s + 15$ nsec, so that the slowest neutron group avoids the non-linearity in the converter response which occurs for short time intervals between the arrivals of the pulses at its inputs. A comparison of Figs. 29(a) and (c) shows that the use of a large delay T_γ inverts the order in which the neutron groups are displayed by the multichannel pulse height analyser.

If a delay with an intermediate value is used (i.e. $\frac{1}{2}T_F < T_\gamma < T_s$), the neutron groups are recorded in a mixed up order. The way in which this happens is deduced in Fig. 29(b). Thus the values of T_γ between $\frac{1}{2}T_F$ and T_s + 15 nsec. are unsuitable.

The use of a suitable delay T_γ enables the energy resolution to be improved by increasing the length of the flight path until the neutron groups in the spectrum are displayed without confusion over the whole range of the time-to-pulse-height converter. The improvement in energy resolution obtained by increasing the length of the flight path was investigated experimentally.

The neutron time-of-flight spectrometer was set up as shown in Fig. 26. The length of the flight path was 2.25 metres and therefore the flight times of the neutron groups associated with the formation of levels at 0.72, 1.74, 2.15, 2.86 and 3.58 MeV in B^{10} in the $Be^9(d,n)B^{10}$ reaction were 82, 94, 101, 117 and 145 nsec respectively. The timing pulses from the γ-ray detector were delayed by about 160 nsec, so that the timing pulses from the neutron detector arrived before the corresponding pulses from the γ-ray detector at the inputs to the time-to-pulse-height converter. A series of time-of-flight spectra of the $Be^9(d,n)B^{10}$ neutrons was recorded.

The $Be^9(d,n\gamma)B^{10}$ neutron time-of-flight spectrum shown in Fig. 30 is the sum of six separate spectra, each of which was recorded in 4 hours. A comparison of Figs.

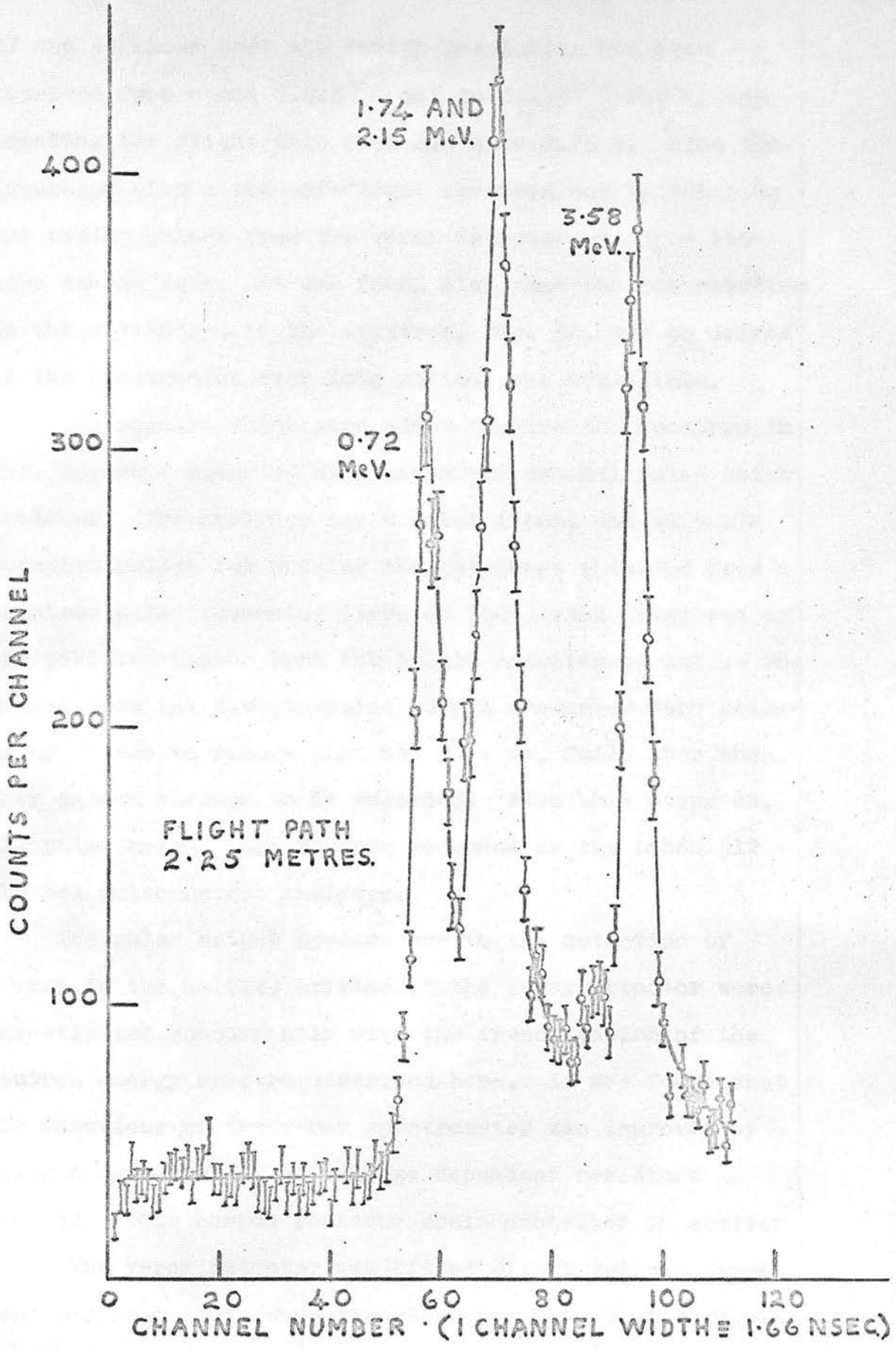

FIG 30. A SPECTRUM OF THE $Be^{9}(d,n\gamma)B^{10}$ NEUTRONS.

27 and 30 shows that the energy resolution has been improved from about $0.21E^{3/2}$ MeV to $0.12E^{3/2}$ MeV by increasing the flight path from 1.3 m to 2.25 m. Also the inversion of the time-of-flight spectrum due to delaying the timing pulses from the γ-ray detector by T_γ = 160 nsec can be seen. It was found also that the contribution to the resolution in the spectrum, Fig. 30, due to drifts in the electronics over long periods was negligible.

The spectra which were added to give the spectrum in Fig. 30, were recorded by a Laben 512 channel pulse height analyser. The analyser has a gated input, and suitable negative pulses for opening the gate were obtained from a Solatron pulse generator (type GO 1005) when triggered by the positive pulses from the triple coincidence unit. The pulses from the time-to-pulse height converter were delayed by 7 μsec to ensure that the gate was fully open when they passed through to be recorded. From this stage on, all pulse height spectra were recorded by the Laben 512 channel pulse height analyser.

The pulse height spectra due to the detection of γ-rays in the NaI(Tℓ) crystal of the γ-ray detector were investigated concurrently with the investigation of the neutron energy spectra described here. It was found that the behaviour of the γ-ray spectrometer was improved by using a dynode chain of voltage dependent resistors instead of the carbon resistor chain described in section 2.2. The γ-ray detector was fitted with a voltage dependent resistor chain when the above neutron time-of-flight

spectra were recorded. The new chain, which does not affect the timing properties of the γ-ray detector, is described in detail in Chapter 4.

The improvement in the energy resolution by improving the instrumental time resolution

The time resolution in the $Be^9(d,n\gamma)B^{10}$ neutron time-of-flight spectra which we have obtained so far is about 10 nsec. In order to improve the resolution it is necessary to consider the factors which cause the spoiling of resolution and to estimate, where possible, the magnitude of the spoiling.

The variation in deuteron energy: The variation in deuteron energy caused by the instability of the accelerating voltage of the H.T. set was observed to be $\pm$ 10 keV. A graph of the flight times per metre flight path for neutrons emitted in the $Be^9(d,n)B^{10}$ reaction at 60^o to the deuteron beam against the energy of the deuterons is shown in Fig. 31. From this graph we see that the time spread is about $\pm$ 0.3 nsec per metre. flight path for the 3.58 MeV neutron group and less than $\pm$ 0.1 nsec for the other groups produced by 600 keV deuterons.

The target thickness: The surface density of the Be^9 film used as the target was estimated to be less than 0.01 mg./cm^2. Using the data for the stopping power of Be^9 published by Kahn[47], the energy lost by 600 keV deuterons

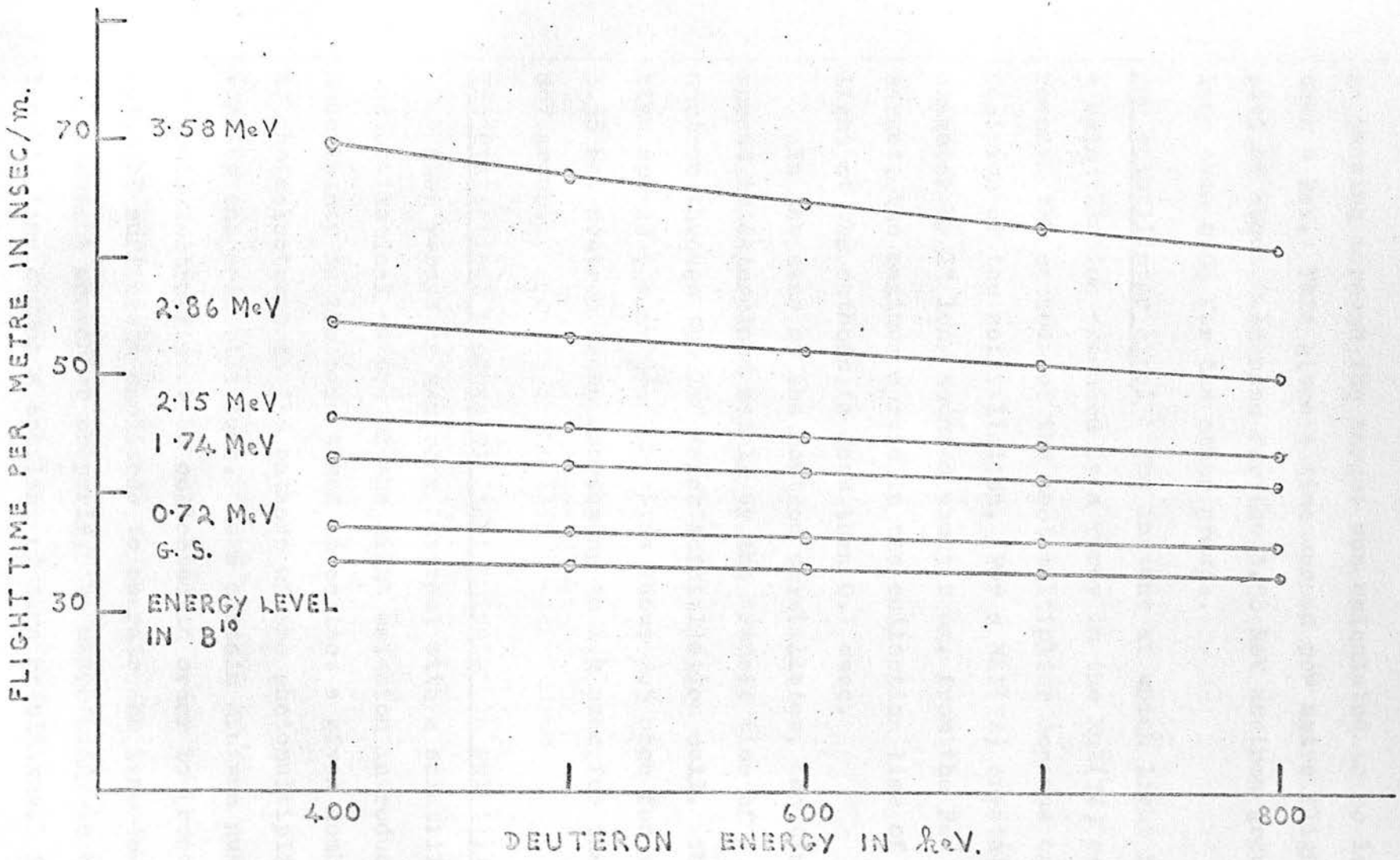

FIG. 31 THE VARIATION OF THE FLIGHT TIME PER METRE WITH DEUTERON ENERGY FOR THE NEUTRON GROUPS FROM THE $Be^9(d,n)B^{10}$ REACTION EMITTED AT 60° TO THE DEUTERON BEAM.

in passing through the target was calculated to be less than 5 keV. This gives a time spread per metre flight path of about 0.15 nsec for the 3.58 MeV neutron group and less than 0.05 for the other groups.

The scintillator size: The instant at which light from a scintillation produced by a γ-ray in the NaI(Tℓ) crystal reaches the cathode of the photomultiplier depends on the position of the scintillation. For a NaI(Tℓ) crystal $1\frac{1}{4}$" diameter by 1" long mounted about 2 cm. from the Be^9 target, the maximum spread in the collection time of the light at the cathode is less than 0.1 nsec.

In the case of the neutron scintillator, the time spread is determined mainly by the transit time of a neutron through the $1\frac{1}{2}$" thick scintillation cell. This time spread (= $\frac{2.7}{\sqrt{E}}$ nsec) is about 2.5 nsec for the 3.58 MeV neutron group decreasing to 1.4 nsec for the 0.72 MeV group.

The statistical process of light emission in scintillators:

When γ-rays or neutrons interact with a scintillator, the statistical nature of the light emission introduces an uncertainty in the time taken to collect a given number of photoelectrons at the cathode of the photomultiplier viewing the scintillations. As a certain minimum number of photoelectrons must be collected in order to produce a pulse of sufficient amplitude to operate the time-to-pulse-height converter properly, the uncertainty in collection time causes a spoiling of time resolution. When

a time-to-pulse-height converter which triggers properly on the first few photoelectrons is used a typical value for the time spread associated with γ-rays depositing energies above 100 keV in a NaI(Tℓ) crystal is about 4 nsec[48]. The corresponding time spread for neutrons depositing energies greater than 200 keV in an NE 213 liquid scintillation cell is about 0.6 nsec[48].

The response of the photomultipliers: The E.M.I. type 6262B photomultipliers used in the time-of-flight spectrometer are capable of giving pulses with minimum rise times of 7 or 8 nsec. The instant at which a pulse from the photomultiplier reaches the trigger level of the time-to-pulse-height converter may occur at any time up to the rise time of the pulse after the detection of the nuclear radiation depending on the amplitude of the pulse. Thus when all sizes of pulses are accepted by the time-to-pulse-height converter the time spread caused by the slow response of the photomultipliers may be as large as 8 ns for each tube. In practice the time spread will be less than this due to the energy selection carried out in the "linear" channels of the spectrometer.

The time-to-pulse-height converter and pulse height analysis equipment: The time spread due to the time-to-pulse height converter and the pulse height analysis equipment was found to be less than 0.5 nsec (Chapter 2). The spoiling of resolution due to long term instabilities in the electronics was found to be very small as mentioned above.

The main contribution to the total time resolution in the spectra obtained so far was attributed to the slow response of the 6262B photomultipliers. It was decided therefore to replace the 6262B tubes used in the γ-ray and neutron scintillation detectors by 56 AVP photomultipliers which can provide pulses with rise times of about 2 nsec.

The statistical process of light emission in the NaI(Tℓ) crystal gave rise to the next largest time spread, but as this type of scintillator was required for reliable energy measurements of the γ-rays, no improvement could be made. The possibility of reducing the time spread due to the thickness of the neutron scintillator by using a thinner one was considered, but as the detection efficiency of the neutron detector would be reduced, it was decided not to change the scintillator.

No attempts were made to reduce the small contributions to the total time resolution due to the other sources mentioned above as it was expected that the minimum time resolution would be determined mainly by the contributions from the NaI(Tℓ) crystal and the relatively thick neutron scintillator.

The improved time-of-flight spectrometer

A γ-ray scintillation detector, Fig. 39, consisting of a NaI(Tℓ) crystal 5" diam. by 4" long mounted on a 58 AVP photomultiplier tube was available in the laboratory and therefore it was decided to use this counter in the time-of-flight spectrometer. The time spread due to the size of the larger NaI(Tℓ) crystal is small, being

about 0.5 nsec when the crystal is 3 cm from the target. The 58 AVP photomultiplier was fitted with a voltage dependent resistor chain which was operated at 2.1 kV with a standing current of 1.7 mA. A more detailed description of the scintillation detector is given in Chapter 4. The use of a larger crystal has the advantage of improving the detection efficiency for the γ-rays by a large factor; the actual improvement depends on the energy of the γ-rays. The 6262B photomultiplier of the neutron detector was replaced by a 56 AVP tube with a dynode chain of voltage dependent resistors. The overall voltage applied to the chain was 2.3 kV, causing a standing current of 0.75 mA to flow through the chain. The circuit diagram of the dynode chain is shown in Fig. 32.

In the general view of the target area shown in Fig. 33, the detectors can be seen mounted beside the far target of the H.T. set. The γ-ray detector was placed about 3 cm from the Be^9 target at an angle of 90^o to the deuteron beam direction. The neutron detector, mounted inside a large wax shield, was placed about 3 m from the target with the flight path at 60^o to the deuteron beam. A time-of-flight spectrum was observed of those neutrons from the $Be^9(d,n\gamma)B^{10}$ reaction coincident with γ-rays detected above a 0.35 MeV threshold in the "linear" channel. The spectrum shown in Fig. 34 was obtained in a 57 hour period with a deuteron current of $\approx 0.1\mu A$. The time resolution of the neutron groups is 5.5 ± 0.5 nsec;

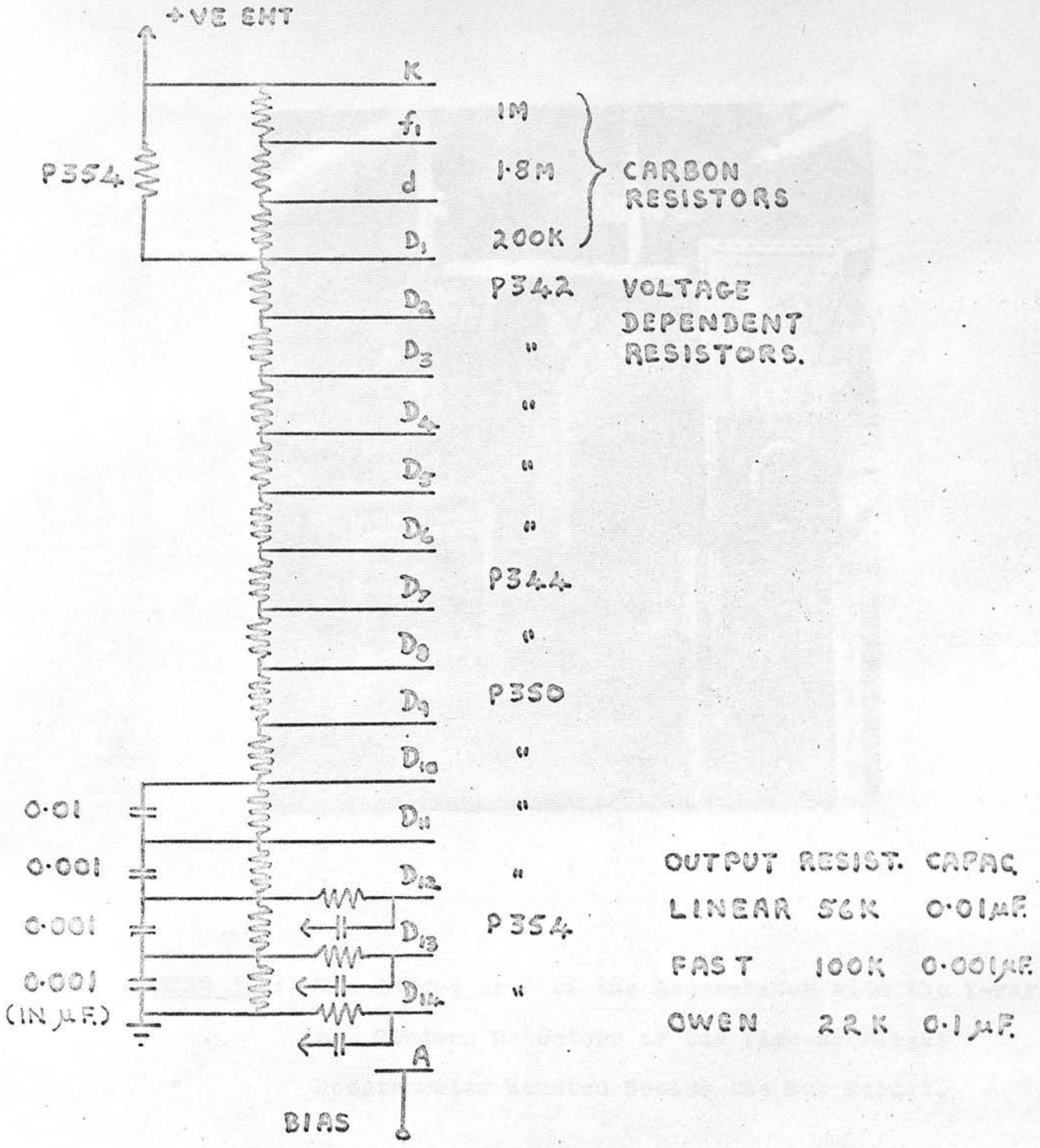

FIG. 32. CIRCUIT DIAGRAM OF DYNODE CHAIN FOR 56AVP PHOTOMULTIPLIER USED IN THE NEUTRON DETECTOR.

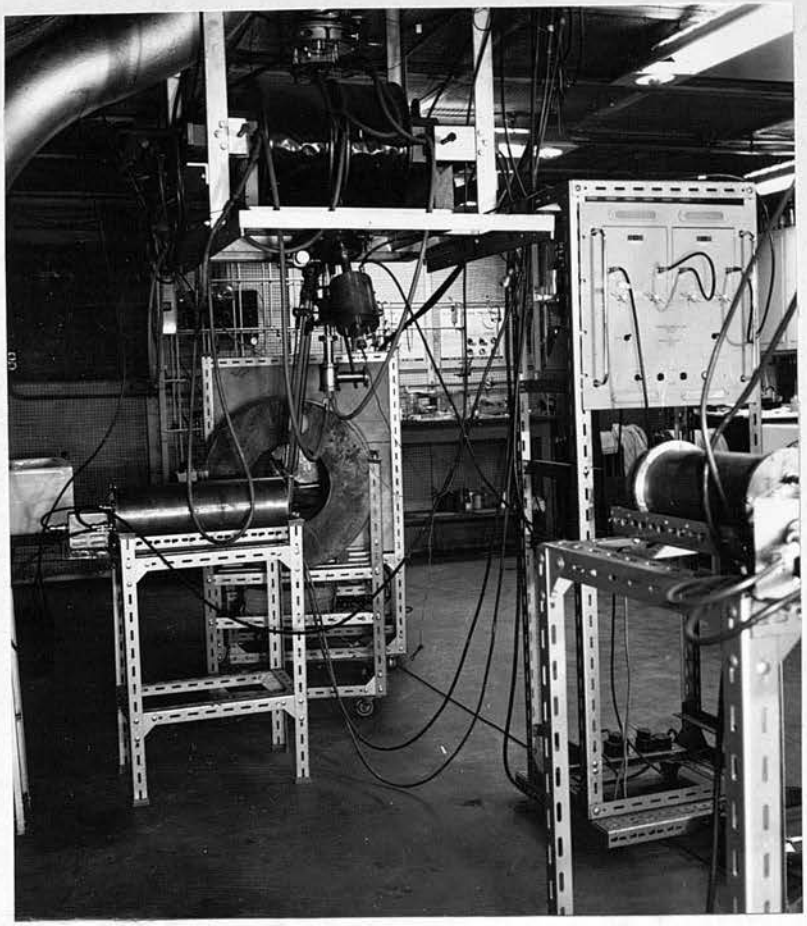

FIGURE 33 : The Target Area of the Accelerator with the γ-ray and Neutron Detectors of the Time-of-Flight Spectrometer Mounted Beside the Far Target.

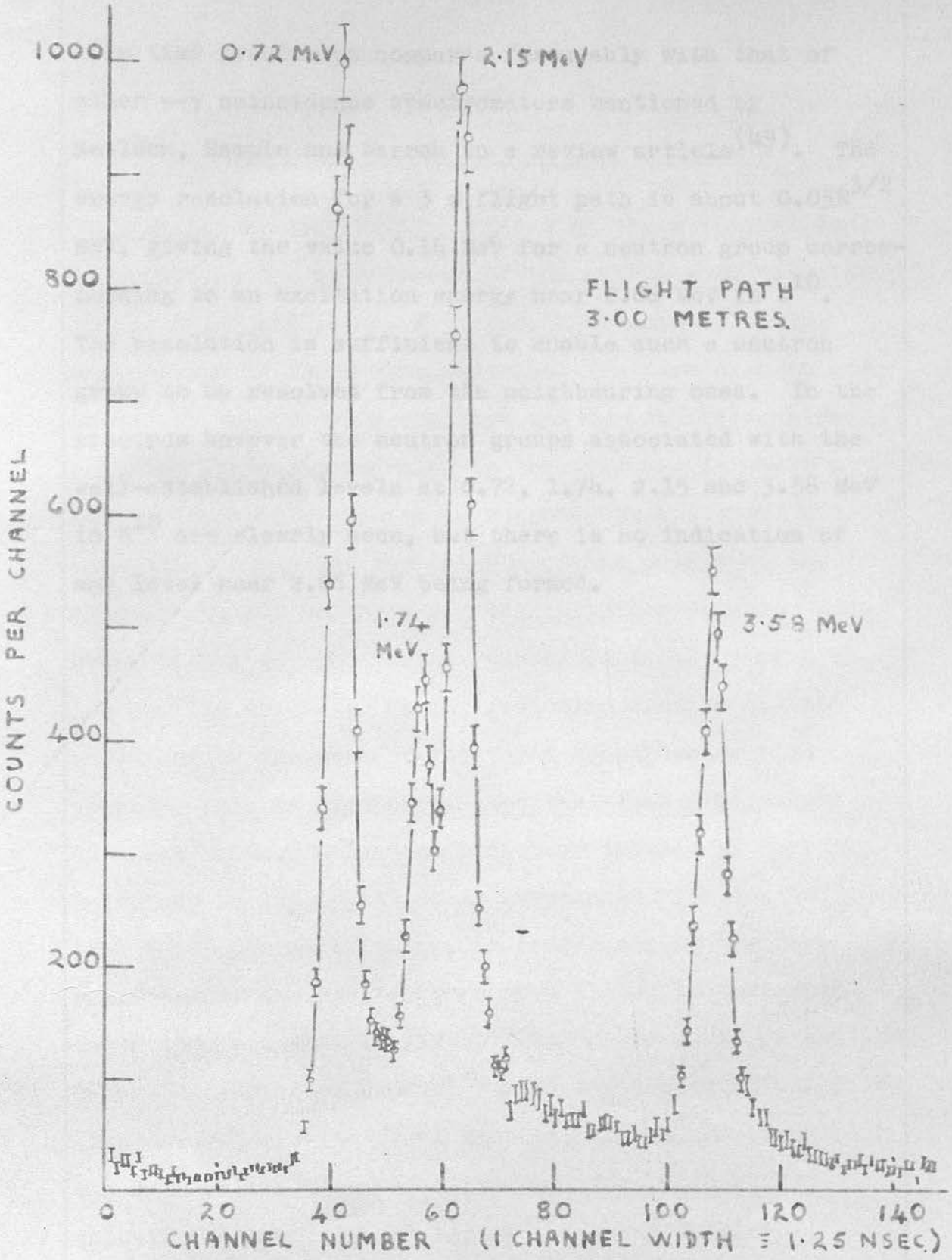

FIG.34 THE SPECTRUM OF THE $Be^{9}(d,n\gamma)B^{10}$ NEUTRONS. COINCIDENT WITH THE B^{10} γRAYS ABOVE 0·35 MeV.

this time resolution compares favourably with that of other n-γ coincidence spectrometers mentioned by Neilson, Sample and Warren in a review article[49]. The energy resolution for a 3 m flight path is about $0.05E^{3/2}$ MeV, giving the value 0.16 MeV for a neutron group corresponding to an excitation energy near 2.86 MeV in B^{10}. The resolution is sufficient to enable such a neutron group to be resolved from the neighbouring ones. In the spectrum however the neutron groups associated with the well-established levels at 0.72, 1.74, 2.15 and 3.58 MeV in B^{10} are clearly seen, but there is no indication of any level near 2.86 MeV being formed.

CHAPTER 4

THE γ-RAY SCINTILLATION SPECTROMETER

An important facility offered by the n-γ coincidence technique is the measurement of the energies of both the neutrons and the γ-rays detected in coincidence. The measurement of the neutron energies has already been discussed in the previous chapters and so now the measurements of the γ-ray energies is considered. In section 4.1 evidence is presented to support the statement made in section 2.2, that the heights of the pulses at the "linear" output of the γ-ray scintillation detector were proportional to the energies deposited by the γ-rays in the NaI(Tℓ) crystal. In the following section 4.2 the variation of the gain of the γ-ray spectrometer with counting rate is discussed. The variation was reduced by using voltage dependent resistors instead of carbon resistors in the dynode chain associated with the EMI type 6262B photomultiplier. A comparison of the performances of the spectrometer when fitted in turn with these dynode chains is given. The dynode chain of voltage dependent resistors used with a 58 AVP photomultiplier is also described. The final section, 4.3 is concerned with the reliability with which the position of an energy selection channel can be set in the γ-ray spectrum.

4.1. The Linearity of the γ-ray Spectrometer

The γ-ray scintillation detector described in section 2.2 was placed about 10 cm from the Be^9 target which was bombarded with 600 keV deuterons. The pulse height distribution at the 9^{th} dynode of the 6262B photomultiplier due to the detection of γ-rays was amplified and then recorded by the Laben 512 channel pulse height analyser. A typical pulse height spectrum is shown in Fig. 35. This spectrum is due to γ-rays with energies of 0.41, 0.72, 1.02, 1.43, 2.15, 2.86 and 3.58 MeV from the $Be^9(d,n)B^{10}$ reaction, and also 0.48 and 3.37 MeV from the competing reactions $Be^9(d,\alpha)Li^7$ and $Be^9(d,p)Be^{10}$ respectively.

The channel numbers of the more prominent peaks in the spectrum at energies of 0.72, 1.02, 1.43, 1.84, 2.35, 2.86 and 3.37 MeV were found, and a graph of these energies against the corresponding channel numbers was plotted, Fig. 35. The peaks at 2.35 and 1.84 MeV are due to the escape of one or two annihilation γ-rays respectively following pair production in the NaI(Tℓ) crystal by 2.86 MeV γ-rays. The photo-peaks of the 2.15 and 3.58 MeV γ-rays are not sufficiently prominent to be useful in this energy-channel number calibration. Also as there is a gradual build up of carbon on the target from diffusion pump oil, and therefore a varying intensity of annihilation γ-rays from the decay of N^{13} formed in the $C^{12}(d,n)N^{13}$ reaction, the peaks near 0.5 MeV have not

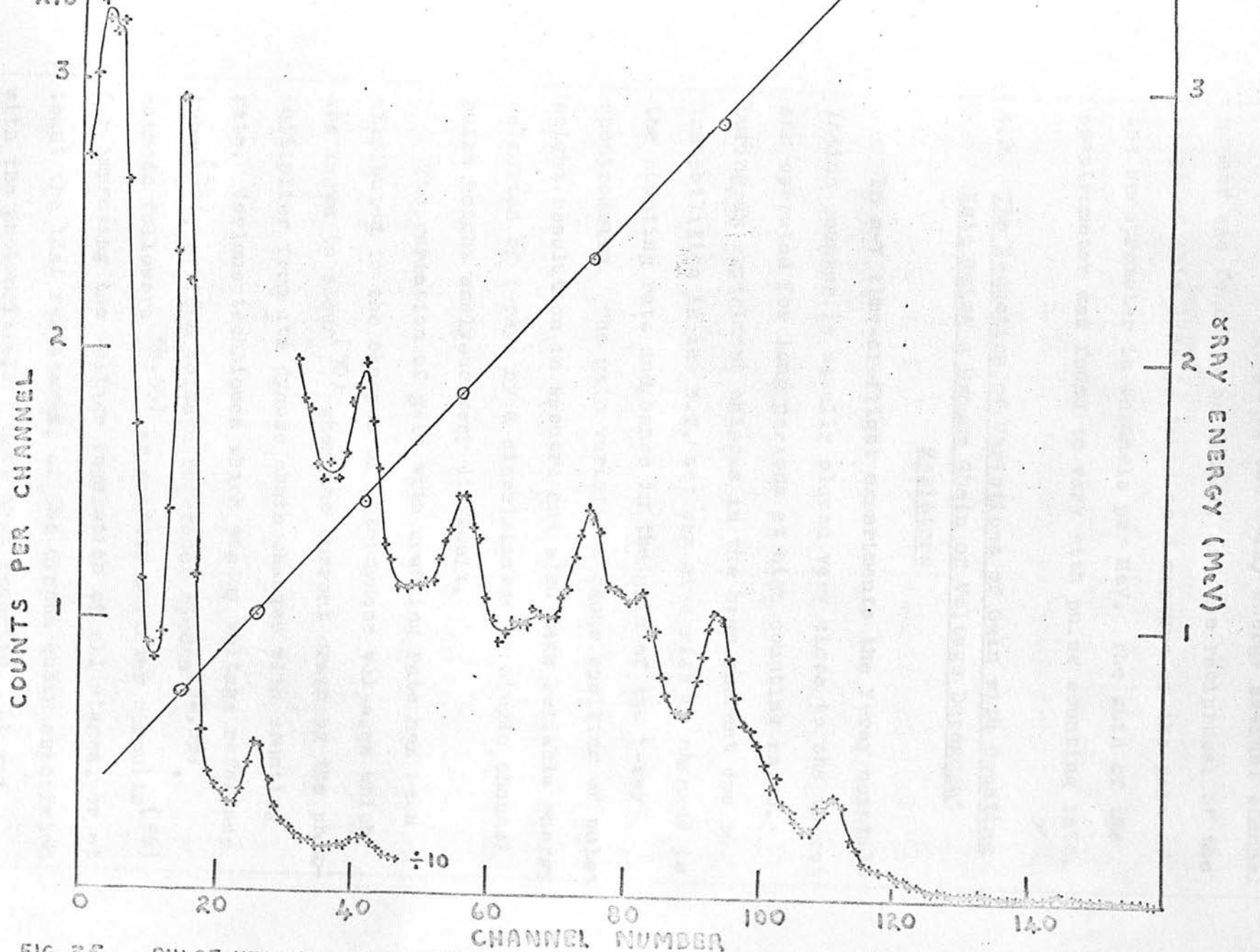

FIG. 35. PULSE HEIGHT SPECTRUM DUE TO γRAYS FROM THE $Be^9 + d$ REACTIONS DETECTED IN THE NaI(Tl) CRYSTAL 1¼" DIAM. BY 1" LONG.

been used. The graph of the γ-ray energy against channel number was found to be linear, and the reciprocal of the slope of this line is taken as a measure of the gain of the spectrometer in channels per MeV. The gain of the spectrometer was found to vary with pulse counting rate.

4.2. The Reduction of Variations of Gain with Counting Rate Using a Dynode Chain of Voltage Dependent Resistors

In n-γ time-of-flight experiments the γ-ray scintillation counter is usually placed very close to the target and operated for long periods at high counting rates. During an experiment changes in the beam current due to instabilities in the H.T. set can give rise to changes in the counting rate and hence in the gain of the γ-ray spectrometer. The gain variations cause spoiling of pulse height resolution in spectra and also make reliable energy selection of γ-rays by a discriminator or single channel pulse height analyser very difficult.

The variation of gain with counting rate has been attributed to the changes of interdynode voltages which are known to occur[50] when the current drawn by the photomultiplier from its dynode chain changes with counting rate. Various techniques which employ voltage reference tubes[51], silicon voltage reference diodes[52,53], cathode followers[54,55] or emitter follower circuits[56] for improving the voltage regulation of all stages, or at least the last few stages, of the dynode chain associated with the photomultiplier have been reported. It was

decided to investigate the use of voltage dependent resistors in dynode chains because such chains are simple, compact and cheap. A comparison of the behaviour of the γ-ray spectrometer fitted, first of all, with a carbon resistor chain and then with a chain of voltage dependent resistors was made by observing the γ-rays from the Be^9+d reactions at various counting rates.

The circuit diagram of the dynode chain associated with the 6262B photomultiplier is given in Fig. 4(a), but for convenience the values of the carbon resistors used are noted in Table 3. The interdynode voltages occurring when the overall voltage applied to the dynode chain is 1.5 kV have been calculated and are recorded in column 3. Voltage dependent resistors giving nominally the same interdynode voltages for the same standing current in the dynode chain were chosen to replace the carbon resistors. The nominal interdynode voltages and the Mullard type numbers of the voltage dependent resistors are recorded in columns 4 and 5 of the table. The overall voltage applied to each chain from an E.H.T. unit (IDL type 532/B) was 1.5 kV, giving a standing current of about 0.75 mA in each case.

The pulse height spectrum of the γ-rays from the Be^9+d reactions was recorded by the pulse height analyser which was set to count for a predetermined live time. The counting rate, which was varied by altering the deuteron beam current incident on the Be^9 target, was calculated by dividing the total number of pulses recorded in all channels by the live time. The counting rate determined in this way gives the number of pulses per second whose amplitudes exceed the 2 volt threshold bias of the analyser.

Position in dynode chain	Carbon resistor chain		Voltage dependent resistor chain	
	Resistor Value k Ω	Nominal inter-dynode voltage	Nominal inter-dynode voltage	Mullard type number
				E299DD/
$K - D_1$	180	110	108	/P344
$D - D_2$	75	45	50	/P336
$D_2^1 - D_3$	75	45	50	/P336
$D_3 - D_4$	75	45	50	/P336
$D_4 - D_5$	75	45	50	/P336
$D_5 - D_6$	75	45	50	/P336
$D_6 - D_7$	150	90	90	/P342
$D_7 - D_8$	150	90	90	/P342
$D_8 - D_9$	180	110	108	/P344
$D_9 - D_{10}$	75	45	50	/P336
$D_{10} - D_{11}$	270	165	161	/P348
$D_{11} - D_{12}$	270	165	161	/P348
$D_{12} - D_{13}$	270	165	161	/P348
$D_{13} - D_{14}$	270	165	161	/P348
$D_{14} - A$	270	165	161	/P348

TABLE 3. Comparison of the dynode chains used with the EMI type 6262B photomultiplier. Both dynode chains operate at 1.5 kV with a standing current of 0.75 mA.

Pulse height spectra were recorded at a number of counting rates between 600 and 17,000 counts per second using the dynode chain of carbon resistors. The pulse height spectra of those γ-rays which deposited energies in excess of 1.2 MeV in the NaI(Tℓ) crystal are shown in Fig. 36 for the counting rates indicated. Immediately after these spectra were recorded the dynode chain was replaced by the voltage dependent resistor one and a similar series of spectra was recorded with counting rates between 600 and 44,000 counts per second, Fig. 37. By comparing Figs 36 and 37, it can be seen that the variation of gain with counting rate was considerably smaller with the dynode chain of voltage dependent resistors than with the carbon resistor chain.

A quantitative comparison of the variations in gain with counting rate was made by determining the gain, in channels per MeV, from the "γ-ray energy versus channel number" calibration lines of the spectra. Since both series of spectra begin with a counting rate of 600 counts per second, the percentage change in gain is defined as $\frac{100(G_n - G_{600})}{G_{600}}$ where G_n is the gain in channels per MeV at a counting rate of n counts per second. The graph of the percentage gain change versus counting rate, Fig. 38, indicates that the range of counting rates over which the percentage gain change remains within chosen limits is increased by a factor of 5 using voltage dependent resistors instead of carbon resistors in the dynode chain.

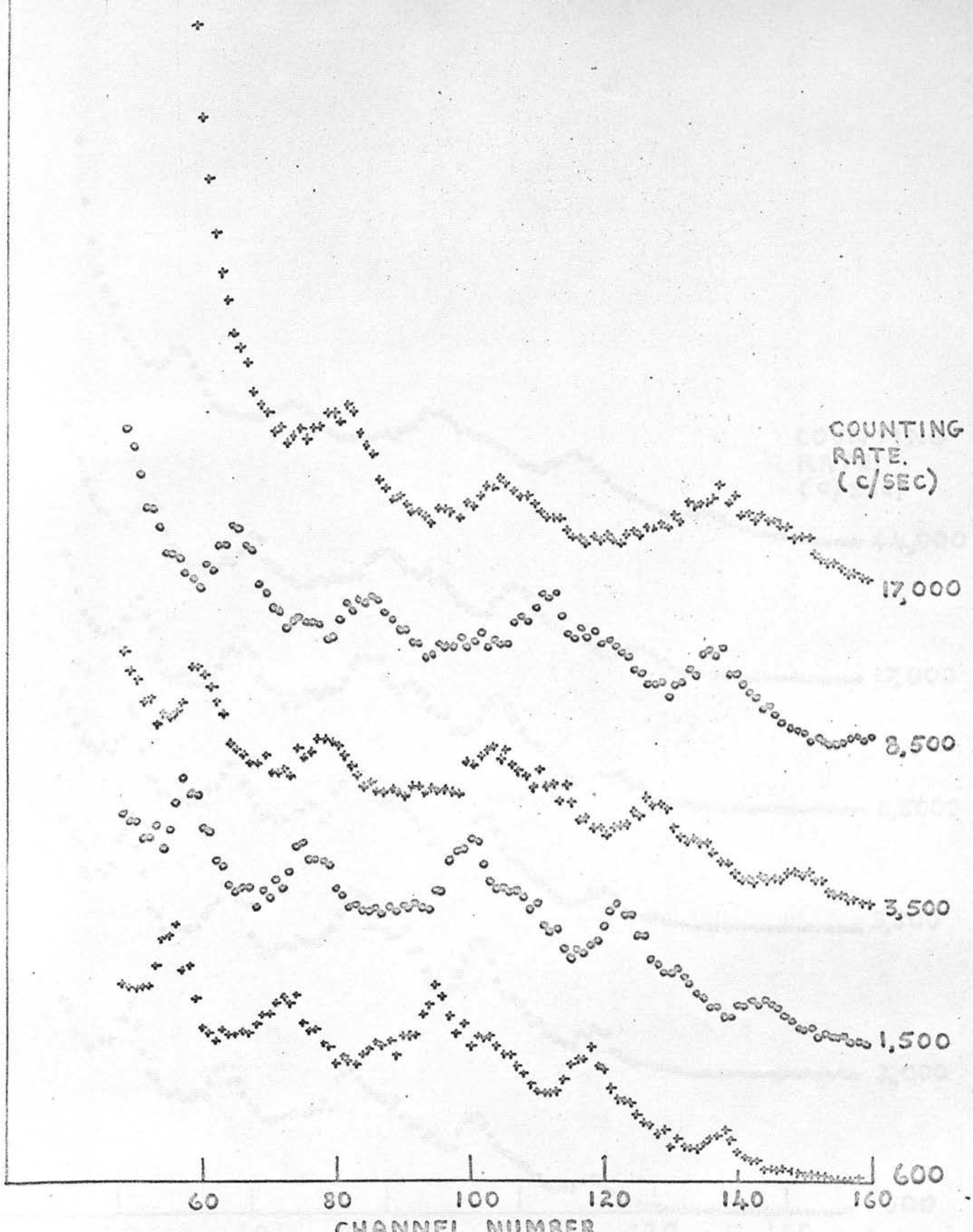

FIG. 36. SERIES OF PULSE HEIGHT SPECTRA DUE TO γ RAYS FROM THE $Be^9 + d$ REACTIONS DETECTED IN A NaI(Tℓ) CRYSTAL 1¼" DIAM. BY 1" LONG AT VARIOUS COUNTING RATES. A DYNODE CHAIN OF CARBON RESISTORS WAS USED WITH THE 6262B PHOTOMULTIPLIER.

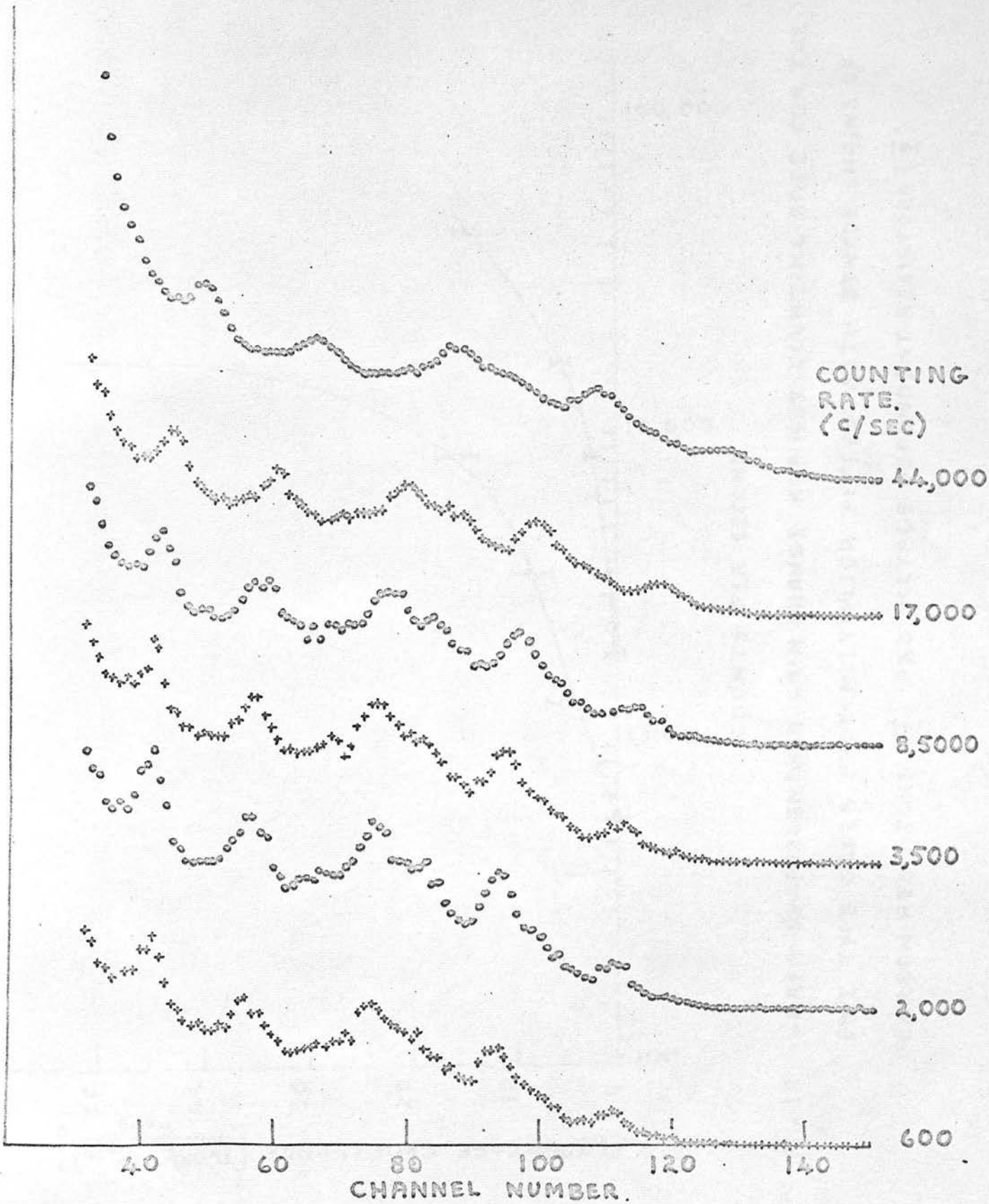

G.37. SERIES OF PULSE HEIGHT SPECTRA SIMILAR TO THOSE OF FIG.36. A DYNODE CHAIN OF VOLTAGE DEPENDENT RESISTORS WAS USED WITH THE 6262B PHOTOMULTIPLIER.

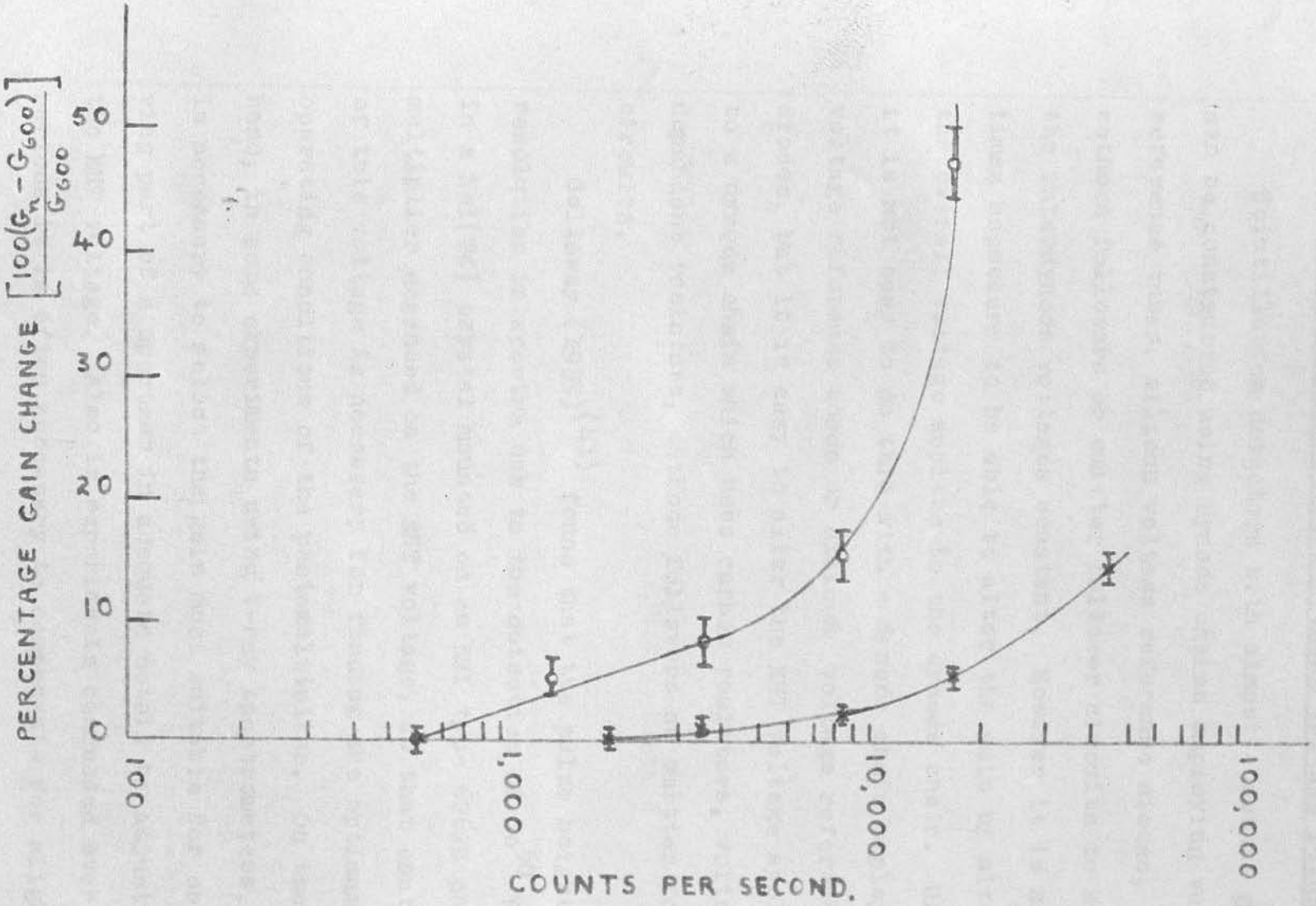

FIG. 38. GRAPH OF PERCENTAGE GAIN CHANGE AGAINST COUNTING RATE FOR THE EMI TYPE 6262B PHOTOMULTIPLIER FITTED WITH DYNODE CHAINS OF CARBON RESISTORS (I) AND VOLTAGE DEPENDENT RESISTORS (I).

Discussion on dynode chains employing voltage regulation

Scintillation detectors with almost constant gains can be constructed using dynode chains employing voltage reference tubes, silicon voltage reference diodes, cathode followers or emitter follower circuits to keep the interdynode voltages constant. However it is sometimes necessary to be able to alter the gain by altering the overall voltage applied to the dynode chain. Usually it is not easy to do this with a dynode chain employing voltage reference tubes or silicon voltage reference diodes, but it is easy to alter the EHT voltage applied to a dynode chain which uses carbon resistors, voltage dependent resistors, cathode followers or emitter follower circuits.

Galloway (1959)[41] found that the pulse height resolution in spectra due to the detection of Co^{60} γ-rays in a NaI(Tℓ) crystal mounted on an EMI type 6262B photomultiplier depended on the EHT voltage, so that control of this voltage is necessary for finding the optimum operating conditions of the photomultiplier. On the other hand, in some experiments using γ-ray spectrometers, it is necessary to select the gain most suitable for observing part of a spectrum in adequate detail by adjusting the EHT voltage. Also in experiments conducted over long periods it is often necessary to compensate for slight changes in the gain of the complete spectrometer by

adjusting the overall voltage applied to the dynode chain.

In those cases where it is necessary to control the EHT voltage, the simplest type of dynode chain providing a useful degree of voltage regulation is one employing voltage dependent resistors. Such a chain is compact, cheap and easily constructed, and the voltage regulation provided may be adequate for many purposes. However, if a very high degree of voltage regulation is required, then it is necessary to use a much more elaborate dynode chain which employs cathode followers or emitter follower type circuits to regulate the interdynode voltages.

A dynode chain of voltage dependent resistors for use with a 58 AVP photomultiplier.

A γ-ray scintillation detector consisting of a NaI(Tℓ) crystal 5" diam. by 4" long coupled directly to the photocathode of a 58 AVP photomultiplier was fitted with a dynode chain of voltage dependent resistors. The photograph of Fig. 39 shows the method of mounting the crystal, photomultiplier and dynode chain inside a cylindrical light-tight container. Details of the dynode chain are given in the circuit diagram, Fig. 40. As a suitable voltage dependent resistor could not be obtained for the position in the dynode chain between the deflection electrode d and the first dynode D_1, a carbon resistor was used. The dynode chain operates at an EHT of 2.1 kV with a standing current of 1.7 mA. A linear output for

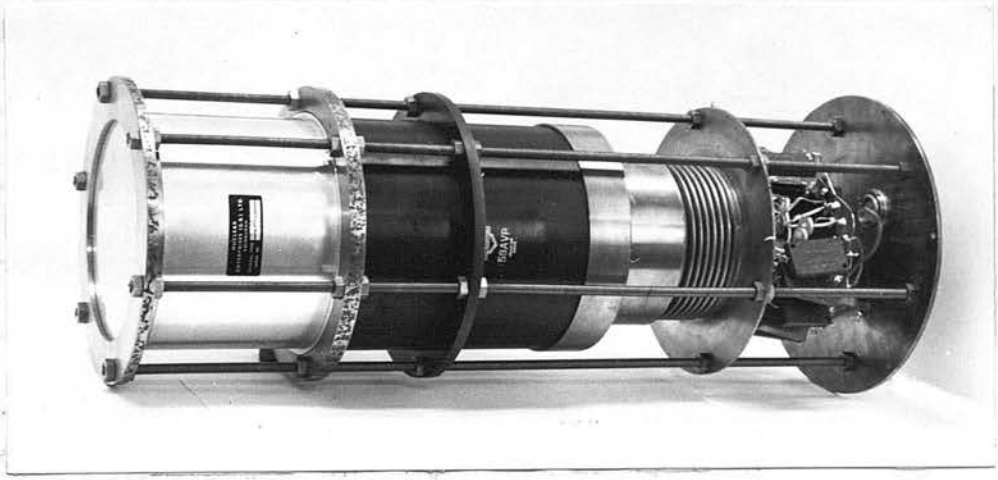

FIGURE 39 : The γ-ray Scintillation Detector Showing the NaI(Tℓ) Crystal 5" Diam. by 4" Long Coupled to the 58 AVP Photomultiplier.

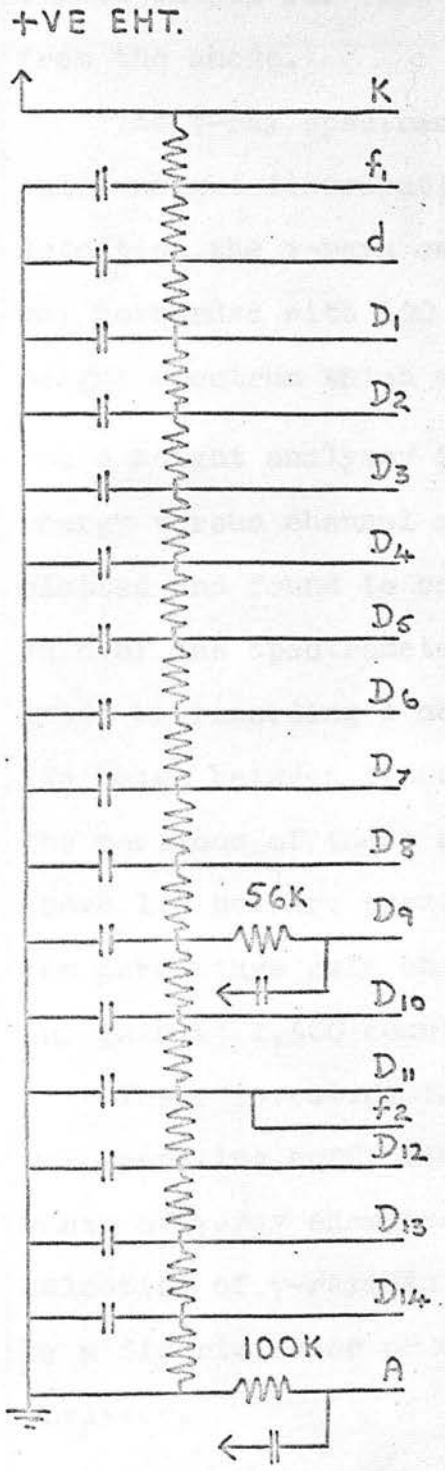

VOLTAGE DEPENDENT RESISTORS SERIES E299DD.
P350
P354
P336

15K CARBON RESISTOR
P344

"
"
"
"
"
"
"
"
"
"
"
"

ALL CAPACITORS ARE 0·01 μF.

FIG.40. CIRCUIT DIAGRAM OF DYNODE CHAIN FOR 58AVP PHOTOMULTIPLIER.

γ-ray spectrometry was provided at the 9^{th} dynode and a fast output for time-of-flight measurements was taken from the anode.

The γ-ray spectrometer was set up to observe the pulse height distribution at the 9^{th} dynode due to the detection the γ-rays emitted from the Be^9 target when it was bombarded with 600 keV deuterons. A typical pulse height spectrum which was recorded by the multichannel pulse height analyser is shown in Fig. 41. A "γ-ray energy versus channel number" calibration curve was plotted and found to be linear. The variation of the gain of the spectrometer with counting rate was investigated by recording a series of spectra at various counting rates between 1,300 and 50,000 counts per second. The portions of these spectra due to γ-rays with energies above 1.3 MeV are presented in Fig. 42 and a graph of the percentage gain change against counting rate based on the gain at 1,300 counts per second is plotted in Fig. 43.

These investigations show that the γ-ray spectrometer was operating sufficiently well to enable reliable measurements of γ-ray energies to be made and also reliable selection of γ-rays in a chosen energy range to be made by a discriminator or a single channel pulse height analyser.

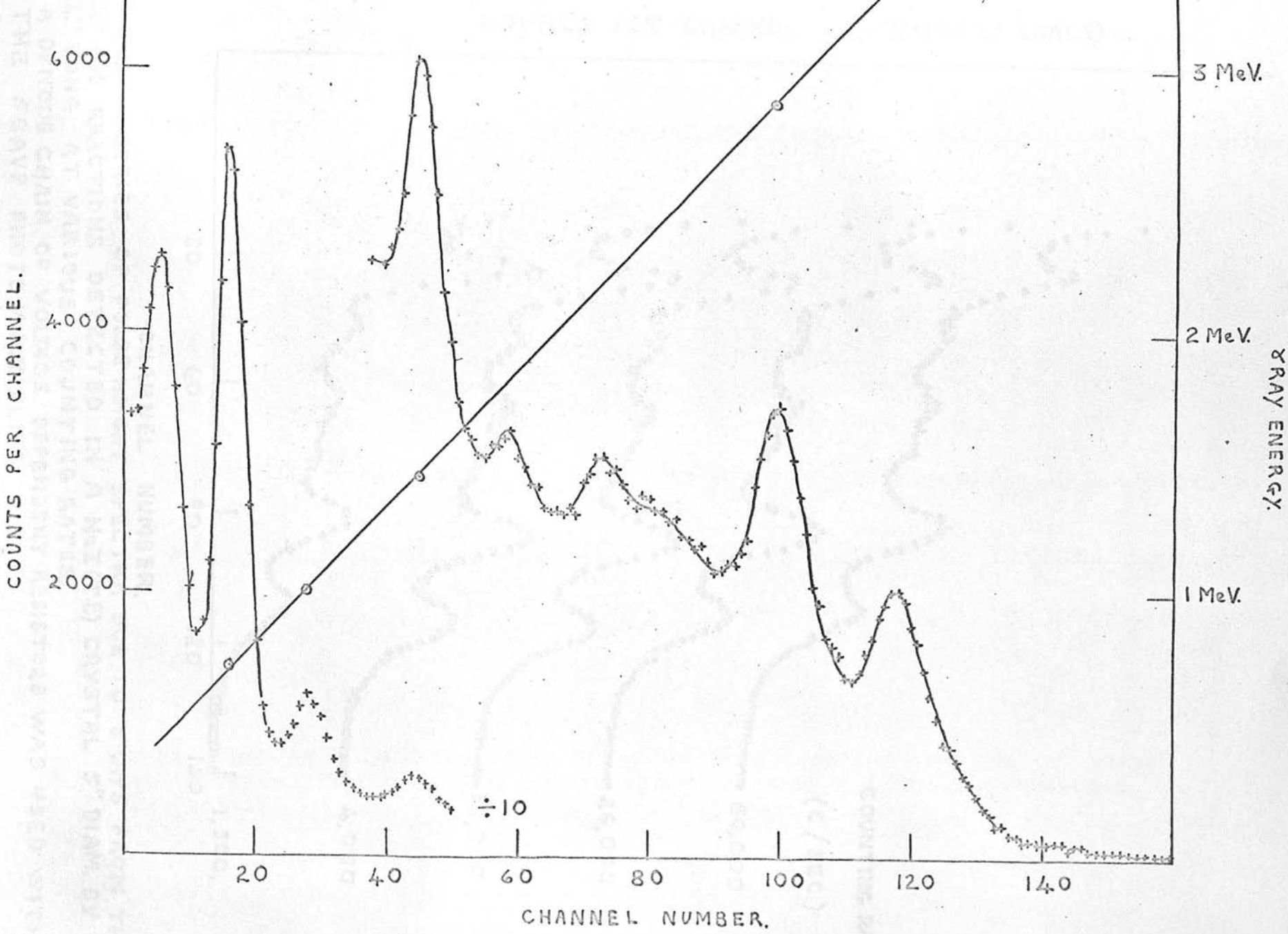

FIG. 41 PULSE HEIGHT SPECTRUM DUE TO γRAYS FROM THE $Be^{9}+d$ REACTIONS DETECTED IN THE NaI(Tℓ) CRYSTAL 5 IN. DIAM. BY 4 IN. LONG.

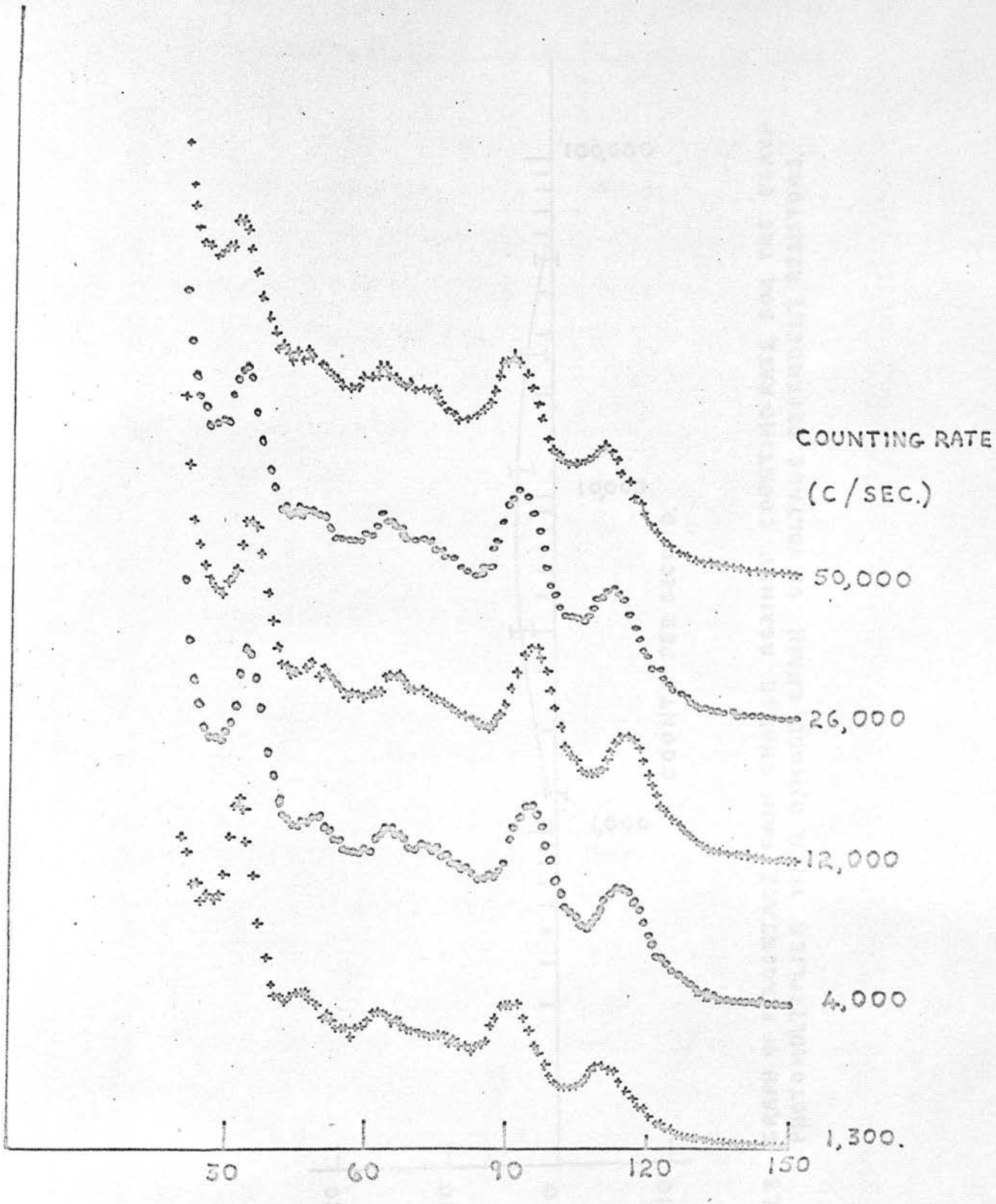

FIG. 42 SERIES OF PULSE HEIGHT SPECTRA DUE TO γRAYS FROM THE $Be^9 + d$ REACTIONS DETECTED IN A NaI(Tℓ) CRYSTAL 5" DIAM. BY 4" LONG AT VARIOUS COUNTING RATES.
A DYNODE CHAIN OF VOLTAGE DEPENDENT RESISTORS WAS USED WITH THE 58AVP PHOTOMULTIPLIER.

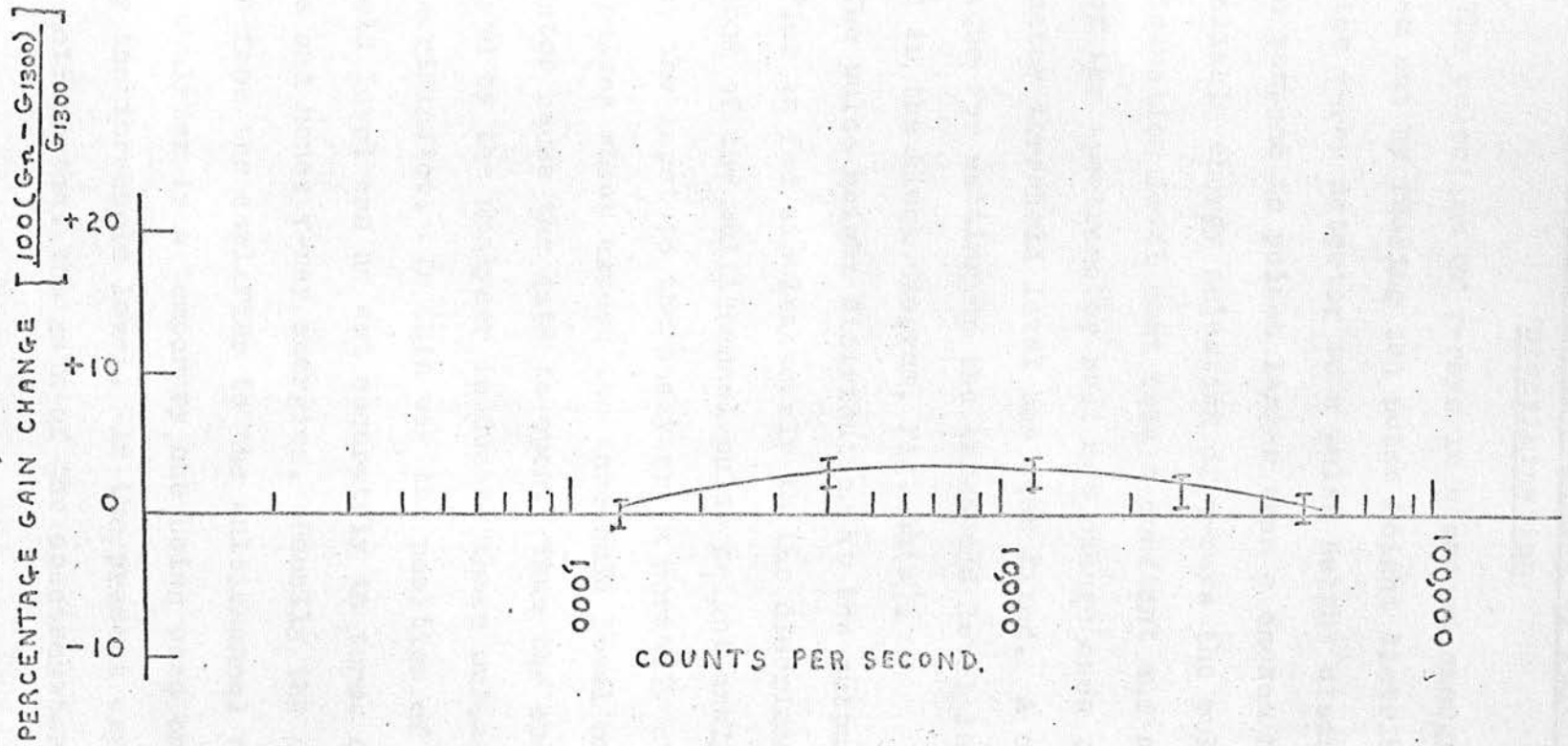

FIG. 43 GRAPH OF PERCENTAGE GAIN CHANGE AGAINST COUNTING RATE FOR THE 58AVP PHOTOMULTIPLIER WITH DYNODE CHAIN OF VOLTAGE DEPENDENT RESISTORS.

4.3. The Selection of γ-ray Energies by Pulse Height Discrimination

The selection of γ-rays in a chosen energy range is carried out by feeding the pulse height distribution from the γ-ray detector to a pulse height discriminator set to respond to pulses larger than a chosen height. For reliable energy selection of γ-rays the pulse height discrimination level must remain constant and also the gain of the spectrometer must not change once the discriminator threshold level has been fixed. A common technique for setting up the threshold level is illustrated in the block diagram, Fig. 44(a).

The pulse height distribution at the output of the amplifier is fed simultaneously to the discriminator and the input of the multichannel pulse height analyser. The gate at the input to the analyser is normally closed, but those pulses which exceed the threshold level of the discriminator cause the gate to open. Thus the spectrum displayed by the analyser is due to those pulses passed by the discriminator. In this way the position of the threshold level can be set accurately in terms of pulse heights and hence γ-ray energies. Usually the direct connection from the amplifier to the multichannel pulse height analyser is a temporary one being used only for setting the threshold level. In the present experiment it was noticed that the gain of the spectrometer changed

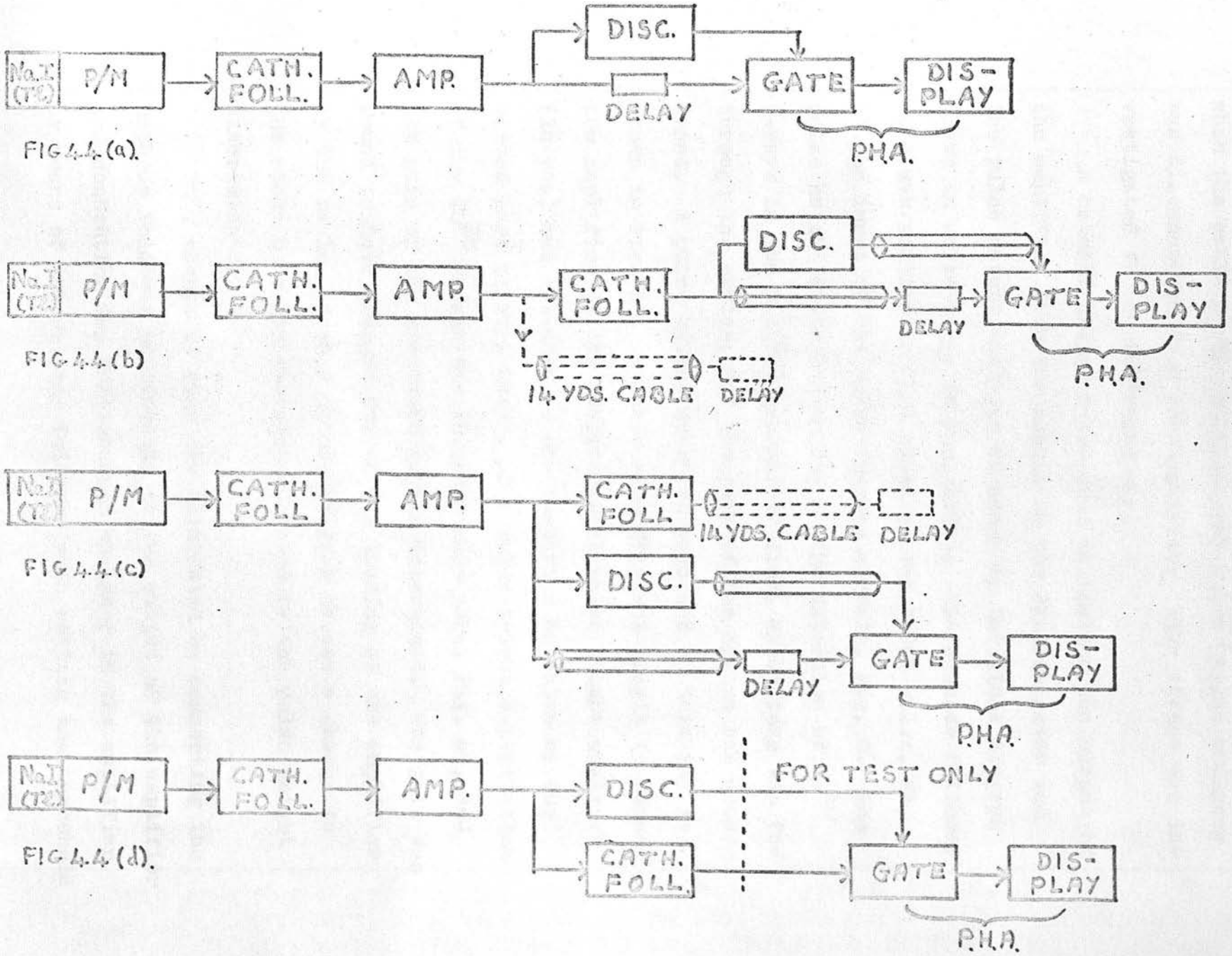

FIG. 4.4 ARRANGEMENTS USED FOR INVESTIGATING THE SETTING OF A GATING CHANNEL

when the cable to the multichannel pulse height analyser was disconnected from the amplifier. This effect was investigated in the following way.

A cathode follower was used to isolate the output of the amplifier from the inputs of the discriminator and the pulse height analyser as shown by the block diagram drawn in solid lines in Fig. 44(b). The cathode follower used was similar to that based on the E88CC valve, V1, at the input of the pulse shaping circuit, Fig. 6. The pulse height distribution due to the detection of Co^{60} γ-rays in the NaI(Tℓ) crystal 5" diam. by 4" long was fed through the system, and the gain of the system was determined. A pulse height spectrum recorded in this way is shown in Fig. 45. A cable of sufficient length to connect the amplifier to the multichannel pulse height analyser (14 yds) was attached to the amplifier as shown by the dotted part of Fig. 44(b). The pulse height distribution of the CO^{60} γ-rays was recorded once more, Fig. 45, and the gain of the spectrometer was determined. The gain was found to have changed due to the loading of the amplifier by the cable. Such a change of gain causes a change in the range of γ-ray energies selected by the pulse height discriminator.

This change of gain was eliminated by connecting the cathode follower permanently to the output of the amplifier and connecting the multichannel analyser to the amplifier by means of the cathode follower when setting the threshold

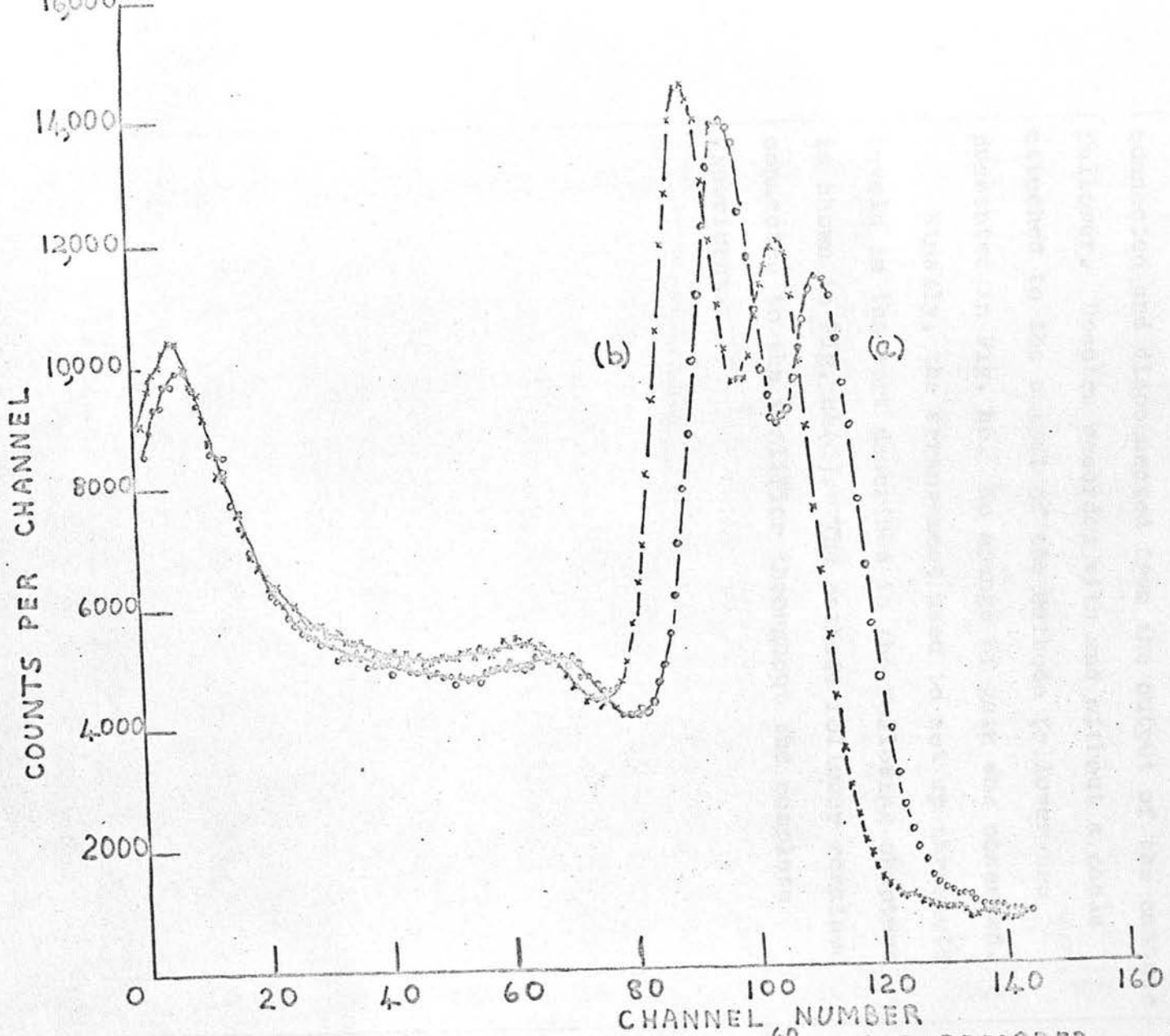

FIG. 45 THE PULSE HEIGHT SPECTRA OF Co^{60} γRAYS RECORDED
(a) WITHOUT THE CABLE ON THE AMPLIFIER IN FIG. 44(b).
(b) WITH THE CABLE ON THE AMPLIFIER IN FIG. 44(b).

level. A test was carried out using the experimental arrangement indicated in Fig. 44(c) to check that the gain of the spectrometer did not change when cables were connected and disconnected from the output of the cathode follower. Spectra recorded with and without a cable attached to the output of the cathode follower are presented in Fig. 46. No change of gain was observed.

Finally, the arrangement used to set up threshold levels in the work described in the following chapters is shown in Fig. 44(d). The cathode follower remained connected to the amplifier throughout the complete experiment.

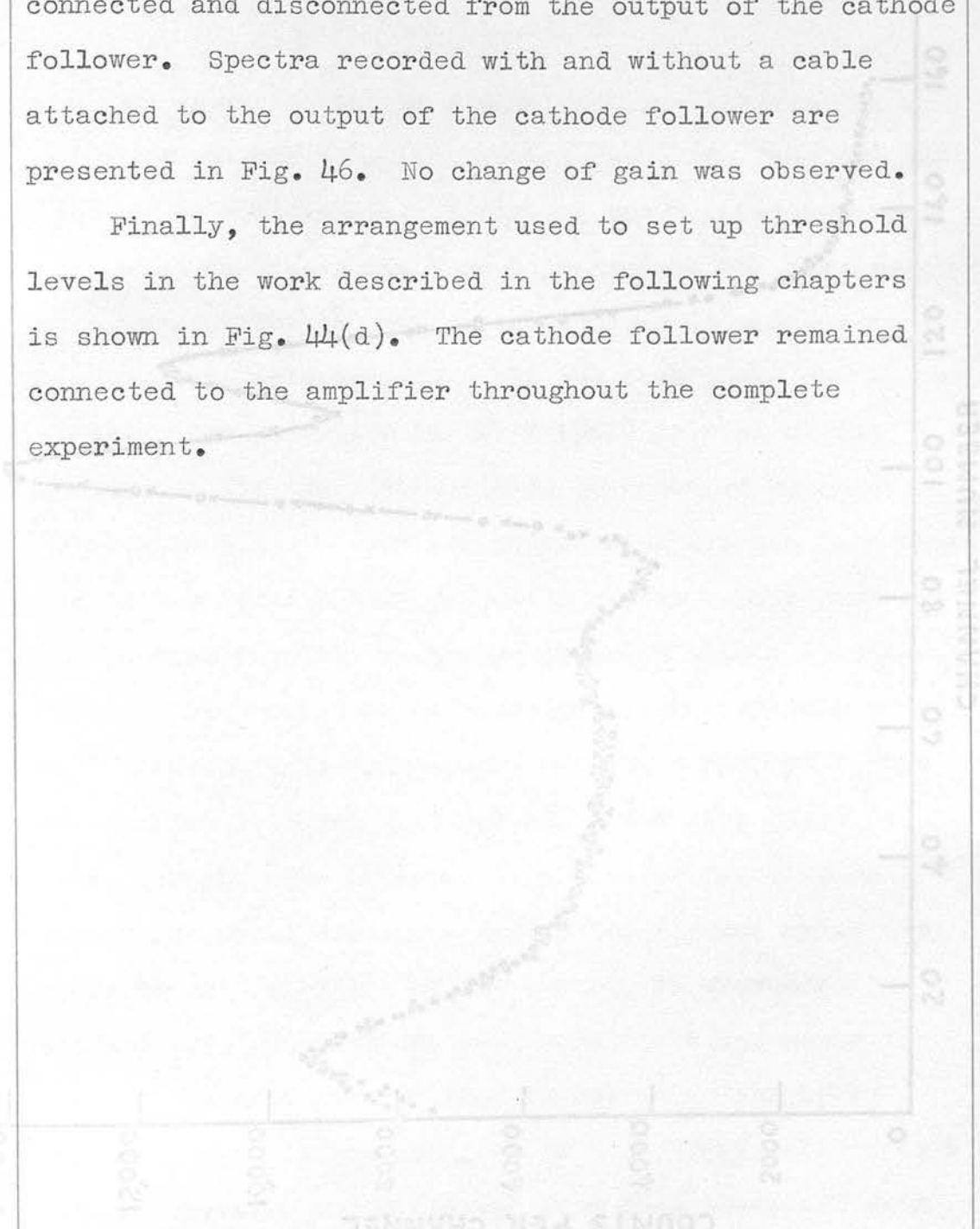

FIG 46 THE PULSE HEIGHT SPECTRA OF Co^{60} γ RAYS RECORDED WITH (×) AND WITHOUT (○) THE CABLE ON THE AMPLIFIER IN FIG 44-(c)

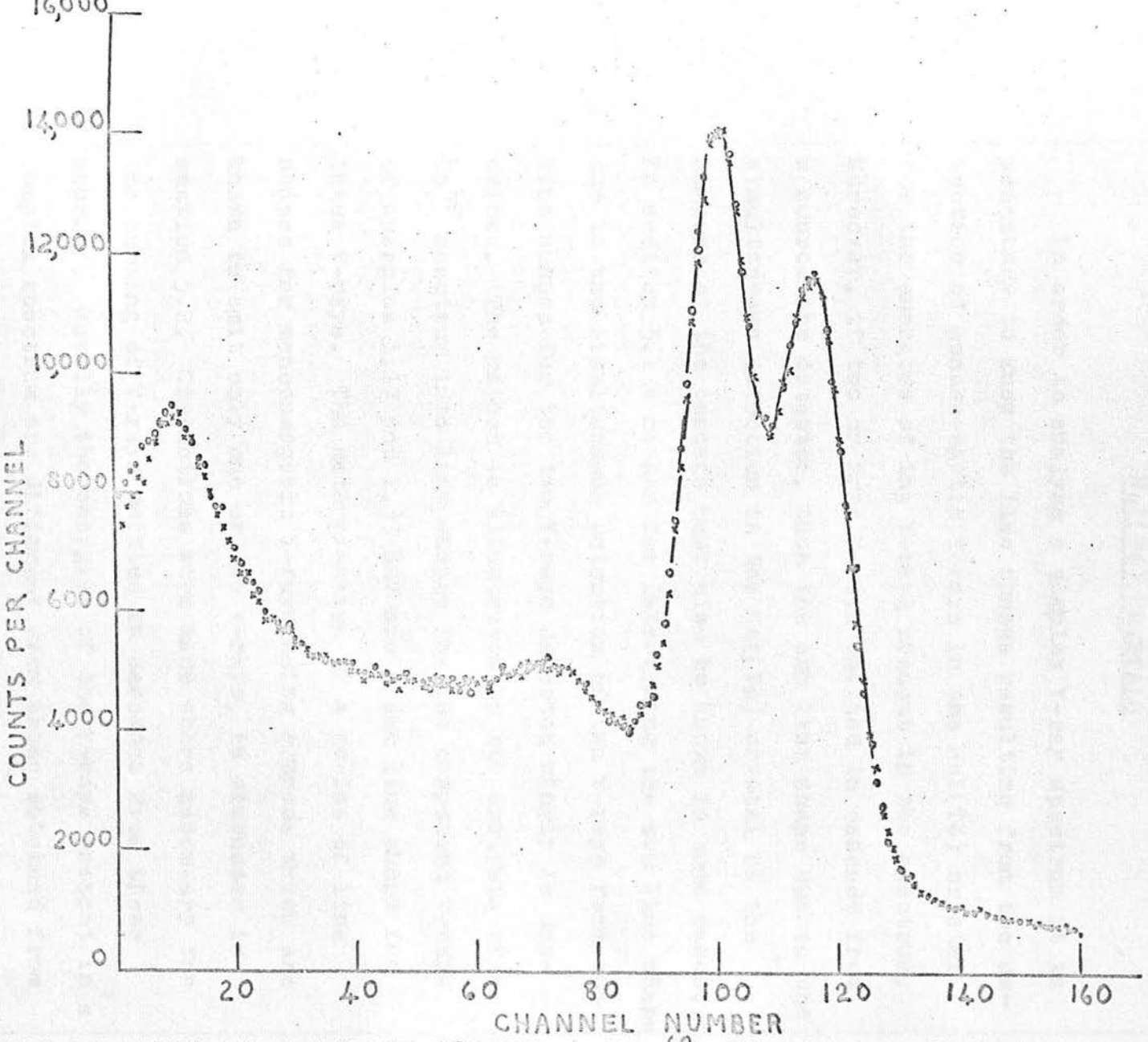

FIG. 4.6 THE PULSE HEIGHT SPECTRA OF Co^{60} γRAYS RECORDED WITH [×] AND WITHOUT [○] THE CABLE ON THE AMPLIFIER IN FIG. 4.4 (c)

CHAPTER 5

THE ANALYSIS OF COMPLEX Υ-RAY SPECTRA OBTAINED WITH NaI(Tℓ) CRYSTALS

In order to analyse a complex Υ-ray spectrum it is necessary to know the line shapes resulting from the detection of monoenergetic Υ-rays in the NaI(Tℓ) crystal for the energies of the Υ-rays present in the spectrum. Moreover, if two or more Υ-rays emitted in cascade from a source are detected, then the sum line shape due to the simultaneous detection in the NaI(Tℓ) crystal of the members of the cascade must also be known in some cases. In section 5.1 a method for determining the sum line shape due to the simultaneous detection of two Υ-rays from the line shapes for the two Υ-rays detected singly is described. The method is illustrated by the analysis of a Co^{60} spectrum into line shapes for the component Υ-rays of energies 1.17 and 1.33 MeV and a sum line shape for these Υ-rays. The determination of a series of line shapes for monoenergetic Υ-rays using sources which are known to emit only one or two Υ-rays, is discussed in section 5.2. Corrections were made where necessary for the summing of Υ-rays emitted in cascades from these sources. Usually the energies of the Υ-rays present in a complex spectrum are different from those obtained from the calibration sources. In section 5.3 a method of interpolation which can be used for finding the line

shapes for γ-rays of any energy in the range from about 0.3 MeV to 4.5 MeV is described. Finally the line shapes for the γ-rays which are emitted in the decay of the low-lying energy levels of B^{10} are presented.

5.1. Determination of Sum Line Shapes for γ-ray Cascades

The line shape due to the energy summing of a pair of γ-rays from a cascade in a small NaI(Tℓ) crystal has been determined experimentally by Vingiani and Monaro (1961)[57] using a sum-coincidence spectrometer with two identical NaI(Tℓ) scintillation detectors. However in the present experiment the energy summing of γ-rays occurred in a large NaI(Tℓ) crystal, 5" diam. by 4" long and a sum-coincidence technique could not be used as only one scintillation detector with a large NaI crystal was available. The following technique was developed therefore to enable the sum line shapes due to two γ-rays to be determined from the line shapes of the γ-rays detected singly in the NaI(Tℓ) crystal.

The line shape of a monoenergetic γ-ray, γ(p) may be specified by the number of counts N(i,p) recorded in the i-th channel of the pulse height spectrum for each channel. A complex γ-ray spectrum, N(i,t) due to two γ-rays, γ(1) and γ(2) emitted in a cascade can be split into components as follows:- $N(i,t) = N(i,1) + N(i,2) + N(i,s)$ where N(i,s) describes the line shape due to the simultaneous detection of γ(1) and γ(2) in the NaI(Tℓ) crystal. Those events recorded in the i-th channel correspond to a

γ-ray (or γ-rays) depositing a total energy in the range $\left[E_o + (i-1)\Delta E\right]$ to $\left[E_o + i\,\Delta E\right]$ in the crystal, where E_o is the "threshold energy" of the multichannel analyser and ΔE is the "energy width" of each channel. When an event is recorded in the k-th channel due to the simultaneous detection of $\gamma(1)$ and $\gamma(2)$, $\gamma(1)$ depositing an energy in the range $\left[E_o + (i-1)\Delta E\right]$ to $\left[E_o + i\,\Delta E\right]$, then the energy deposited in the crystal by $\gamma(2)$ must lie in the range $\left[(k-i-1)\Delta E\right]$ to $\left[(k-i+1)\Delta E\right]$. Such events occurring separately would be recorded in the i-th channel of the $\gamma(1)$ line shape and either the j-th or (j+1)th channel of the $\gamma(2)$ line shape, where

$$j = \left[k - i - \frac{E_o}{\Delta E}\right].$$

Now the probability of γ-ray, $\gamma(p)$ being recorded in the i-th channel is proportional to $N(i,p)$, and therefore the probability of the simultaneous detection of $\gamma(1)$ and $\gamma(2)$ giving an event in channel k is given by

$$N(k,s) \propto \sum_i N(i,1)\left[a(j,2)N(j,2) + a(j+1,2)N(j+1,2)\right] .$$

The constant $a(j,2)$ is the fraction of the $\gamma(2)$ γ-rays detected in the energy range $\left[E_o + (j-1)\Delta E\right]$ to $\left[E_o + j\,\Delta E\right]$ which contribute to sum events recorded in the k-th channel when the $\gamma(1)$ γ-rays deposit energies between $\left[E_o + (i-1)\Delta E\right]$ and $\left[E_o + i\Delta E\right]$ in the crystal; the remaining $\left[1 - a(j,2)\right]$ of the γ-rays contribute to sum events recorded in the (k-1)th channel. We now assume

that the number of counts per channel $N(j,p)$ of the $\gamma(p)$ line shape varies smoothly and slowly from the j-th to the $(j+1)$th channel so that $N(j,p) \approx N(j+1,p)$ and $a(j,p) \approx \frac{1}{2}$. The number of counts in the k-th channel of the sum line shape then reduces to $N(k,s) \alpha \sum_i N(i,1)N(j,2)$ with $j = \left[k - i - \frac{E_o}{\Delta E}\right]$. The condition that $N(j,p) \approx N(j+1,p)$ may be realized in practice by displaying the $\gamma(p)$ line shapes over a sufficiently large number of channels. These calculations enable the complex γ-ray spectrum, $N(i,t)$ to be analysed into the line shapes $N(i,1)$, $N(i,2)$ and $N(i,s)$. It is implicit in the above argument that the line shape $N(j,2)$ results from the same number of γ-rays from the source as $N(j,1)$.

The relative intensities of the component line shapes in the above spectrum may be calculated from the source-to-scintillator geometry and the detection efficiency of the scintillator. Suppose the source emits N_o γ-ray cascades per second with no angular correlation between the directions of emission of the two γ-rays $\gamma(1)$ and $\gamma(2)$. The probability $P(p)$ of γ-ray $\gamma(p)$ depositing its full energy in the crystal is $\frac{\omega}{4\pi} f(p) N_o$, where $f(p)$ is the photopeak detection efficiency for a γ-ray of energy $E(p)$ incident on the particular NaI(Tℓ) crystal, and ω is the average solid angle subtended by the crystal at the source. The probability $P(1,2)$ of both $\gamma(1)$ and $\gamma(2)$ depositing their full energy in the crystal is

$$P(1,2) = P(1)P(2) = \left(\frac{\omega}{4\pi}\right)^2 f(1)\, f(2)\, N_o .$$

Now the area A(p) of the photopeak of the $\gamma(p)$ line shape is proportional to the probability of $\gamma(p)$ being detected alone and depositing its full energy in the crystal.

Thus $A(1) \propto \frac{\omega}{4\pi} f(1) N_o \left[1 - \frac{\omega}{4\pi} F(2)\right]$ where F(2) is the total detection efficiency of the NaI(Tℓ) crystal for γ-ray, $\gamma(2)$, and similarly for A(2). The relative intensities of the $\gamma(1)$, $\gamma(2)$ and sum line shapes in the complex spectrum N(i,t) as given by the areas of their full energy peaks are therefore

$$A(1) : A(2) : A(s)$$
$$\equiv f(1)\left[1 - \frac{\omega}{4\pi} F(2)\right] : f(2)\left[1 - \frac{\omega}{4\pi} F(1)\right] : \frac{\omega}{4\pi} f(1) f(2) .$$

The argument can be extended to deal with several γ-rays emitted in a cascade. Higher orders of summing may occur when 3, 4, 5.... γ-rays are detected simultaneously in the scintillator. However the probability of three γ-rays being detected simultaneously is extremely small and usually it is sufficient to consider only the summing due to pairs of γ-rays. The pulse height spectrum due to the detection of the γ-rays in a cascade is given fairly accurately by the addition in the appropriate proportions of the line shapes of the individual γ-rays and the sum line shapes due to all pairs of γ-rays. The intensities of the line shapes are chosen so that the area of the photopeak A(k) of γ-ray $\gamma(k)$ is

$N_o \frac{\omega}{4\pi} f(k) \left[1 - \frac{\omega}{4\pi} \sum_{i \neq k} F(i)\right]$ and the area of the sum peak due to two γ-rays $\gamma(k)$ and $\gamma(\ell)$ is $N_o \left(\frac{\omega}{4\pi}\right)^2 f(k)\, f(\ell)$ for some fixed value of N_o.

In the present experiment the summing of γ-rays occurred in a NaI(Tℓ) crystal 5" diam. by 4" long placed 3 cm. from the source. For such an arrangement the geometrical efficiency $\frac{\omega}{4\pi}$ is $\frac{2}{7}$ and the total detection efficiency $F(i)$ for γ-rays $\gamma(i)$ in the crystal is less than 1. In the terms $\left[1 - \frac{\omega}{4\pi} F(i)\right]$ which appear in the above formulae, $\frac{\omega}{4\pi} F(i) \leqslant 1$ and therefore these terms can be evaluated fairly accurately using only approximate values for $F(i)$. The variations of the total detection efficiency and the photopeak detection efficiency with γ-ray energy are similar[58,59,60] and so it was decided to use photopeak detection efficiencies throughout the calculations. The error introduced by making this approximation is small compared to the other inaccuracies and is taken into account in the following work.

The analysis of a Co^{60} γ-ray spectrum.

A 20 μC Co^{60} source was placed centrally about 3 cm from the surface of the large NaI(Tℓ) crystal and the pulse height distribution due to the detection of the 1.17 - 1.33 MeV γ-ray cascade was recorded by the multichannel pulse height analyser. The Co^{60} γ-ray spectrum, corrected for electronic noise and the low level background activity present in the laboratory, is shown in Fig. 47.

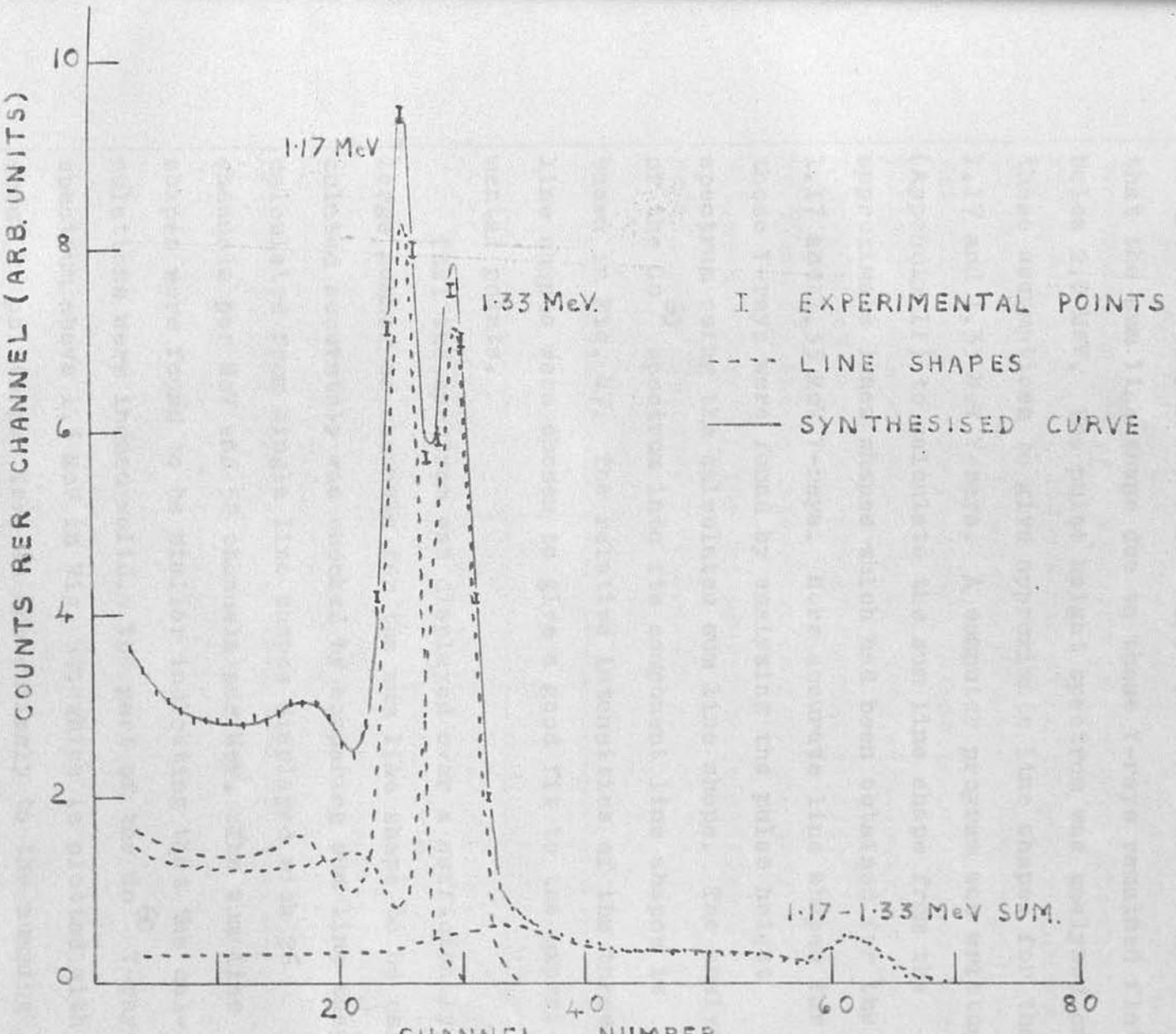

FIG. 47. THE 1·17 AND 1·33 MeV γRAYS FROM Co^{60}.

Initially it was assumed that the line shapes for γ-rays of energies 1.17 and 1.33 MeV were similar and that the sum line shape due to these γ-rays remained flat below 2.0 MeV. The pulse height spectrum was analysed on these assumptions to give approximate line shapes for the 1.17 and 1.33 MeV γ-rays. A computer program was written (Appendix II) to calculate the sum line shape from the approximate lines shapes which had been obtained for the 1.17 and 1.33 MeV γ-rays. More accurate line shapes for these γ-rays were found by analysing the pulse height spectrum using the calculated sum line shape. The analysis of the Co^{60} spectrum into its component line shapes is shown in Fig. 47. The relative intensities of the three line shapes were chosen to give a good fit to the experimental points.

That the spectrum was displayed over a sufficiently large number of channels for the sum line shape to be calculated accurately was checked by comparing sum line shapes calculated from single line shapes displayed with 26 channels per MeV and 52 channels per MeV. The sum line shapes were found to be similar indicating that the calculations were indeed valid. The part of the Co^{60} γ-ray spectrum above 1.5 MeV in Fig. 47, which is plotted with about 26 points per MeV, is due entirely to the summing of the 1.17 and 1.33 MeV γ-rays in the NaI(Tℓ) crystal, and is in good agreement with the calculated line shape. We conclude that for spectra displayed with more than 25

channels per MeV, the sum line shapes can be determined fairly accurately by the above method.

The calculated and the observed intensities of the components in the Co^{60} spectrum are in good agreement, see Table 4. The photopeak detection efficiencies used in the calculations were taken from the curve in Fig. 48. The variation of the photopeak detection efficiency of a NaI(Tℓ) crystal 5" diam. by 4" long with γ-ray energy was obtained from the data of Jarczyk et al.[58] and Weitkamp[59], and by interpolation from the data of Miller and Snow[60] for the source-to-scintillator separations indicated.

Line shape	1.17 MeV	1.33 MeV	2.5 MeV (sum)
Observed intensities	48 ± 1	46 ± 1	5.3 ± 0.3
Calculated intensities	49 ± 4	45 ± 3	5.7 ± 0.4

Table 4. The Relative Intensities of the Line Shapes as Given by the Areas of the Full Energy Peaks.

This method of dealing with the summing of γ-rays in a NaI(Tℓ) crystal enables the pulse height distribution for a γ-ray cascade to be analysed fairly accurately into the line shapes of the individual γ-rays and the sum line shape. Alternatively the pulse height distribution for a γ-ray cascade can be constructed from the line shapes of the individual γ-rays, with a typical accuracy of about $\pm$ 10%.

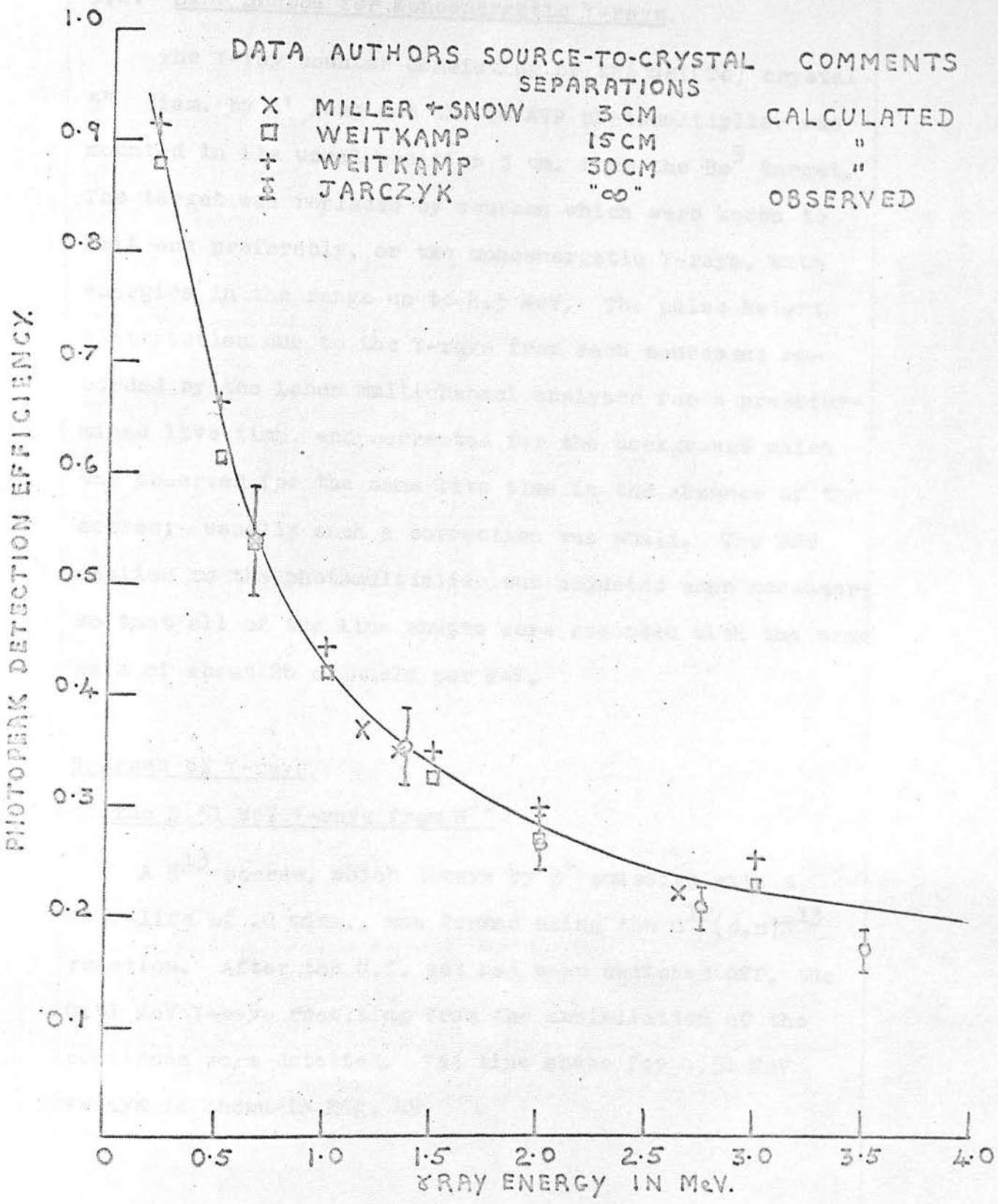

FIG. 48 THE VARIATION OF THE PHOTOPEAK DETECTION EFFICIENCY WITH γRAY ENERGY FOR A NaI(Tℓ) CRYSTAL 5" DIAM. BY 4" LONG.

5.2. Line Shapes for Monoenergetic Υ-rays.

The Υ-ray counter consisting of the NaI(Tℓ) crystal 5" diam. by 4" long and the 58 AVP photomultiplier was mounted in its usual position 3 cm. from the Be^9 target. The target was replaced by sources which were known to emit one preferably, or two monoenergetic Υ-rays, with energies in the range up to 4.5 MeV. The pulse height distribution due to the Υ-rays from each source was recorded by the Laben multichannel analyser for a predetermined live time, and corrected for the background which was observed for the same live time in the absence of the source; usually such a correction was small. The EHT applied to the photomultiplier was adjusted when necessary so that all of the line shapes were recorded with the same gain of about 26 channels per MeV.

Sources of Υ-rays.

The 0.51 MeV Υ-rays from N^{13}

A N^{13} source, which decays by β^+ emission with a half-life of 10 mins., was formed using the $C^{12}(d,n)N^{13}$ reaction. After the H.T. set had been switched off, the 0.51 MeV Υ-rays resulting from the annihilation of the positrons were detected. The line shape for 0.51 MeV Υ-rays is shown in Fig. 49.

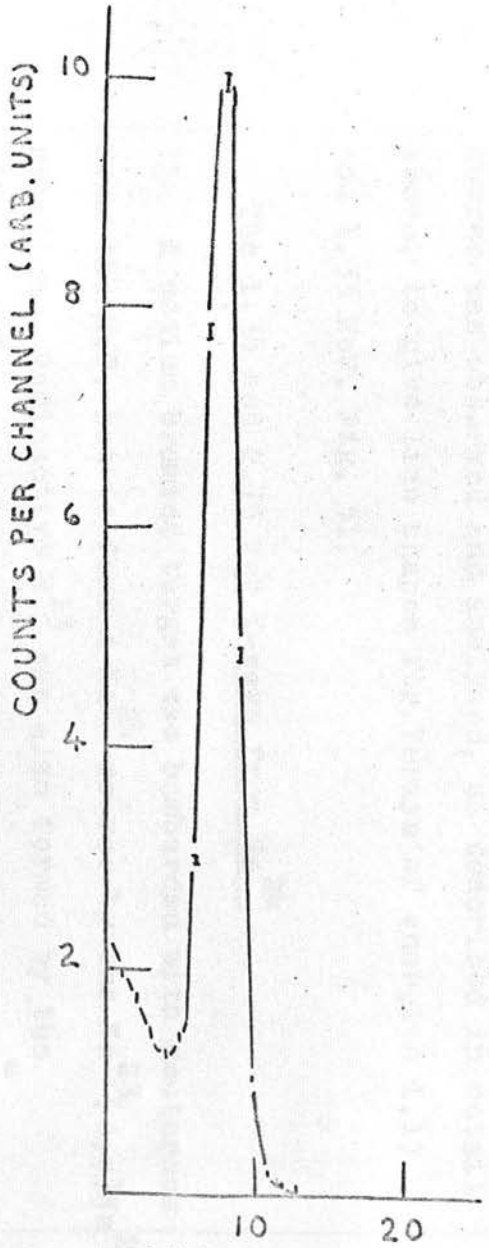

FIG. 49 0·51 MeV γ RAYS FROM THE β^+ DECAY OF N^{13}.

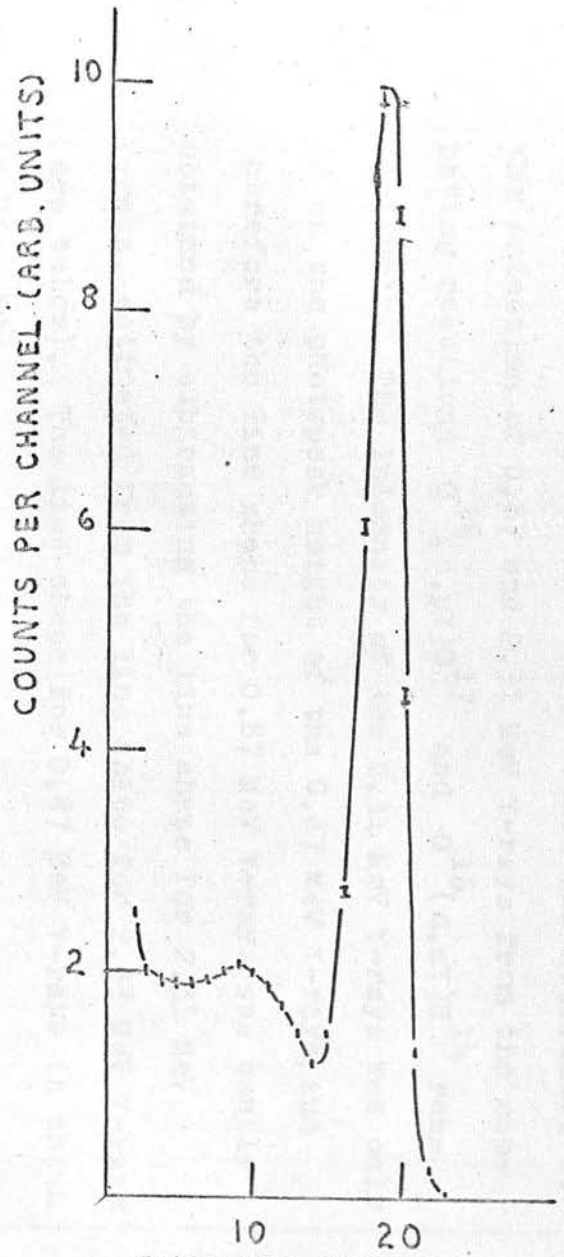

FIG. 50 0·87 MeV γ RAYS FROM THE $O^{16}(d,p)O^{17}$ REACTION.

The 0.87 MeV γ-rays from O^{17}

The pulse height distribution due to the γ-rays emitted when deuterons from the H.T. set struck a quartz target was recorded. The distribution was attributed to the detection of 0.87 and 2.31 MeV γ-rays from the competing reactions $O^{16}(d,p\gamma)O^{17}$ and $O^{16}(d,\alpha\gamma)N^{14}$ respectively. The intensity of the 2.31 MeV γ-rays was only 1% of the photopeak height of the 0.87 MeV γ-rays, and therefore the line shape for 0.87 MeV γ-rays was easily obtained by subtracting the line shape for 2.31 MeV γ-rays, estimated from the line shape for 2.37 MeV γ-rays (see below). The line shape for 0.87 MeV γ-rays is shown in Fig. 50.

The 1.17 and 1.33 MeV γ-rays from Co^{60}

The spectrum of the γ-rays emitted from a Co^{60} source was observed and analysed, as described in detail above, to give line shapes for γ-rays of energies 1.17 and 1.33 MeV, Fig. 51.

The 1.38 and 2.75 MeV γ-rays from Na^{24}

A sodium bromide target was bombarded with deuterons from the H.T. set to form a Na^{24} source by the $Na^{23}(d,p)Na^{24}$ reaction. Radioactive N^{13} was also formed by the $C^{12}(d,n)N^{13}$ reaction due to the contamination of the target and the target holder with carbon from the diffusion pump oil. As the half-lifes of N^{13} and Na^{24} are about 10 mins. and 15 hours respectively, the pulse height

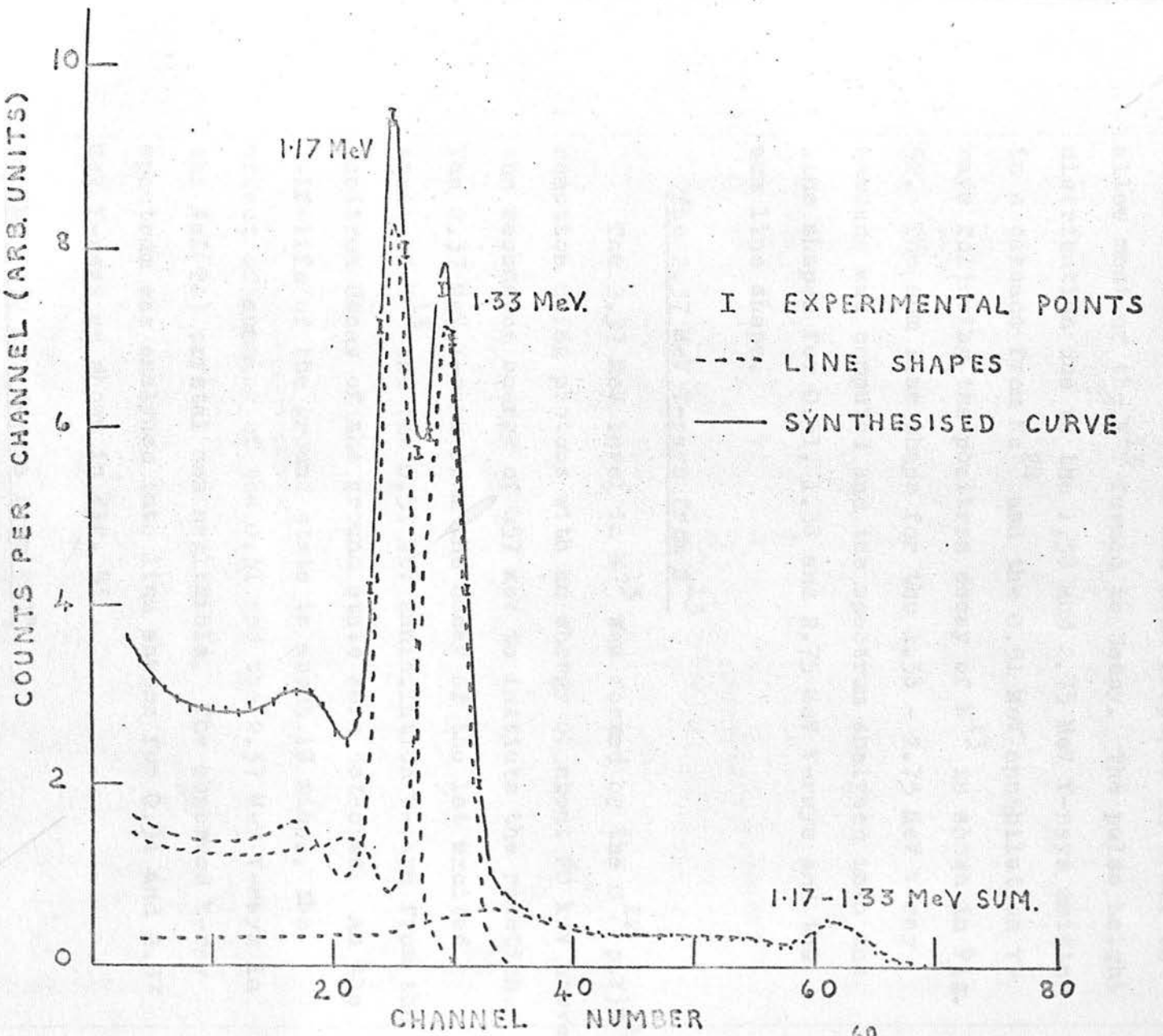

FIG. 51. THE 1·17 AND 1·33 MeV γRAYS FROM Co^{60}.

distribution of the γ-rays from the target was recorded 2 hours after the source had been prepared in order to allow most of the N^{13} formed to decay. The pulse height distribution due to the 1.38 and 2.75 MeV γ-rays emitted in a cascade from Na^{24} and the 0.51 MeV annihilation γ-rays following the positron decay of N^{13} is shown in Fig. 52. The sum line shape for the 1.38 - 2.75 MeV γ-ray cascade was computed and the spectrum analysed into the line shapes for 0.51, 1.38 and 2.75 MeV γ-rays and the sum line shape.

The 2.37 MeV γ-rays from N^{13}

The 2.37 MeV level in N^{13} was formed by the $C^{12}(p,\gamma)N^{13}$ reaction using protons with an energy of about 20 keV above the resonance energy of 457 keV to initiate the reaction. The 2.37 MeV γ-rays from the decay of the 1st excited state of N^{13} and the 0.51 MeV annihilation γ-rays from the positron decay of the ground state were detected. As the half-life of the ground state is about 10 mins., the effect of summing of the 0.51 and the 2.37 MeV γ-rays in the NaI(Tℓ) crystal was negligible. The observed γ-ray spectrum was analysed into line shapes for 0.51 and 2.37 MeV γ-rays as shown in Fig. 53.

The 2.62 MeV γ-rays from ThC"

The pulse height distribution due to the γ-rays emitted from a source which consisted of a mixture of ThB and ThC was recorded. The portion of the distribution

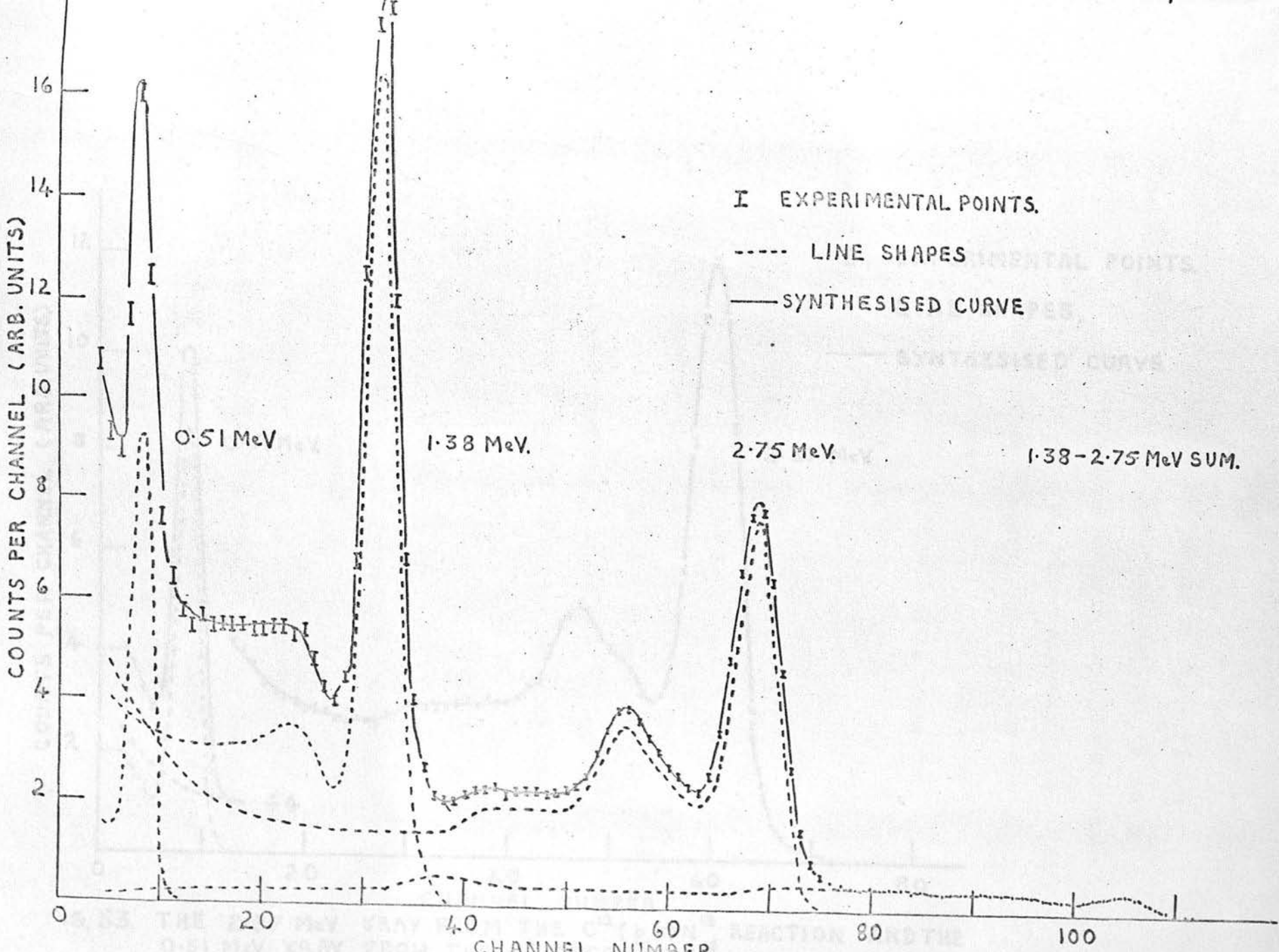

FIG. 52. THE 1·38 AND 2·75 MeV γRAYS FROM Na^{24} AND THE 0·51 MeV γRAY FROM N^{13}.

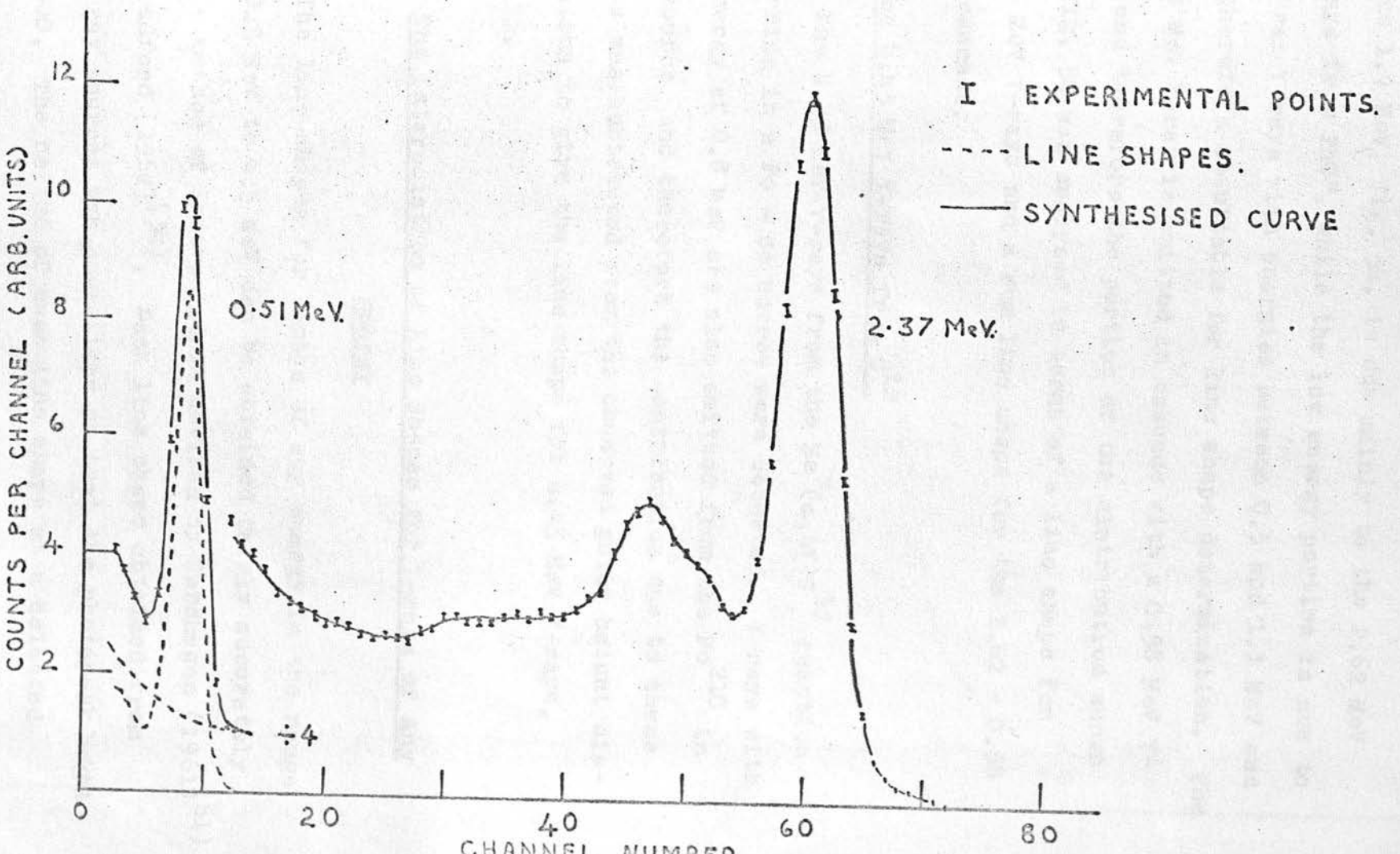

FIG. 53. THE 2·37 MeV γRAY FROM THE $C^{12}(p,\gamma)N^{13}$ REACTION AND THE 0·51 MeV γRAY FROM THE β^+ DECAY OF N^{13}.

above 1.4 MeV, Fig. 54, is due mainly to the 2.62 MeV γ-rays from ThC", while the low energy portion is due to several γ-rays with energies between 0.5 and 1.1 MeV and is therefore unsuitable for line shape determination. The 2.62 MeV γ-ray is emitted in cascade with a 0.58 MeV γ-ray and therefore the portion of the distribution shown in Fig. 54 was analysed in terms of a line shape for 2.62 MeV γ-rays and a sum line shape for the 2.62 - 0.58 MeV cascade.

The 4.43 MeV γ-rays from C^{12}

The 4.43 MeV γ-rays from the $Be^{9}(\alpha,n\gamma)C^{12}$ reaction occurring in a Po - Be source were observed. γ-rays with an energy of 0.8 MeV are also emitted from the Po^{210} in the source, and therefore the contribution due to these γ-rays was subtracted from the observed pulse height distribution to give the line shape for 4.43 MeV γ-rays, Fig. 55.

5.3. The Interpolation of Line Shapes for γ-rays of Any Energy

The line shapes for γ-rays of any energy in the range from 0.3 MeV to 4.5 MeV can be obtained fairly accurately using a method of interpolation devised by Nordhagen (1961)[61] and Bradford (1962)[34]. Each line shape obtained from the γ-ray sources was normalized so that the photopeak height was 1000. The height of each line shape at a selected

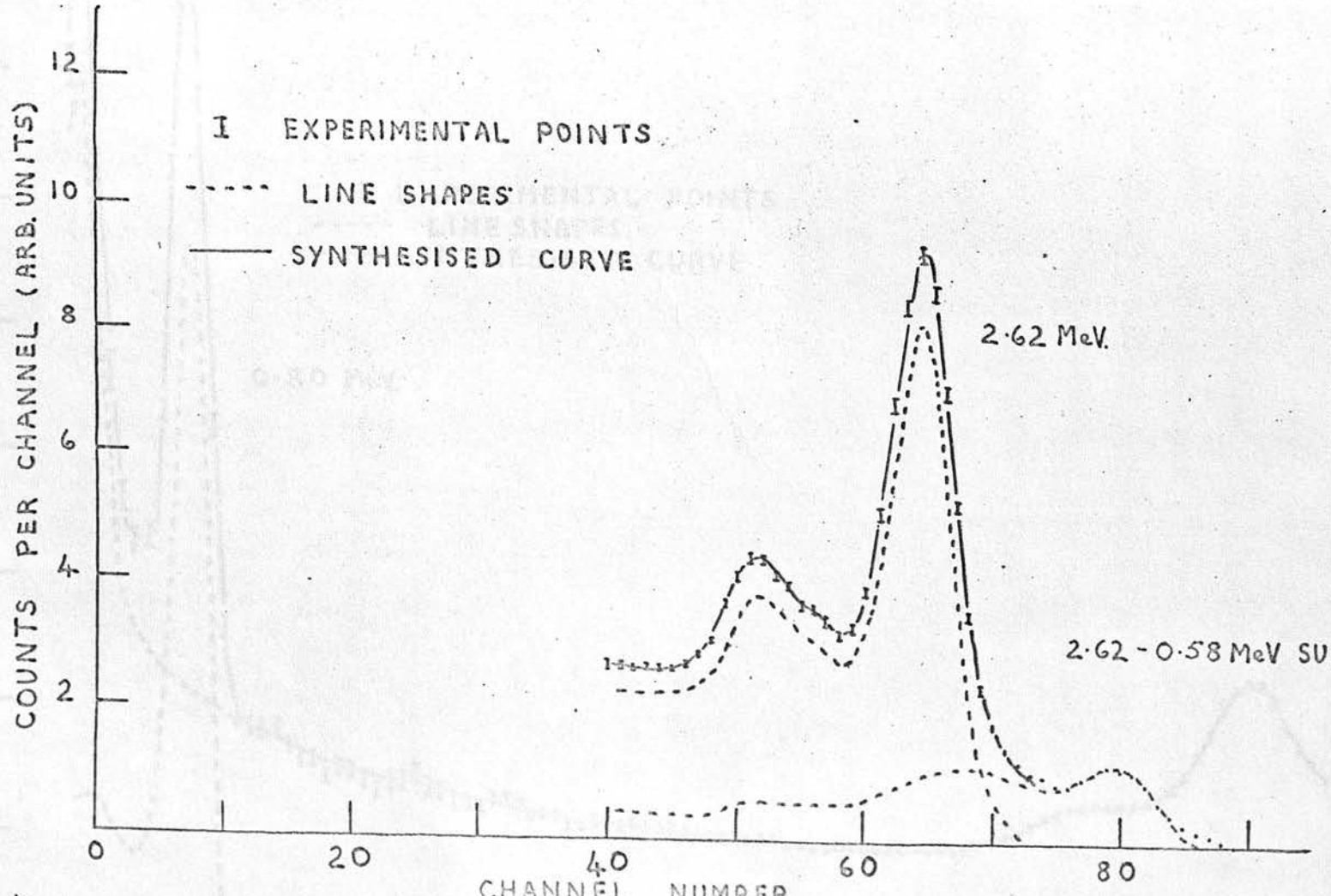

FIG. 54 THE 2·62 MeV γRAY FROM ThC".

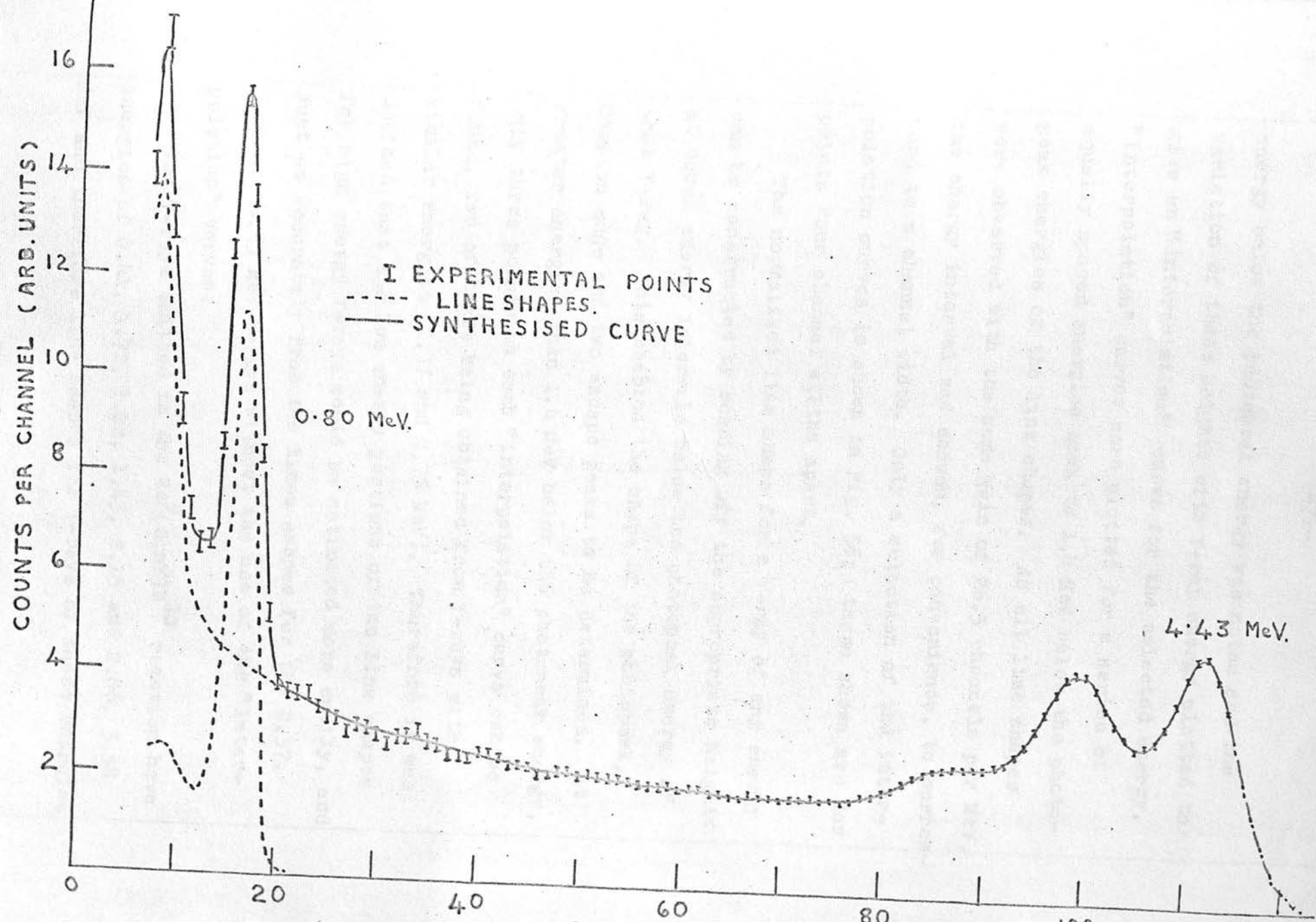

FIG. 55. THE 4·43 MeV γRAY FROM THE $Be^{9}(\alpha, n\gamma)C^{12}$ REACTION AND THE

energy below the photopeak energy was noted and the variation of these heights with γ-ray energy plotted to give an "interpolation" curve for the selected energy. "Interpolation" curves were plotted for a series of equally spaced energies down to 1.4 MeV below the photopeak energies of the line shapes. As all line shapes were observed with the same gain of 26.5 channels per MeV, the energy interval was chosen, for convenience, to correspond to a channel width. Only a selection of the interpolation curves is shown in Fig. 56; those shown are for points four channel widths apart.

The normalized line shape for a γ-ray of any energy can be constructed by reading off the appropriate heights at equal energy intervals below the photopeak energy of that γ-ray. This enables the shape of the photopeak, Compton edge and two escape peaks to be determined. At greater energies than 1.4 MeV below the photopeak energy, only three points on each "interpolation" curve can be found, two of these being obtained from γ-rays with similar energies (2.37 and 2.75 MeV). Therefore it was decided that the low energy portions of the line shapes for high energy γ-rays could be estimated more easily, and just as accurately from the lines shapes for the 2.37, 2.75 and 4.43 MeV γ-rays without the use of the "interpolation" curves.

The γ-rays emitted in the $Be^{9}(d,n\gamma)B^{10}$ reaction have energies of 0.41, 0.72, 1.02, 1.43, 2.15 and 2.86, 3.58 MeV and therefore line shapes for γ-rays of these energies

were constructed, Figs. 57-60, the accuracies of the line shapes being estimated from the spread of the points on the interpolation curves.

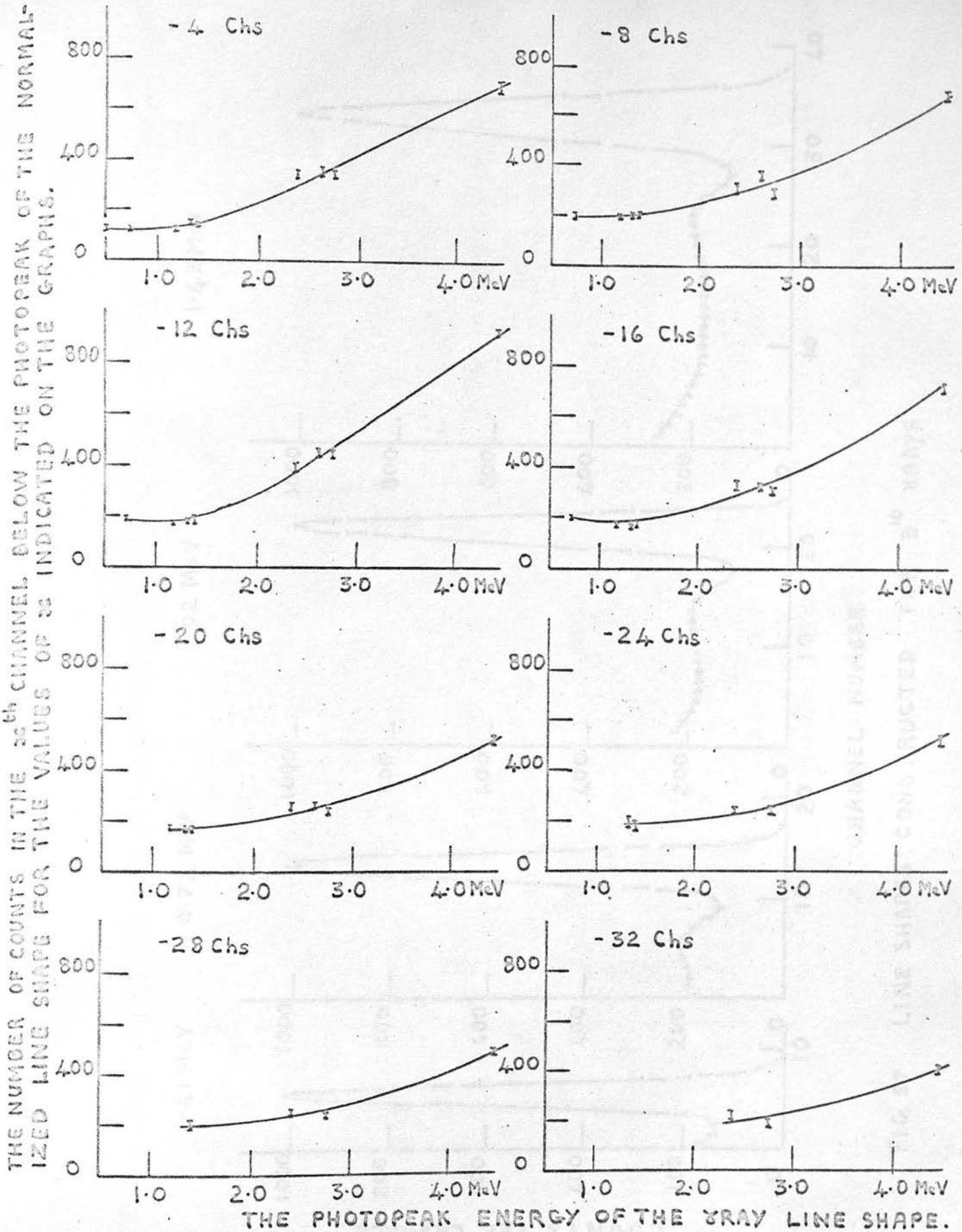

FIG 56. CURVES SHOWING HOW THE PULSE HEIGHT DISTRIBUTION FOR MONO-ENERGETIC γ-RAYS VARIES WITH γ-RAY ENERGY.

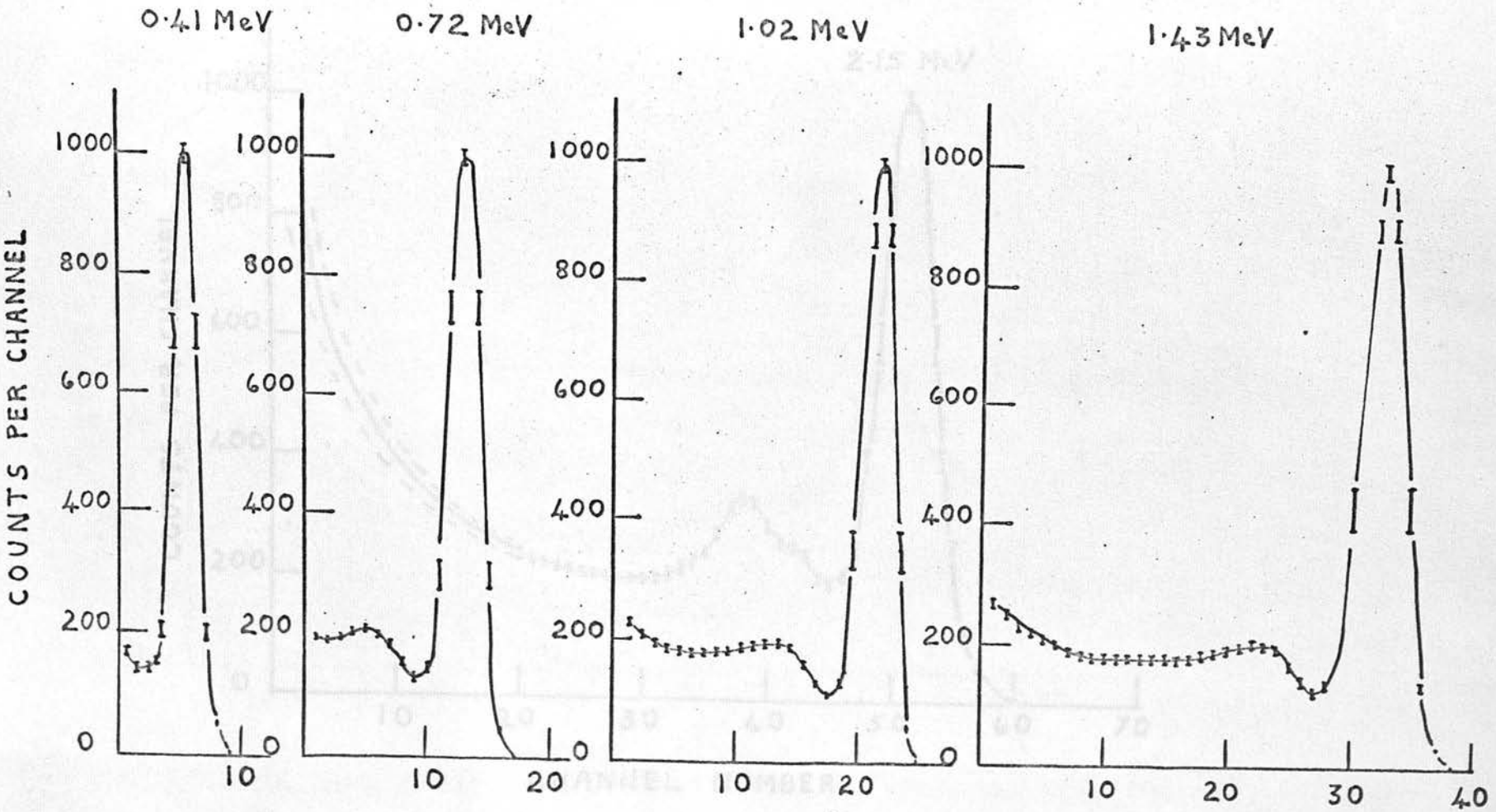

FIG. 57 LINE SHAPES CONSTRUCTED FOR B^{10} γRAYS

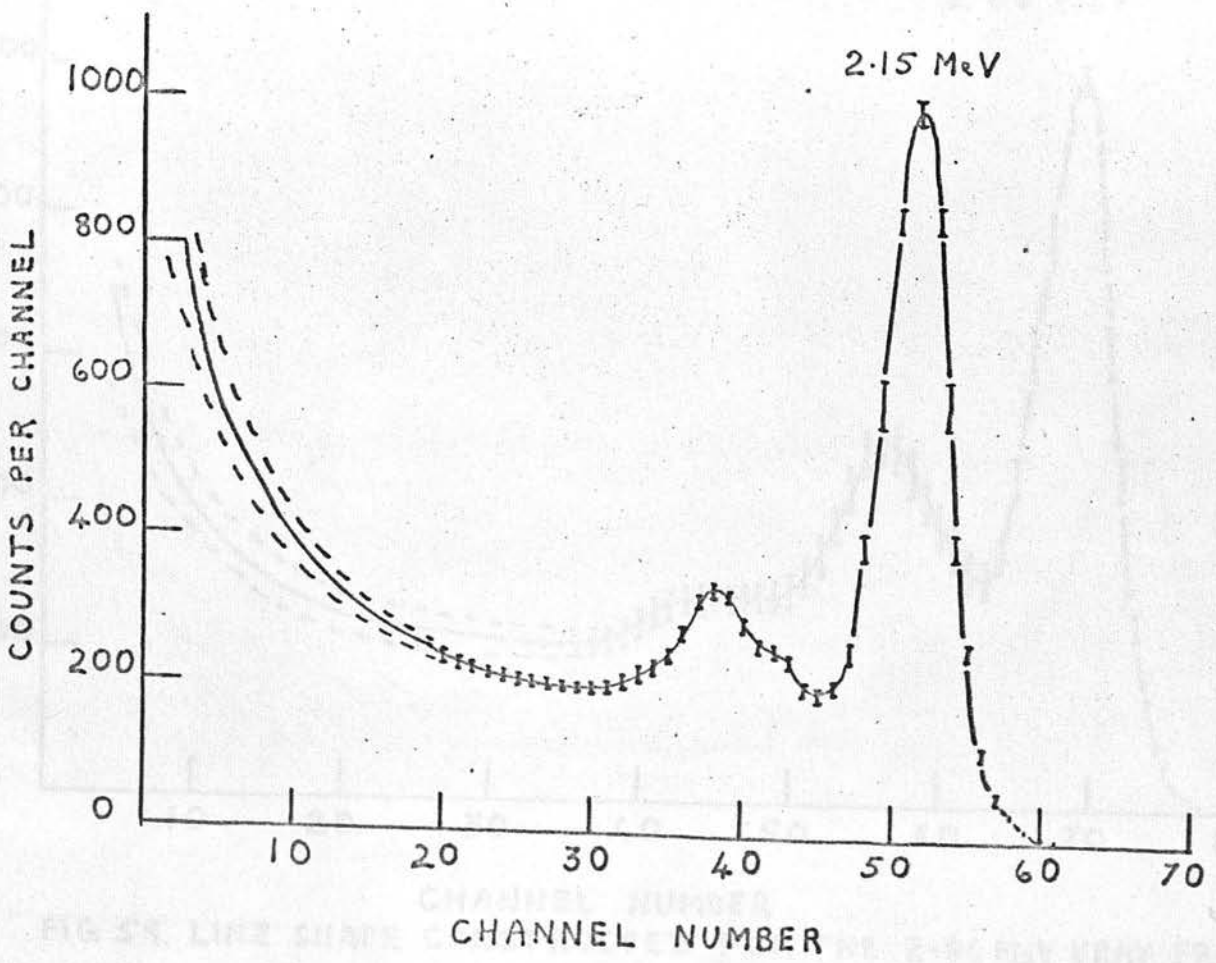

FIG. 58. LINE SHAPE CONSTRUCTED FOR THE 2·15 MeV γ RAY FROM B^{10}.

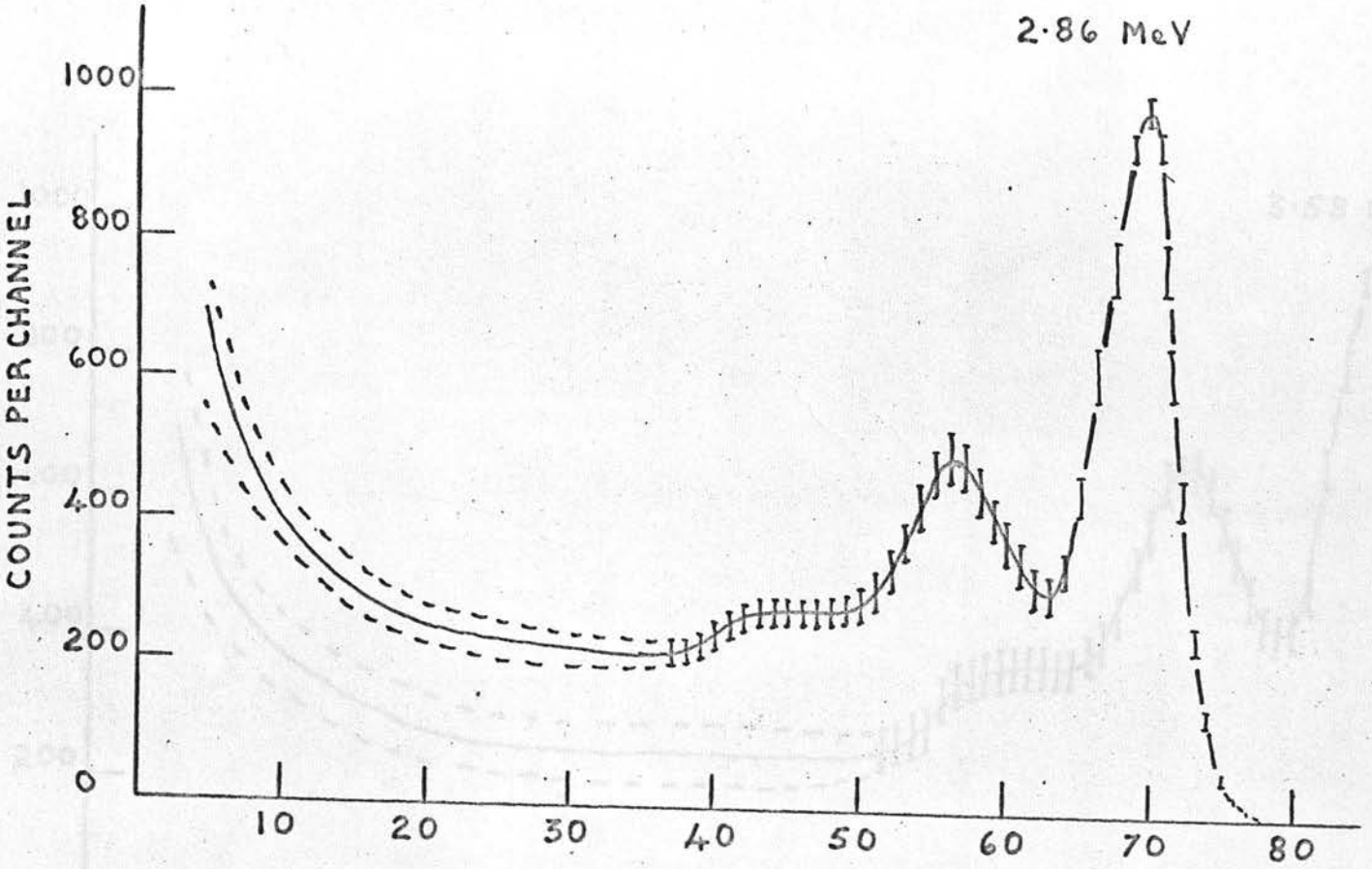

FIG. 59. LINE SHAPE CONSTRUCTED FOR THE 2·86 MeV γRAY FROM B^{10}.

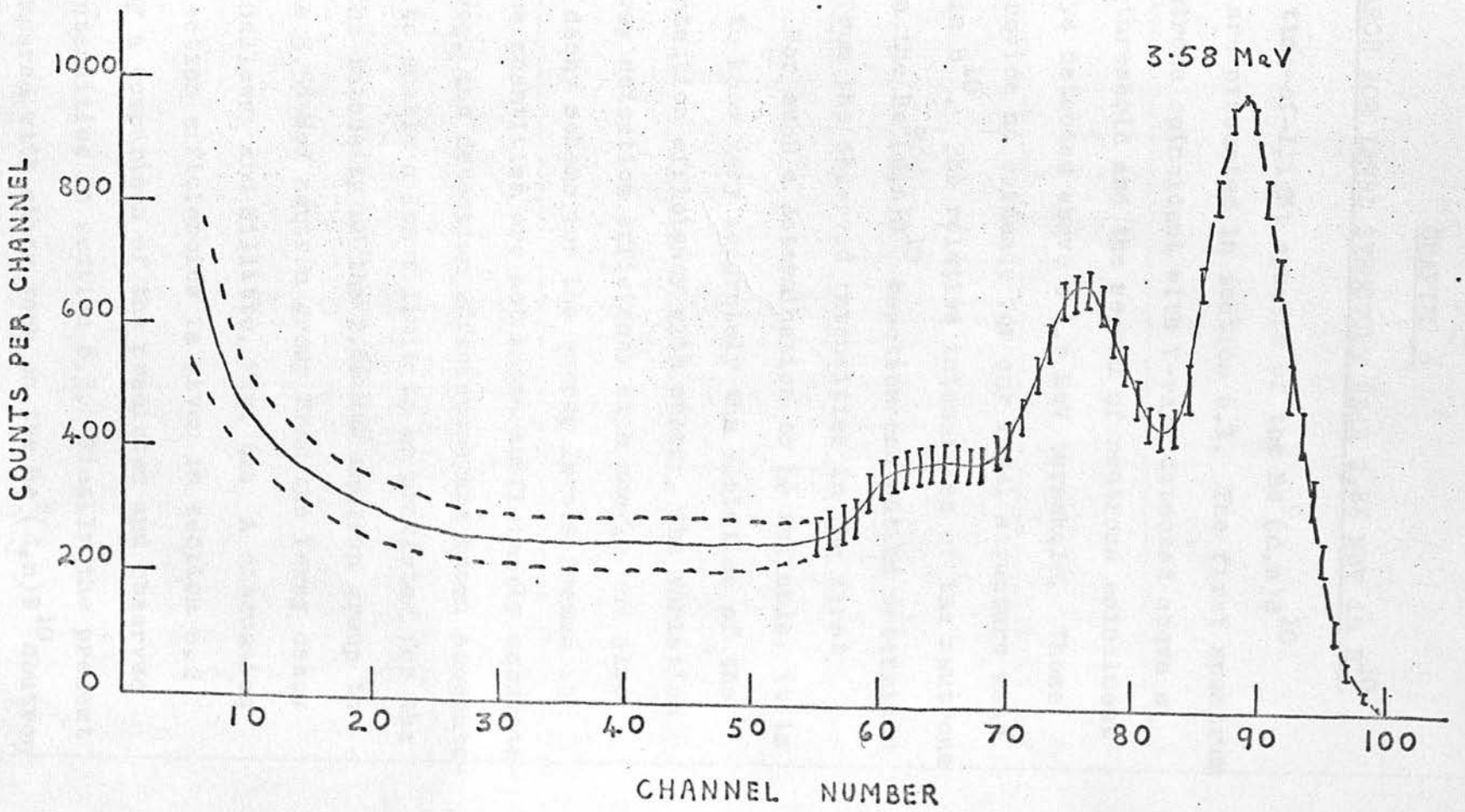

FIG. 60 LINE SHAPE CONSTRUCTED FOR THE 3·58 MeV γRAY FROM B^{10}.

CHAPTER 6

A SEARCH FOR LEVEL STRUCTURE NEAR 2.86 MeV in B^{10}

Two time-of-flight spectra of the $Be^9(d,n)B^{10}$ neutrons are presented in section 6.1. The first spectrum is of neutrons coincident with γ-rays detected above a 0.35 MeV threshold and the second of neutrons coincident with γ-rays detected above a 1.6 MeV threshold. These spectra provide no evidence for any level structure near 2.86 MeV in B^{10}. The relative intensities of the neutrons emitted in the $Be^9(d,n)B^{10}$ reaction can not be determined reliably from the observed intensities in the first spectrum. For such a determination to be reliable, it is necessary to know very accurately the variation of the neutron detection efficiency with energy, the variation of the γ-ray detection efficiency with energy and also the γ-ray decay scheme for the energy levels formed in B^{10}. These quantities are not known sufficiently accurately. However, the detection efficiences are known accurately enough to enable a lower limit to be predicted for the ratio of the intensity of the 2.86 MeV neutron group to that of the 3.58 MeV neutron group from the γ-ray decay scheme of Galloway and Sillitto, Fig. 61. A discussion of the detection efficiencies is given in section 6.2 followed by a comparison of the predicted and observed relative intensities in section 6.3. Finally the present work is compared with other work on the $Be^9(d,n)B^{10}$ neutron energy spectrum in section 6.4.

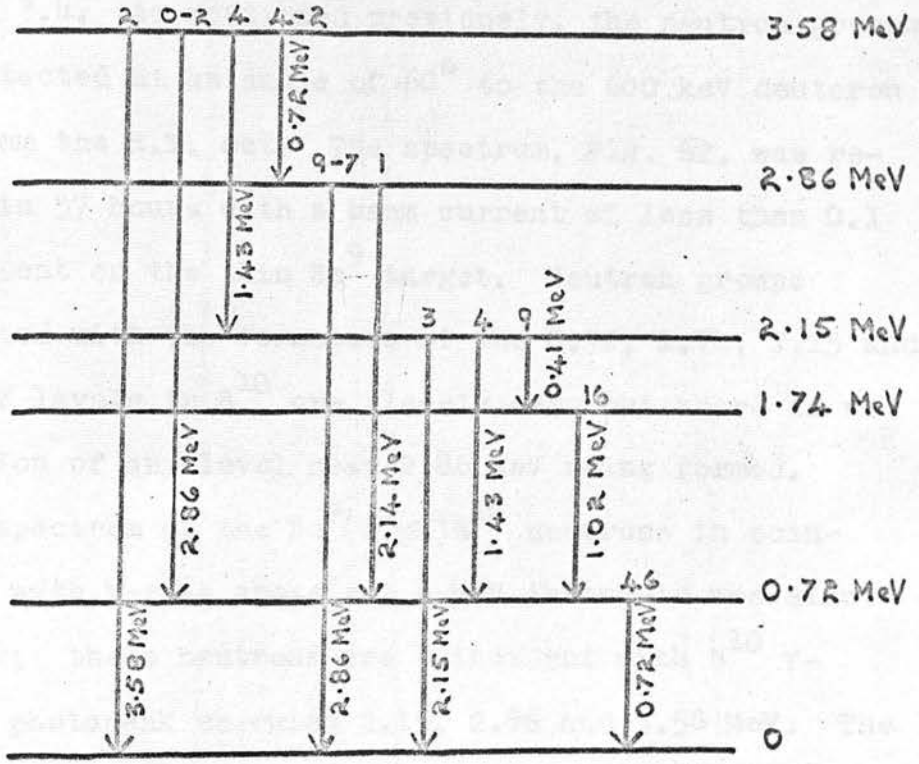

FIG. 61 THE B^{10} DECAY SCHEME PROPOSED BY GALLOWAY AND SILLITTO. (THE RELATIVE INTENSITIES OF THE γRAYS EMITTED FROM THE $Be^{9}(d,n\gamma)B^{10}$ REACTION FOR 600 keV DEUTERONS ARE INDICATED.)

6.1. $Be^9(d,n\gamma)B^{10}$ Neutron Time-of-flight Spectra

A time-of-flight spectrum of the $Be^9(d,n\gamma)B^{10}$ neutrons coincident with γ-rays above a 0.35 MeV threshold in the slow channel was recorded with the spectrometer set up as described in the latter part of section 3.4. As mentioned previously, the neutron groups were detected at an angle of 60° to the 600 keV deuteron beam from the H.T. set. The spectrum, Fig. 62, was recorded in 57 hours with a beam current of less than 0.1 μA incident on the thin Be^9 target. Neutron groups associated with the formation of the 0.72, 1.74, 2.15 and 3.58 MeV levels in B^{10} are clearly seen but there is no indication of any level near 2.86 MeV being formed.

A spectrum of the $Be^9(d,n\gamma)B^{10}$ neutrons in coincidence with γ-rays above a 1.6 MeV threshold was also recorded; these neutrons are coincident with B^{10} γ-rays of photopeak energies 2.15, 2.86 and 3.58 MeV. The spectrum, Fig. 63, was recorded in 97 hours under the same conditions as the previous one. The two prominent peaks are due to the formation of the 2.15 and 3.58 MeV levels in B^{10}. The very small peaks near channels 38 and 50 are attributed to the result of γ-ray summing in the NaI(Tℓ) crystal enabling the neutrons associated with the 0.72 and 1.74 MeV levels to be recorded. As in the previous spectrum there is no indication of a peak corresponding to any level near 2.86 MeV in B^{10}, although the energy resolution in both spectra is sufficient to enable such a peak to be resolved from the neighbouring ones.

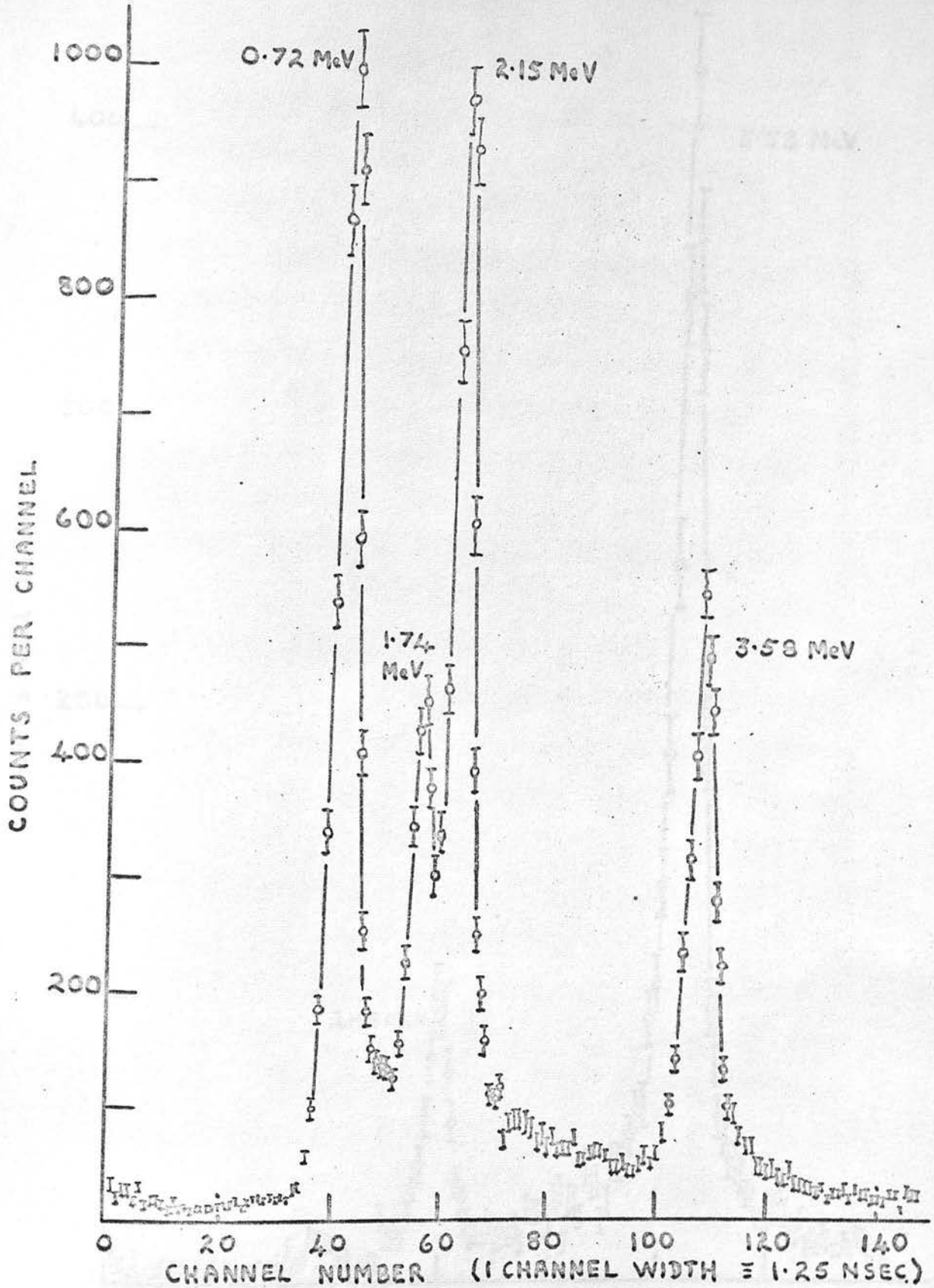

FIG. 62. THE SPECTRUM OF THE $Be^{9}(d,n\gamma)B^{10}$ NEUTRONS. COINCIDENT WITH THE B^{10} γRAYS ABOVE 0·35 MeV.

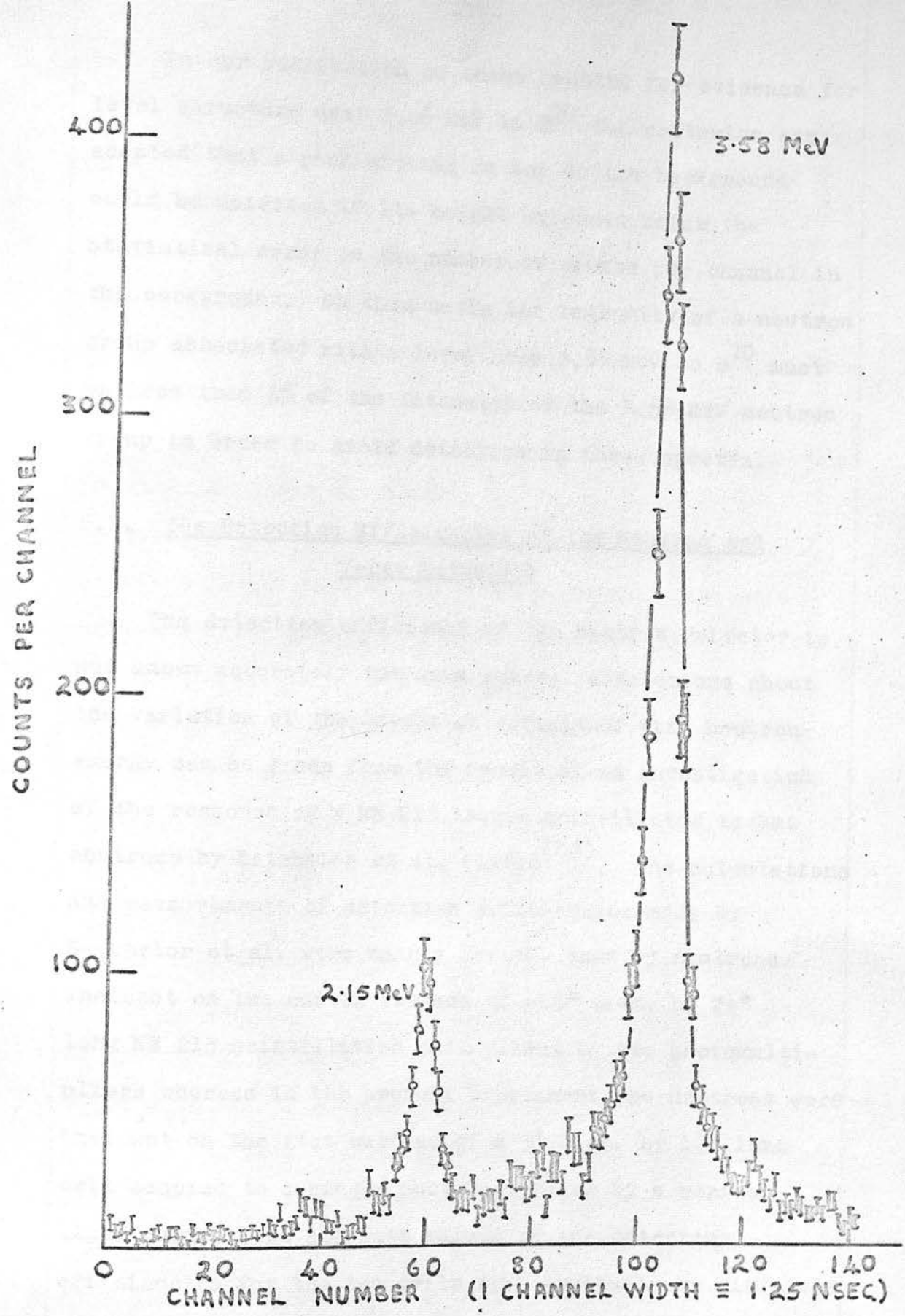

FIG. 63. THE SPECTRUM OF THE $Be^{9}(d,n\gamma)B^{10}$ NEUTRONS COINCIDENT WITH THE 2·15, 2·86 AND 3·58 MeV B^{10} γRAYS

In our examination of these spectra for evidence for level structure near 2.86 MeV in B^{10} the criterion was adopted that a peak sitting on top of the background could be detected if its height exceeded twice the statistical error in the number of counts per channel in the background. On this basis the intensity of a neutron group associated with a level near 2.86 MeV in B^{10} must be less than 3% of the intensity of the 3.58 MeV neutron group in order to avoid detection in these spectra.

6.2. The Detection Efficiencies of the Neutron and γ-ray Detectors

The detection efficiency of the neutron detector is not known accurately but some general conclusions about the variation of the detection efficiency with neutron energy can be drawn from the result of an investigation of the response of a NE 213 liquid scintillator to fast neutrons by Batchelor et al. (1961)[62]. The calculations and measurements of detection efficiencies made by Batchelor et al. were mainly for the case of neutrons incident on the curved surface of a 2" diam. by $2\frac{1}{2}$" long NE 213 scintillation cell viewed by two photomultipliers whereas in the present experiment the neutrons were incident on the flat surface of a 5" diam. by $1\frac{1}{2}$" long cell coupled to a single photomultiplier by a conical light guide. The absolute values of the detection efficiencies for the two cells will obviously be different

but it is expected that the variation of detection efficiency with energy will be similar in the two cases, since it is determined mainly by the variation of the (n,p) scattering cross-section with neutron energy[49,62]. The variation of the detection efficiency of the NE 213 scintillation spectrometer with neutron energy observed by Batchelor et al. is reproduced in Fig. 64. The neutron energy at which the detection threshold was set was determined by the discriminator thresholds in the slow and Owen channels of the spectrometer.

In the various spectra which were obtained, the relative intensities of the neutron groups associated with the 0.72, 1.74 and 2.15 MeV levels in B^{10} were always about the same, but the ratio of the intensity of the neutron group associated with the 3.58 MeV level to that of the group associated with the 0.72 MeV level varied from 1.1 in Fig. 30 to about 0.5 in Fig. 62. (See also Fig. 27.) The variation is attributed to differences in the settings of the thresholds in the slow and Owen channels of the spectrometer giving different values for the detection efficiency for the 1.25 MeV neutrons emitted in the formation of the 3.58 MeV level in B^{10}. Such large changes in the detection efficiency for the 1.25 MeV neutrons indicate that these neutrons were just above the detection threshold, and that in the spectra of Figs. 62 and 63, at least, the neutrons of higher energy associated with any level near 2.86 MeV in B^{10} should be detected more efficiently than those associated with the 3.58 MeV level.

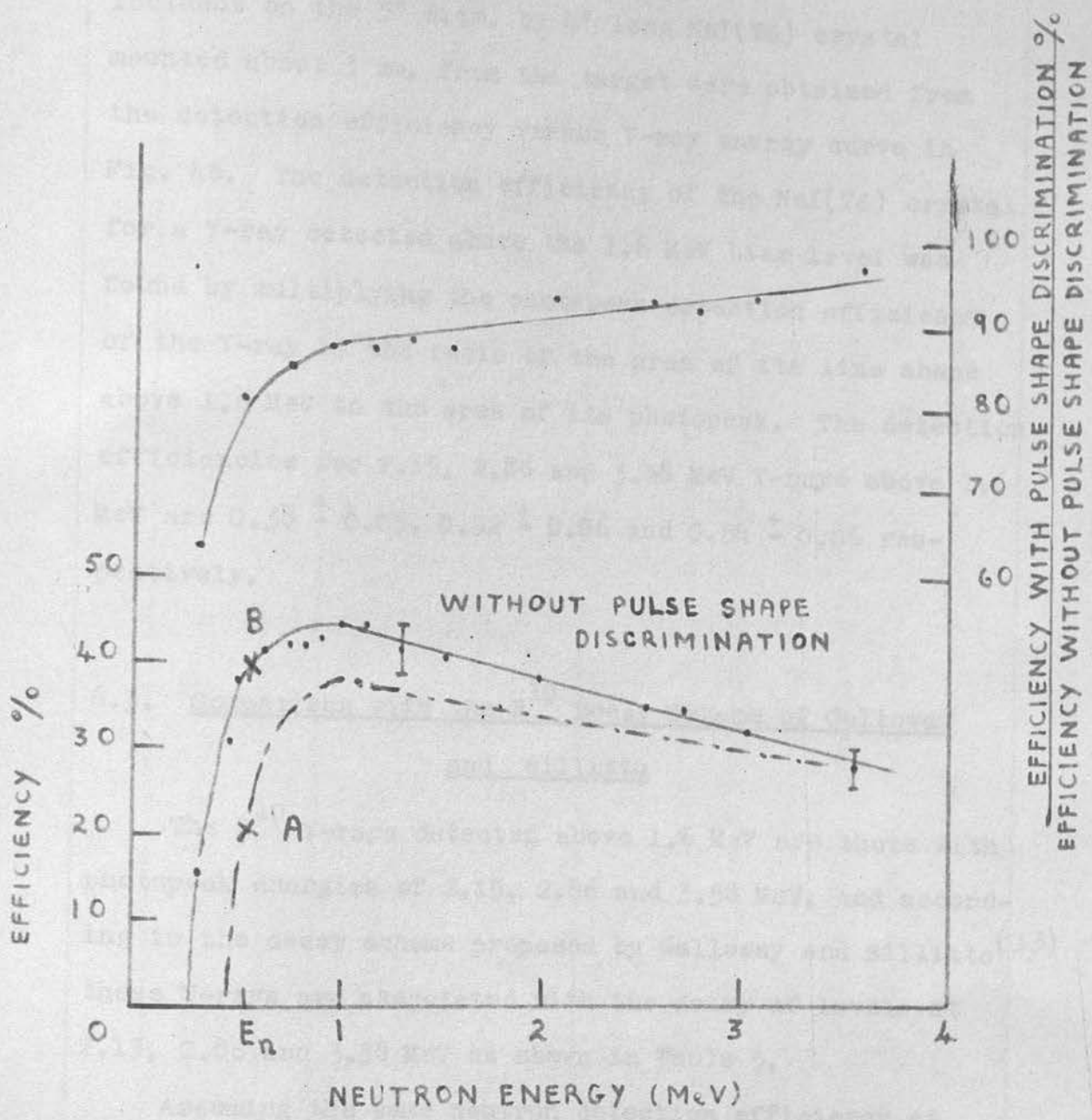

FIG. 64. TYPICAL VARIATION OF DETECTION EFFICIENCY OF A NE 213 SCINTILLATOR WITH NEUTRON ENERGY. THE DATA WERE TAKEN FROM BATCHELOR ET. AL. FOR A NEUTRON SCINTILLATOR 2" DIAM. BY 2½" LONG. THE DETECTION EFFICIENCY FOR A NEUTRON OF ENERGY E_n CAN VARY FROM A LOW VALUE AT "A" TO A HIGH VALUE AT "B" DUE TO A CHANGE IN THE DETECTION THRESHOLD.

The photopeak detection efficiencies for B^{10} γ-rays incident on the 5" diam. by 4" long NaI(Tℓ) crystal mounted about 3 cm. from the target were obtained from the detection efficiency versus γ-ray energy curve in Fig. 48. The detection efficiency of the NaI(Tℓ) crystal for a γ-ray detected above the 1.6 MeV bias level was found by multiplying the photopeak detection efficiency of the γ-ray by the ratio of the area of its line shape above 1.6 MeV to the area of its photopeak. The detection efficiencies for 2.15, 2.86 and 3.58 MeV γ-rays above 1.6 MeV are 0.38 ± 0.05, 0.52 ± 0.06 and 0.54 ± 0.06 respectively.

6.3. Comparison with the B^{10} Decay Scheme of Galloway and Sillitto

The B^{10} γ-rays detected above 1.6 MeV are those with photopeak energies of 2.15, 2.86 and 3.58 MeV, and according to the decay scheme proposed by Galloway and Sillitto[33] these γ-rays are associated with the decay of levels at 2.15, 2.86 and 3.58 MeV as shown in Table 5.

Assuming the same neutron detection efficiency at 2.86 MeV as at 3.58 MeV, and using the detection efficiencies calculated above for the B^{10} γ-rays above the 1.6 MeV bias level, it was estimated that according to the decay scheme proposed by Galloway and Sillitto, the intensity of the neutron group associated with the level at 2.86 MeV should be at least 66% of the intensity of the

Energy Level in B^{10} (MeV)	Energy of γ-ray from B^{10} in MeV			Calculated intensity of neutron group forming level in B^{10}
	2.15	2.86	3.58	
2.15	15	-	-	12 ± 2
2.86	5	35	-	41 ± 6
3.58	7	25	13	47 ± 7

Table 5. The numbers in columns 2, 3 and 4 of the table give the percentage of the B^{10} γ-rays of photopeak energies 2.15, 2.86 and 3.58 MeV, which are emitted in the decay of levels at 2.15, 2.86 and 3.58 MeV, distributed according to the energies of the γ-rays and levels. The data is based on the decay scheme proposed by Galloway and Sillitto[33].

group associated with the 3.58 MeV level in the spectrum shown in Fig. 63. However there is no indication of a neutron group associated with the hypothetical 2.86 MeV level in B^{10}, and the intensity of such a group must be less than 3% of the intensity of the 3.58 MeV neutron group to avoid detection. Possibly, due to difficulties in interpolation and extrapolation, the line shapes for the B^{10} γ-rays used by Galloway and Sillitto in the analysis of their γ-ray spectra were less accurate than expected, and this led to a misinterpretation of the data. In any case the neutron time-of-flight measurement gives direct evidence about the formation of the B^{10} levels in the $Be^9(d,n)B^{10}$ reaction, whereas γ-ray coincidence spectrometry gives only indirect evidence. This fact has been pointed out by Galloway (1959)[41] and Bradford (1962)[34].

We conclude that there is no evidence for level structure near 2.86 MeV in B^{10}.

6.4. Comparison with Other $Be^9(d,n)B^{10}$ Neutron Energy Spectra

The early work (summarized in Chapter 1) on the $Be^9(d,n)B^{10}$ neutron energy spectrum was carried out using very inefficient techniques which made it difficult to obtain spectra of good statistical accuracy. Bayman (1954)[63] has studied the effect of statistical fluctuations on spectra of poor statistical accuracy by considering

frequency distributions obtained by random sampling of a well-defined parent distribution. His work indicates that spurious peaks could be observed in spectra of similar statistical accuracy to the early energy spectra of the $Be^9(d,n)B^{10}$ neutrons, even when such spectra were smoothed over several channels. Also if the peaks result from purely random fluctuations in the number of counts per channel, then one would expect these spurious peaks to occur at different energies in different spectra. It is interesting to note that the peaks in spectra, which have been attributed to level structure near 2.8 MeV in B^{10}, have been seen at various energies between 2.7 MeV and 3.2 MeV, and on occasions it has been suggested that there are two levels near 2.7 and 3.1 MeV. The most likely explanation of the peaks near 2.86 MeV in B^{10} in the $Be^9(d,n)B^{10}$ neutron energy spectra is that they are due to statistical fluctuations in the background. Whether or not this is the complete explanation of these peaks does not alter our conclusions. Any level in B^{10} formed with sufficient intensity for the neutron group to be detected in earlier spectra would certainly be detected in the present experiment.

Recently in this laboratory, Maydan (1965)[64] obtained a time-of-flight spectrum of the neutrons from the $Be^9(d,n)B^{10}$ reaction for 600 keV deuterons using the beam-pulsing system which he fitted to the accelerator. This spectrum showed no evidence for any level structure near 2.86 MeV in B^{10}.

We conclude that the recent time-of-flight spectra of the $Be^{9}(d,n)B^{10}$ neutrons, which have been obtained with good statistical accuracy and with adequate energy resolution, provide no evidence for the formation of any level near 2.86 MeV in B^{10}.

CHAPTER 7

THE γ-RAY DECAY OF THE 3.58 MeV LEVEL IN B^{10}

The n-γ coincidence time-of-flight spectrometer was used to measure the branching ratios for the γ-ray decay of the 3.58 MeV level in B^{10}. In section 7.1 a description is given of the experimental arrangement and the setting up of the spectrometer to select the γ-rays which were coincident with the neutron group emitted in the formation of the 3.58 MeV level in the $Be^{9}(d,n\gamma)B^{10}$ reaction. Also described in this section is a simple check on the operation of the spectrometer which was made using Na^{22} and Po - Be sources. The spectrum of the γ-rays from the decay of the 3.58 MeV level is presented in section 7.2. The spectrum was analysed to give the branching ratios of the 3.58 MeV level using cascade line shapes which were calculated, taking into account summing of pairs of γ-rays in each cascade, from the interpolated line shapes for the B^{10} γ-rays. The present measurements are compared with other measurements of the branching ratios and with theoretical calculations of the ratios in section 7.3.

7.1. The Experimental Arrangement for Observing the γ-rays from the 3.58 MeV Level in B^{10}

The spectrometer was set up around the Be^{9} target as shown in Fig. 65. Since there is no level structure between the 2.15 and 3.58 MeV levels in B^{10}, the detection

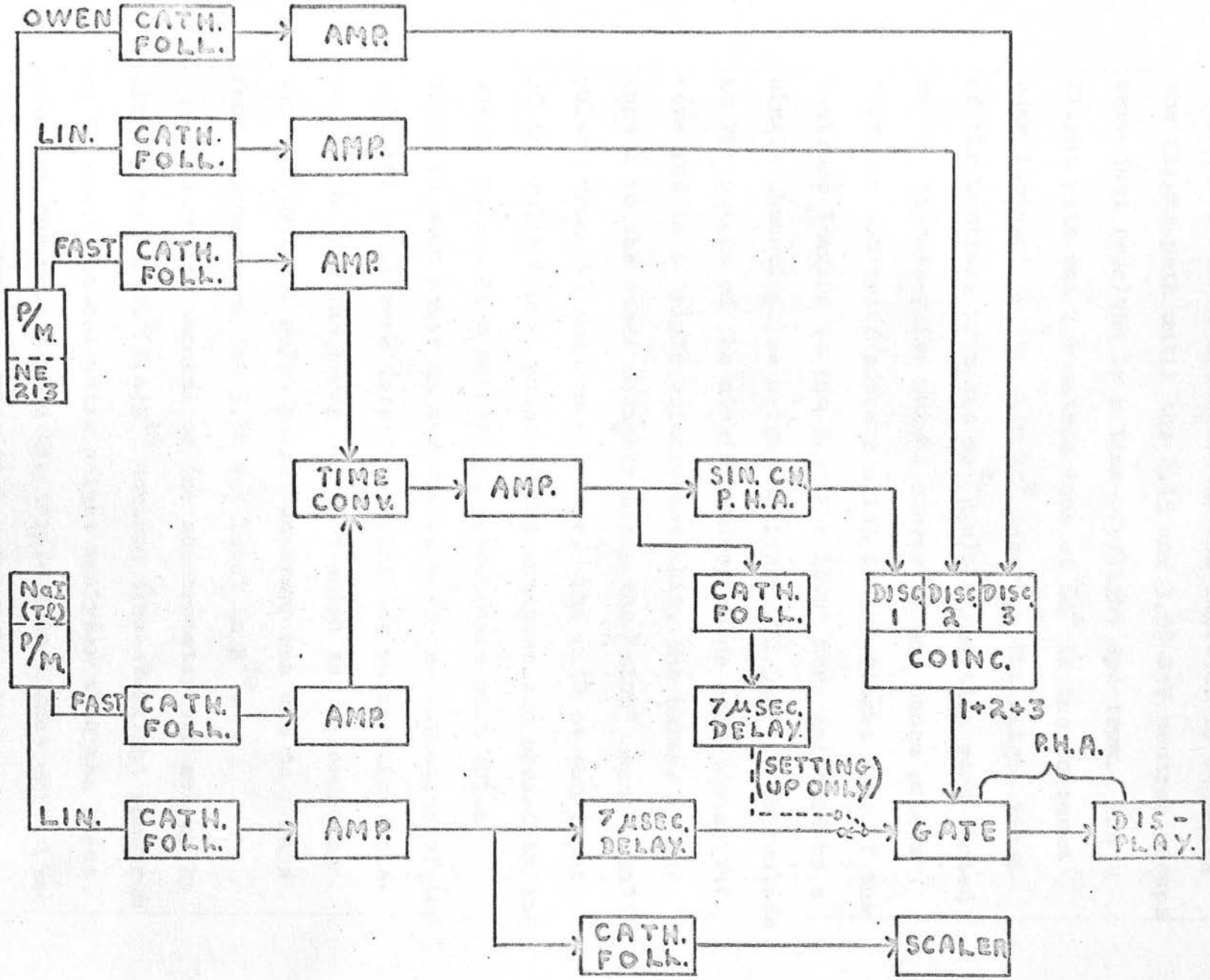

FIG. 6-5 NEUTRON TIME-OF-FLIGHT SPECTROMETER FOR BRANCHING RATIO MEASUREMENTS.

efficiency of the spectrometer was improved by reducing the flight path until the 2.15 and 3.58 MeV neutron groups were just resolved in a time-of-flight spectrum. The flight path was 1.6 metres long at 60° to the deuteron beam incident on the thin Be^9 target. The flight times of the neutrons from the $Be^9(d,n)B^{10}$ reaction were sorted by the time-to-pulse height converter and those pulses from the converter corresponding to the flight time of the neutrons leading to the 3.58 MeV level were selected by a single channel pulse height analyser (NE 5103). The pulses at the output of the single channel pulse height analyser were fed to a triple coincidence unit, the pulses at the inputs to the other channels being the "slow" and "Owen" pulses from the neutron detector. The gate at the input of the multichannel pulse height analyser was opened by the output pulses from the triple coincidence unit which occurred when neutrons associated with the formation of the 3.58 MeV level were detected. Thus the pulse height distribution from the γ-ray detector which was recorded by the multichannel pulse height analyser was due to γ-rays from the decay of the 3.58 MeV level in B^{10}.

The gating channel of the spectrometer was set up by displaying the $Be^9(d,n)B^{10}$ neutron time-of-flight spectrum on the multichannel pulse height analyser with the input gated by the pulses from the triple coincidence unit. (See dotted connection in Fig. 65.) When the single channel pulse height analyser was operated as a simple discriminator

with a very low threshold bias, all of the $Be^{9}(d,n\gamma)B^{10}$ neutron groups were recorded in the gated spectrum. The spectrum, Fig. 66, was recorded in 15 mins. using a deuteron beam current of about 0.1 μA. The position and width of the window of the single channel pulse height analyser was adjusted to select the 3.58 MeV neutron group. The setting of the gating channel is indicated in position A in Fig. 66.

The time-of-flight spectrum, Fig. 66, as well as showing the setting of the gating channel on the neutron group associated with the 3.58 MeV level, shows that the triple coincidence part of the spectrometer was operating correctly. A further check on the operation of the spectrometer was made using radioactive sources. The spectrometer was set up to record γ-ray spectra gated by the triple coincidence requirements and a 0.2 mC Na^{22} source which emits annihilation γ-rays and 1.28 MeV γ-rays was placed midway between the γ-ray and neutron detectors. No pulses were recorded by the multichannel pulse height analyser confirming that the pulse shape discrimination circuits were operating correctly. (There is no prompt coincidence peak due to γ-ray coincidences in the time-of-flight spectrum shown in Fig. 66).

In addition to the Na^{22} source a 0.4 μC Po - Be neutron source was placed as near as possible to the neutron scintillator giving a neutron counting rate of about 30 counts per sec. The Po - Be source was very weak

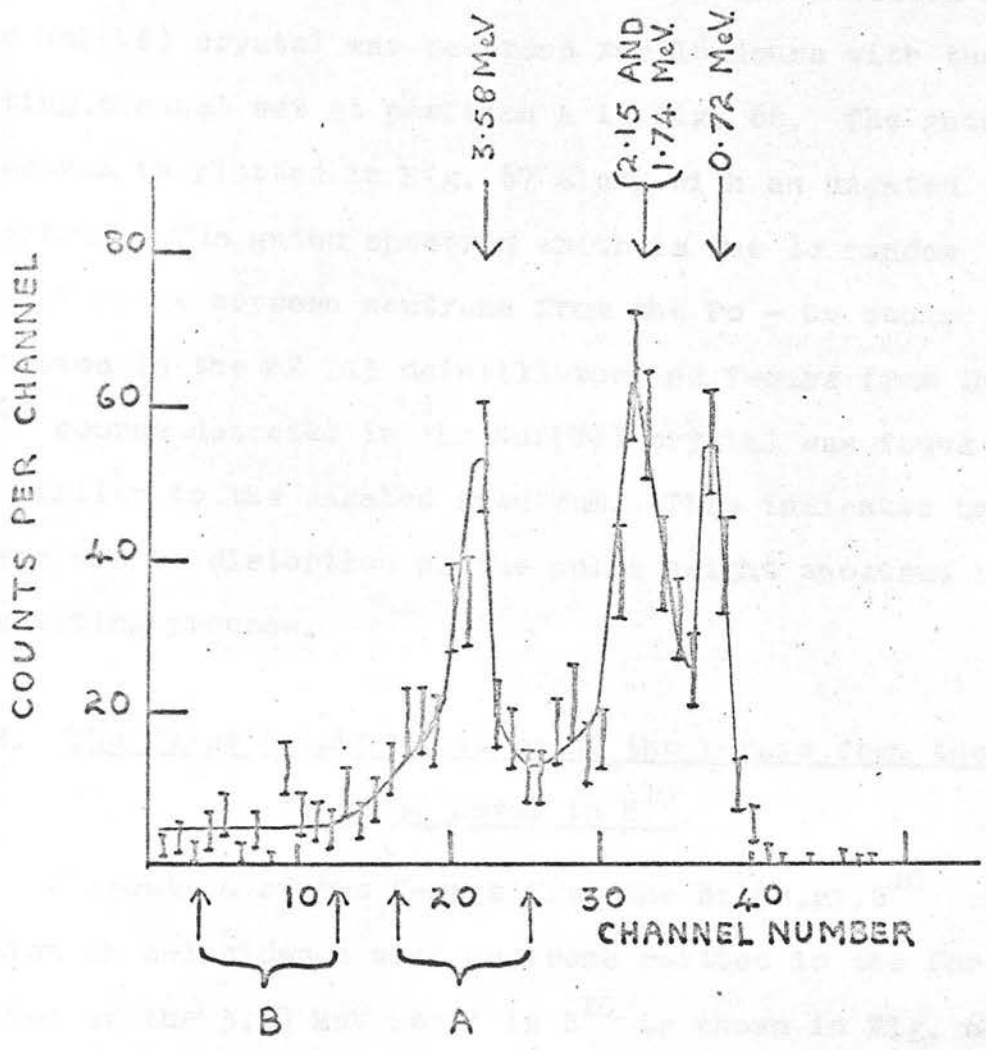

FIG 66 A TIME-OF-FLIGHT SPECTRUM OF THE $Be^{9}(d,n\gamma)B^{10}$ NEUTRONS.

A - POSITION OF GATING CHANNEL ON THE 3·58 MeV GROUP.

B - POSITION OF GATING CHANNEL ON THE BACKGROUND.

and was also far away from the γ-ray scintillator so that very few γ-rays from the source were detected in the NaI(Tℓ) crystal. A spectrum of the γ-rays detected in the NaI(Tℓ) crystal was recorded for 18 hours with the gating channel set at position A in Fig. 66. The gated spectrum is plotted in Fig. 67 along with an ungated spectrum. The gated spectrum which is due to random coincidences between neutrons from the Po - Be source detected in the NE 213 scintillator and γ-rays from the Na^{22} source detected in the NaI(Tℓ) crystal was found to be similar to the ungated spectrum. This indicates that there was no distortion of the pulse height spectrum in the gating process.

7.2. The Pulse Height Spectrum of the γ-rays from the 3.58 MeV Level in B^{10}.

A spectrum of the γ-rays from the $Be^{9}(d,n\gamma)B^{10}$ reaction in coincidence with neutrons emitted in the formation of the 3.58 MeV level in B^{10} is shown in Fig. 68. This spectrum was recorded in 36 hours using a deuteron beam current of about 0.1 μA. The setting of the gating channel on the 3.58 MeV neutron group was checked at frequent intervals during the run, but it was found that no adjustments were necessary.

The background in the spectrum due to random coincidences was estimated by setting the 'gating channel' on the flat background at B in the time-of-flight spectrum shown in Fig. 66. A spectrum of the γ-rays

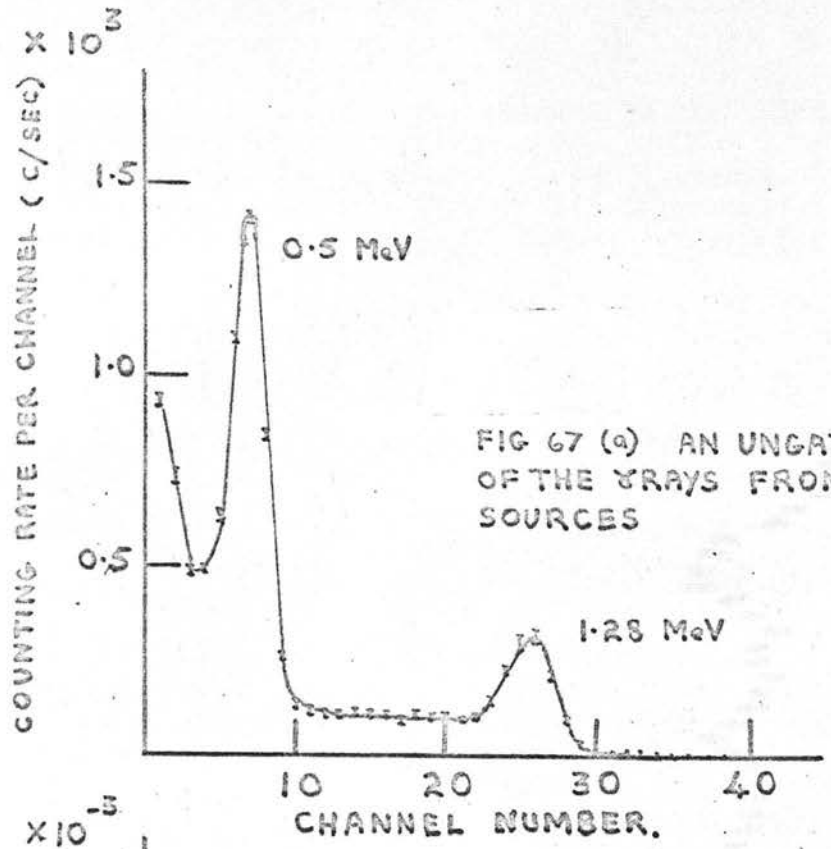

FIG 67 (a) AN UNGATED SPECTRUM OF THE γRAYS FROM Na^{22} AND Po-Be SOURCES

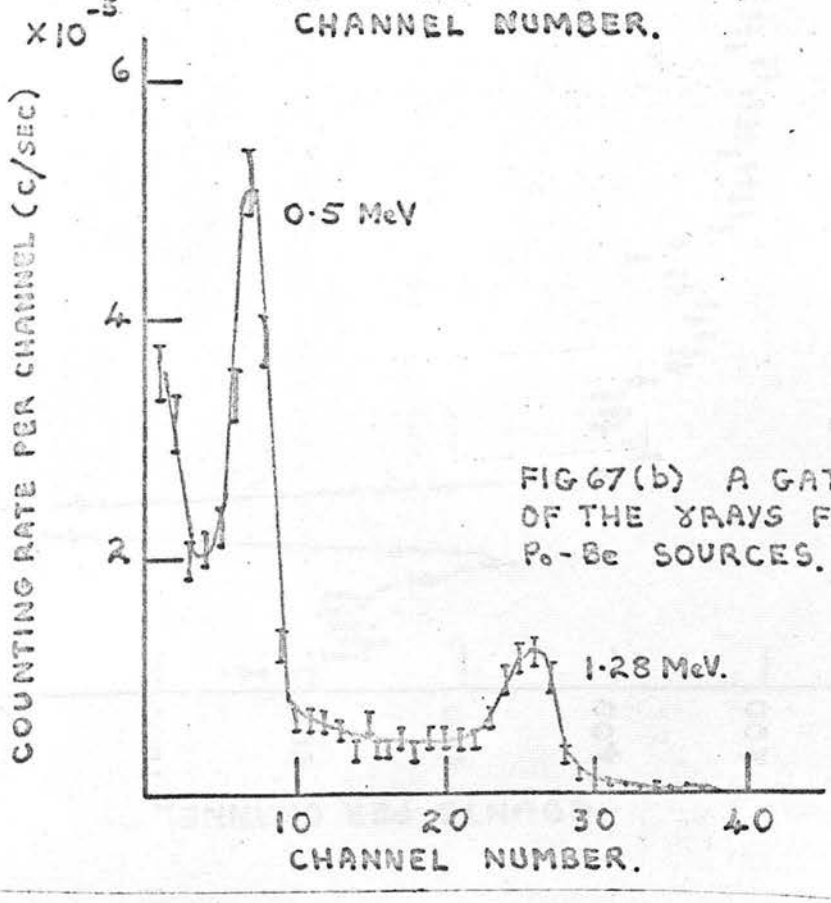

FIG 67 (b) A GATED SPECTRUM OF THE γRAYS FROM Na^{22} AND Po-Be SOURCES.

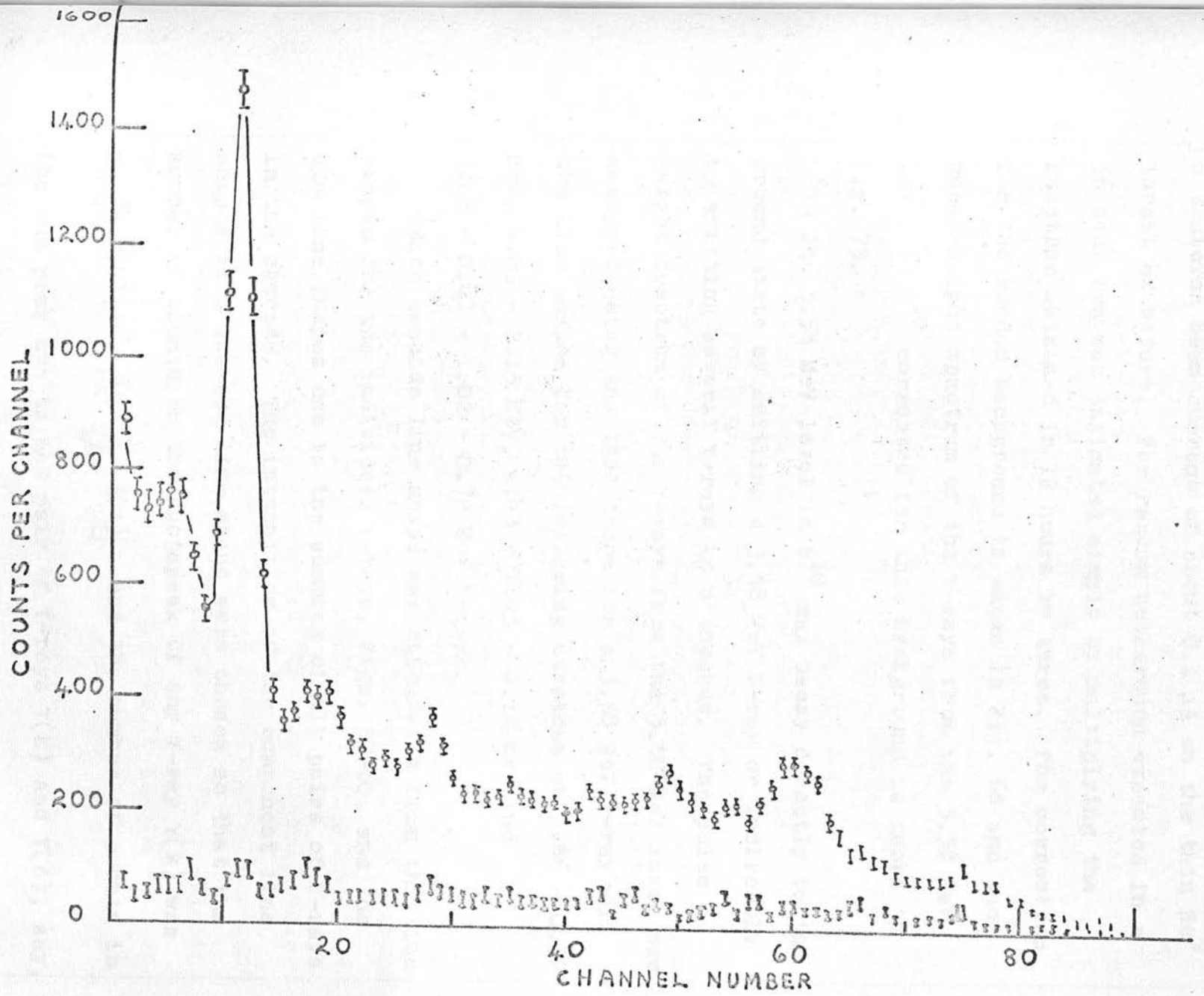

FIG 68 THE SPECTRUM OF THE γRAYS FROM THE DECAY OF THE 3·58 MeV LEVEL IN B^{10}. THE CORRECTION FOR BACKGROUND IS ALSO SHOWN.

coincident with the neutrons in the background of the time-of-flight spectrum was recorded for 12 hours using a deuteron beam current of about 0.1 μA on the thin Be^9 target as before. The random background expected in a 36 hour run was estimated simply by multiplying the spectrum obtained in 12 hours by three. The correction for the random background is shown in Fig. 68 and the pulse-height spectrum of the γ-rays from the 3.58 MeV level in B^{10} corrected for this background is shown in Fig. 73.

The 3.58 MeV level in B^{10} may decay directly to the ground state by emitting a 3.58 MeV γ-ray or indirectly by emitting several γ-rays in a cascade. The pulse height spectrum of the γ-rays from the 3.58 MeV level was analysed using the line shape for a 3.58 MeV γ-ray and the line shapes for the following cascades of 2.86 - 0.72 MeV, 1.43 - 2.15 MeV, 1.43 - 1.43 - 0.72 MeV and 1.43 - 0.41 - 1.02 - 0.72 MeV γ-rays.

Each cascade line shape was calculated from the line shapes for the individual γ-rays, Figs. 57-60, and the sum line shapes due to the summing of all pairs of γ-rays in the cascade. The intensities of the component line shapes in a cascade line shape were chosen so that the number of counts in the photopeak of any γ-ray $\gamma(k)$ was $N_o \frac{\omega}{4\pi} f(k)\left[1 - \frac{\omega}{4\pi} \sum_{i \neq k} f(i)\right]$ and the number of counts in the sum peak due to any pair of γ-rays $\gamma(k)$ and $\gamma(\ell)$, say,

was $N_o(\frac{\omega}{4\pi})^2 f(\ell)\ f(k)$, as described in section 5.1. The number N_o of cascades of each type was arbitrarily chosen as 10^5. The computer program which was written to calculate the cascade line shapes from the individual shapes is given in Appendix III. The calculated cascade line shapes are shown in Figs. 69-72.

The accuracies of the cascade line shapes were estimated taking into account the statistical inaccuracies of the lines shapes Figs. 57-60 and the photopeak detection efficiencies of the γ-rays. In the calculation of the sum line shape for a pair of γ-rays emitted in a cascade, it was assumed that there was no angular correlation between the directions of emission of the two γ-rays. In the case of the B^{10} γ-rays, the γ-ray coincidence experiments of Shafroth and Hanna (1954)[31] and more recently Segel et al. (1966)[40] indicate that the angular anisotropies are less than 10 - 15% for pairs of B^{10} γ-rays.

The analysis of the pulse height spectrum of the γ-rays from the 3.58 MeV level in terms of the cascade line shapes is shown in Fig. 73. The curve which is synthesised from the five cascade line shapes, fits the experimental points well over most of the spectrum, but the fit is not so good in the energy range from 2.0 to 2.5 MeV. However, it seems probable that the fit could be improved if triple summing which occurs when three γ-rays of a cascade interact simultaneously with the NaI(Tℓ) crystal, were taken into

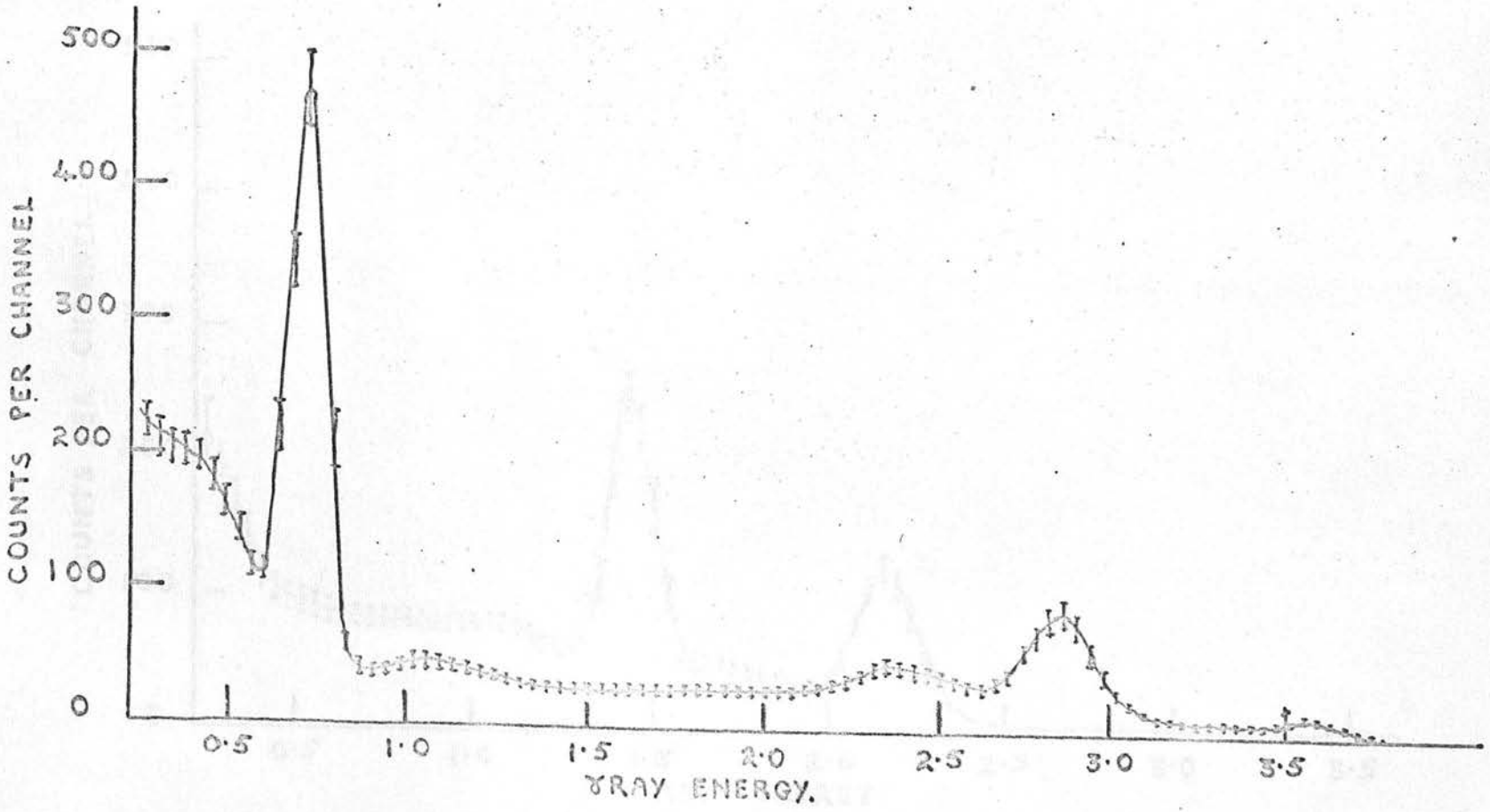

FIG. 61 THE LINE SHAPE FOR THE 2·86 - 0·72 MeV CASCADE.

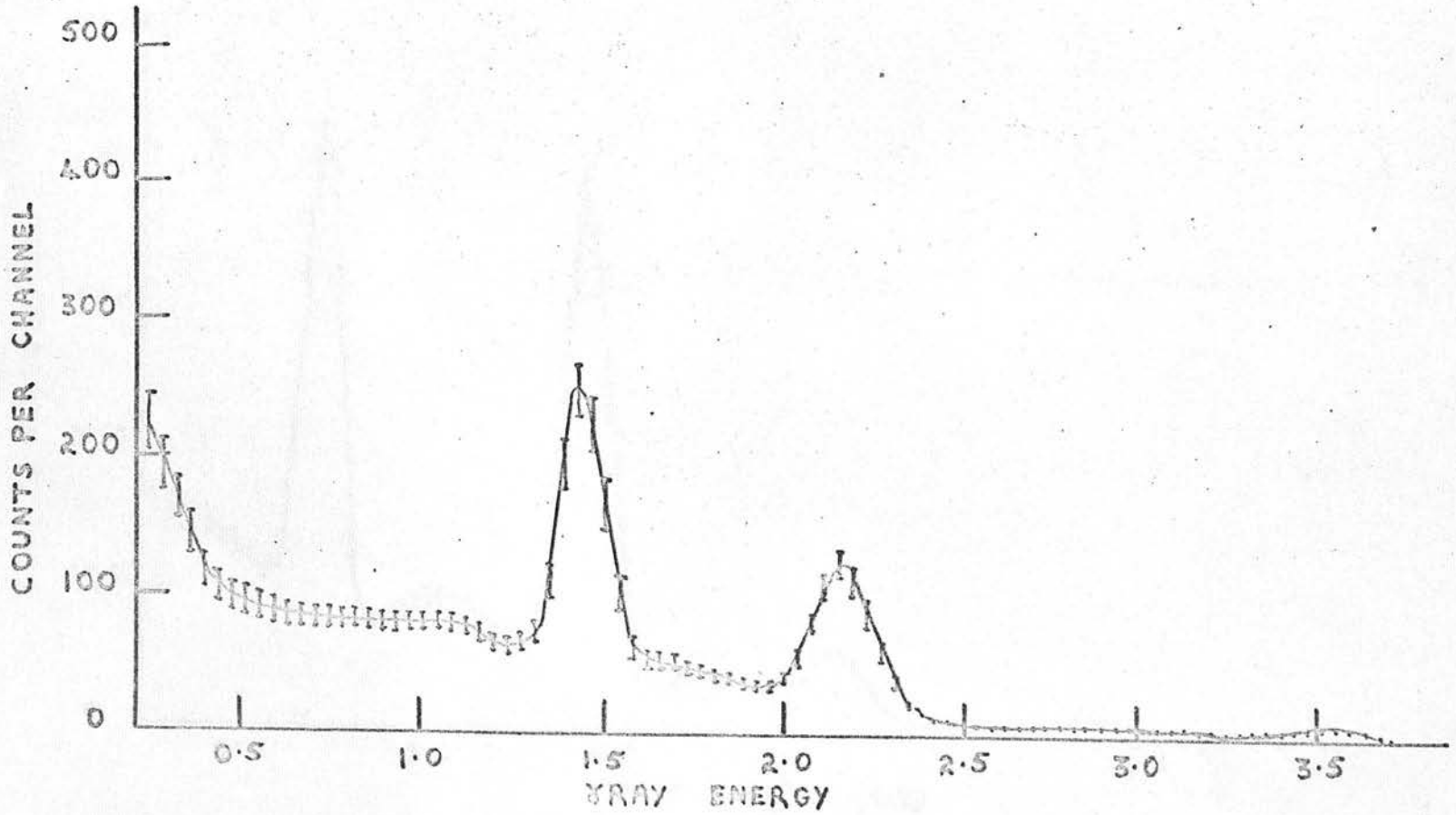

FIG. 70. THE LINE SHAPE FOR THE 1·43 – 2·15 MeV CASCADE

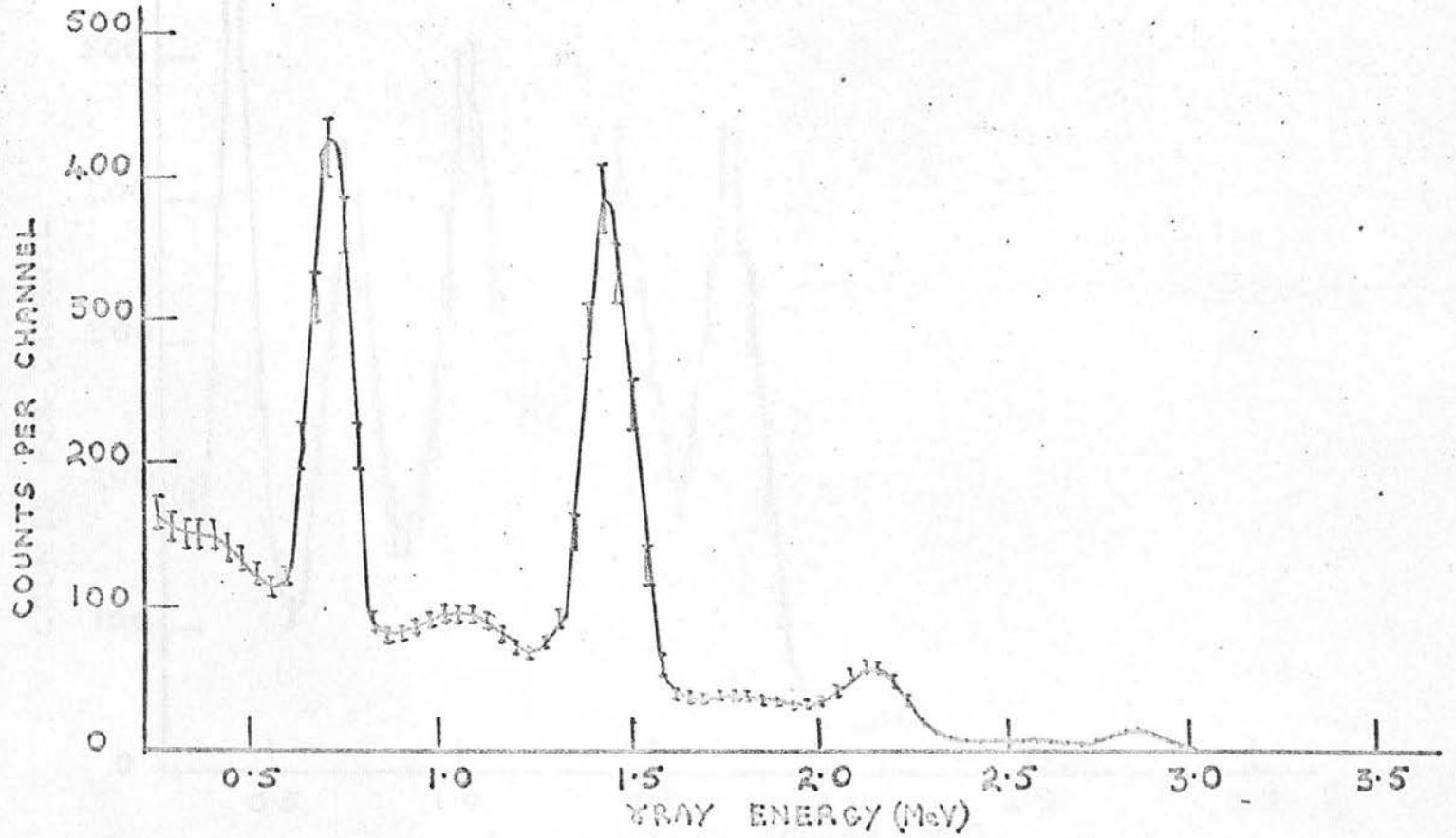

FIG. 71 THE LINE SHAPE FOR THE 1·43 - 1·43 - 0·72 MeV CASCADE.

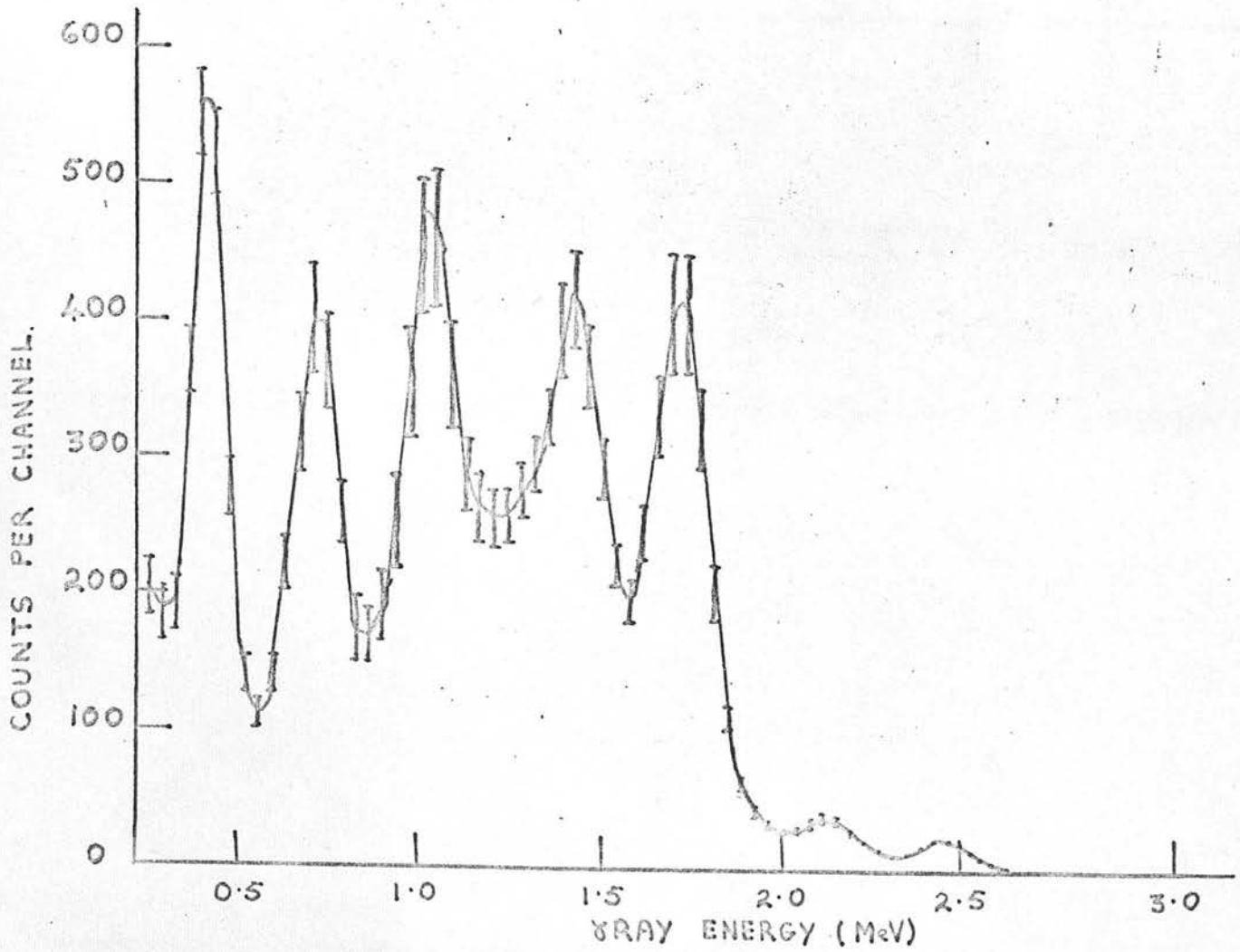

FIG. 72. THE LINE SHAPE FOR THE 1·43-0·41-1·02-0·72 MeV CASCADE.

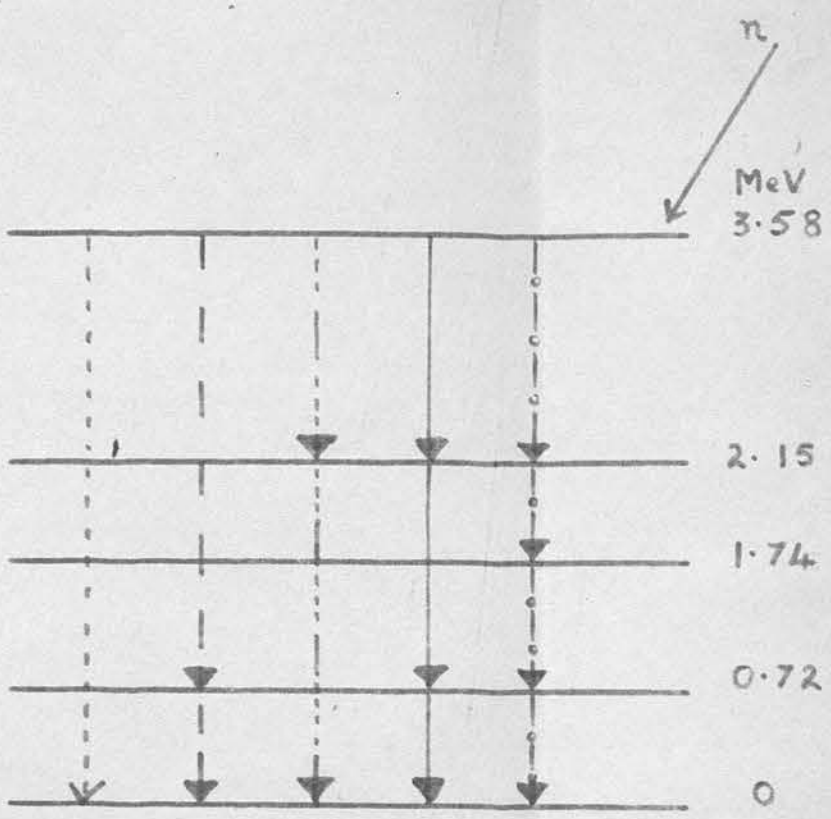

THE γ-RAY CASCADES FROM THE 3·58 MeV LEVEL IN B^{10}.

FIG. 73. THE SPECTRUM OF THE γ-RAYS FROM THE 3·58 MeV LEVEL IN B^{10}.

account. The only cascades in which triple summing can occur are the 1.43 - 1.43 - 0.72 and 1.43 - 0.41 - 1.02 - 0.72 MeV γ-ray cascades giving sum peaks at 3.58 MeV (1.43 - 1.43 - 0.72), 3.17 MeV (1.43-1.02-0.72), 2.86 MeV (1.43 - 0.41 - 1.02), 2.56 MeV (1.43 - 0.41-0.72) and 2.15 MeV (0.41 - 1.02 - 0.72). Normally triple sum peaks are weak, but in those cases where both the 0.41 MeV and the 0.72 MeV γ-rays are detected (with a high detection efficiency) along with another γ-ray, the triple sum peak may be sufficiently intense to enable it to be observed in the spectrum.

The relative intensities of the cascades emitted in the decay of the 3.58 MeV level determined from the analysis of the spectrum in Fig. 73, are given in Table 6.

Cascade identified by γ-ray energies in MeV.	Relative Intensity %
3.58	19 ± 4
2.86 - 0.72	70 ± 7
1.43 - 2.15	3.6 ± 1.8
1.43 - 1.43 - 0.72	3.0 ± 1.5
1.43 - 0.41 - 1.02 - 0.72	4.5 ± 0.9

Table 6. The relative intensities of the cascades emitted from the 3.58 MeV level in B^{10}.

The relative intensities given in the above table have not been corrected for absorption of the B^{10} γ-rays

in the target, the target holder and the photomultiplier housing. Bradford (1962)[34] found such a correction was very small, and as there is less absorbing material between the target and NaI(Tℓ) crystal in the present experimental arrangement, it was decided that a correction for absorption was unnecessary.

The relative intensities of the cascades decaying through the 2.15 MeV level give the 0.41 : 1.43: 2.15 branching ratio of the level as $40 \pm 8 : 26 \pm 13 : 32 \pm 16$. These admittedly inaccurate values of the branching ratio agree with the values obtained by other workers, Table 1.

The percentage of the cascades decaying through the 2.15 MeV level was determined from the sum of the contributions from the three cascades. Although the relative intensities of the three cascades can be altered over a wide range of values, the total intensity of the three cascades can only be altered by about $\pm$ 20% without spoiling the fit of the synthesised curve to the experimental points. The relative intensities of the cascades from the 3.58 MeV level in B^{10} decaying directly to the ground state and through the 0.72 MeV and 2.15 MeV levels were determined as $19 \pm 4 : 70 \pm 7 : 11 \pm 2$.

7.3. Discussion of Experimental Measurements

It was pointed out in Chapter 1 that the reliability of the measurements of the branching ratios for the 3.58 MeV level in B^{10} given in Table 1, depended on whether there is a level at 2.86 MeV or not. As no level structure

has been found near 2.86 MeV in B^{10} all of the measurements except those of Galloway and Sillitto[33] are free from criticism on this score. If we disregard the measurements of Galloway and Sillitto, the remaining measurements indicate that the ratio of the intensities of the 3.58 and 2.86 MeV γ-rays from the decay of the 3.58 MeV level is about 1 : 4. The results presented here are in complete agreement with this conclusion.

Evidence for a transition between the 3.58 and 1.74 MeV levels by emission of a 1.84 MeV γ-ray has been reported by Singh (1959)[37] and Hornyak et al. (1964)[38]. The analysis of the γ-ray spectrum in the present experiment was performed without including a 1.84 MeV γ-ray line shape. In fact the spectrum of Fig. 73 could not be analysed satisfactorily using the branching ratios proposed by Hornyak et al. As the evidence for a 1.84 MeV γ-ray has been obtained only when large NaI(Tℓ) crystals were used to detect the γ-rays, the peaks in the spectra attributed to 1.84 MeV γ-rays may possibly be due to the summing of B^{10} γ-rays in the crystal.

Singh (1959) used a scintillation detector with a NaI(Tℓ) crystal 5" diam. by 6" long to detect the B^{10} γ-rays and therefore the peak at 1.84 MeV which he attributed to a 1.84 MeV γ-ray may be explained by the summing of the 0.72 MeV and 1.02 MeV γ-rays and also the 0.41 MeV and 1.43 MeV γ-rays.

The NaI(Tℓ) crystals used by Hornyak et al. in their

coincidence experiments were 7.6 cm. diam. by 7.6 cm. long. They state that a correction for summing of the 0.72 and 1.02 MeV γ-rays from the decay of the 1.74 MeV level was made but there is no mention of a correction for the summing of the 1.43 and 0.41 MeV γ-rays. It seems possible therefore that part of the small peak at 1.84 MeV in their γ-ray spectrum could be attributed to the summing of the 1.43 and 0.41 MeV γ-rays from the decay of the 3.58 MeV level in B^{10}.

Recently, Segel et al. (1966)[40] have measured, using a γ-ray coincidence technique, the branching ratio of the 3.58 MeV level in B^{10} which was populated by the $B^{10}(p,p'\gamma)B^{10}$ reaction. The value of 12 : 76 : 12 (3.58 : 2.86 : 1.43) which they obtained and the value of 19 : 70 : 11 from the present measurement of the branching ratio of the 3.58 MeV level agree very well. Segel et al. have also made a search for γ-ray transitions from the 3.58 MeV level to the 1.74 MeV level, and they conclude that the branching ratio for this transition is less than 0.3% of the total decay. It is interesting to note that these values for the branching ratio are in fair agreement with the value of 20 : 60 : 20 first proposed by Ajzenberg-Selove and Lauritsen in 1955[1].

A value for the 3.58 MeV branching ratio was calculated in 1957 by Kurath[65] using the intermediate coupling model for the nuclei in the 1p shell proposed by Inglis[66]. The energy level scheme for B^{10} predicted by this model depends on a parameter a/K which measures the

relative spin-orbit and central energy contributions to the excitation energy of the nucleus. The level scheme calculated for $^{a}/K = 4.5$ gives a fairly good fit to the experimental data, but the corresponding branching ratio for the 3.58 MeV level in B^{10} does not agree with the experimental values. The branching ratios of the 3.58 MeV and 2.15 MeV levels are recorded in Table 7.

More recently Cohen and Kurath (1965)[67] have calculated 3.58 MeV branching ratios using effective interactions for the nucleons in the 1p shell for j-j and L-S coupling schemes. The interaction parameters were determined using the experimental values of the excitation energies of the levels in the nuclei of the 1p shell and also the binding energies of the ground states of the nuclei relative to the $(1s)^4$ core. The energy level schemes for B^{10} agree fairly well with the experimental data for both treatments. The branching ratio for the 3.58 MeV level calculated using data taken from nuclei of mass numbers 8 to 16 are recorded in Table 7 for the j-j coupling scheme (the parameters of this scheme are the two-body matrix elements, 2BME) and the L-S coupling scheme of the nucleons in a potential well (POT). Similar calculations were carried out for the j-j scheme using data from the nuclei of mass numbers 6 to 16, and the branching ratio obtained for the 3.58 MeV level is recorded in Table 7.

The calculations of the branching ratios by Cohen

Transition	Kurath[65]	Kurath and Cohen[67]			Experiment
	Inglis $^{a}/K = 4.5$	(8-16)POT	(8-16)2BME	(6-16)2BME	
3.58 → 0	66	71	41	0	19
3.58 → 0.72	33	14	32	23	70
3.58 → 2.15	1	15	27	77	11
2.15 → 0	6	-	not calculated	-	25
2.15 → 0.72	12 (13)*	35	34	23	25 (33)*
2.15 → 1.74	82 (17)*	65	66	77	50 (67)*

Table 7. Branching ratios of the 3.58 MeV and 2.15 MeV levels in B^{10}. (Notation as in reference (67)).

* These figures give the percentage of the decays of the 2.15 MeV level to the 0.72 MeV level and the 1.74 MeV level.

and Kurath were for M1 transitions only, and therefore the value of the branching ratio for the 2.15 MeV level does not include the decay to the ground state. The data for the 2.15 MeV level is also recorded in Table 7.

The calculated and experimental values for the branching ratio for the 3.58 MeV level in B^{10} do not agree. In the case of the 2.15 MeV branching ratio the agreement between the experimental value and the values calculated by Cohen and Kurath using data obtained from nuclei between the mass numbers 8 and 16, is very good. However, Cohen and Kurath state in their article on the branching ratios that they do not expect very good agreement between the calculated and experimental values for the branching ratios in all cases, since the values are extremely sensitive to the wave function used in the calculation.

7.4. Conclusion

The present investigation indicates that the decay scheme for B^{10} has energy levels at 0.72, 1.74, 2.15 and 3.58 MeV. The 3.58 MeV level decays directly to the ground state, the 0.72 MeV level and the 2.15 MeV level with a branching ratio of $19 \pm 4 : 70 \pm 7 : 11 \pm 2$. No evidence is presented for γ-ray transitions between the 3.58 MeV and the 1.74 MeV levels, but the present measurements would not be inconsistent with a branching ratio of less than 3% for the decay of the 3.58 MeV level to the

1.74 MeV level. The calculated values for the branching ratio of the 3.58 MeV level do not agree with the experimental values. The value for the 3.58 MeV branching ratio from the present experiment is consistent with the generally accepted branching ratio for the 2.15 MeV level of 25 ; 25 : 50 for γ-ray transitions to the ground state, the 0.72 MeV level and the 1.74 MeV level in B^{10} respectively.

CHAPTER 8

SUGGESTIONS FOR THE EXPERIMENTAL INVESTIGATION OF SOME PROPERTIES OF THE C^{11} NUCLEUS.

Energy levels are known to exist at 2.00, 4.32, 4.81, 6.35 and 6.49 MeV in C^{11} (2) and the γ-ray decay of these levels has been investigated by Freeman (1962)(68) using the $B^{10}(d,n\gamma)C^{11}$ reaction and by Roush et al. (1965)(69) using the $Be^{9}(He^{3},n\gamma)C^{11}$ reaction. In his article Freeman states that although the value of $\frac{3}{2}$ is generally favoured for the spin of the 4.81 MeV level in C^{11}, a value of $\frac{1}{2}$ can not be rejected on the basis of the experimental evidence, since the spin value assigned to the level depends on the type of reaction mechanism used to interpret the angular distribution of the neutrons associated with the level. However, Freeman points out that the discovery of an anisotropy in the γ-rays from the decay of the level would be sufficient to rule out a spin of $\frac{1}{2}$.

It is proposed that the neutron time-of-flight spectrometer should be used to measure the angular distribution of the 4.81 MeV γ-rays from the decay of the third excited state in C^{11} populated by the $B^{10}(d,n\gamma)C^{11}$ reaction. It would appear to be sufficient to select the γ-rays coincident with the neutron groups associated with the 4.32 and 4.81 MeV levels, and therefore a short flight path could be used to give a high detection efficiency. Since the photopeak of the 4.81 MeV γ-rays should be entirely clear of all the other γ-rays emitted from the

4.32 and 4.81 MeV levels, it should be possible to determine the intensity of the 4.81 MeV γ-ray by measuring the area of its photopeak without an elaborate analysis of the γ-ray spectrum being necessary.

In order to carry out the proposed experiment it will be necessary to design a collimator which will define the solid angle subtended by the NaI(Tℓ) crystal at the target more precisely. Also it will be necessary to monitor the $B^{10}(d,n)C^{11}$ reaction rate during the measurement of the angular distribution of the 4.81 MeV γ-ray.

Roush et al. have shown that the 6.35 MeV level in C^{11} decays directly to the ground state and through intermediate states at 2.00 and 4.43 MeV. The energy resolution in γ-ray spectra obtained using NaI(Tℓ) crystals is not good enough to distinguish between the decay of the 6.35 MeV level through the 2.00 MeV level with the emission of 4.35 and 2.00 MeV γ-rays in cascade and the decay through the 4.32 MeV level with the emission of 2.03 and 4.32 MeV γ-rays. Therefore the 6.35 MeV level has been shown to decay directly to the ground state and by the emission of γ-ray cascades with a branching ratio of 65 : 35. Roush et al. suggest that the intermediate level in the γ-ray cascade is the one at 2.00 MeV, since this would be consistent with the level at 6.35 MeV in C^{11} being the analogue of the level at 6.81 MeV in the mirror nucleus, B^{11}. However it would be desirable to investigate this experimentally. An examination of the

γ-rays from the decay of the C^{11} energy levels, using a lithium-drifted-germanium detector, with high energy resolution, should be able to resolve this ambiguity about the decay of the 6.35 MeV level in C^{11}.

ACKNOWLEDGEMENTS

I wish to thank Professor N. Feather, F.R.S. for his encouragement and for the facilities provided for this experiment, and also Mr. R.M. Sillitto for his interest and very helpful advice. I am grateful to my colleagues, Dr. R.B. Galloway and Dr. G. Bradford for their valuable help and support.

For two years I held an Edinburgh University Studentship and I thank the University for this financial assistance. I am also indebted to the Royal Society and the Department of Scientific and Industrial Research for grants given to purchase equipment.

The technical assistance of Mr. A. Headridge and the staff of the Engineering Workshop and Mr. C. McAnna of the Electronics Workshop is gratefully acknowledged. I thank Mr. W. Wilson for dealing efficiently with my queries and the ordering of components for the spectrometer. I am grateful to Mr. H.J. Napier for his help and for maintaining and operating the H.T. set, often at inconvenient hours. I thank also Mr. G. Turnbull of the H.T. Laboratory for his willing assistance.

APPENDIX I.

The Computer Program for Calculating the Flight Times per Metre of Neutrons Emitted in a (d,n) reaction.

When a deuteron of mass m_d and energy E_d (MeV) interacts with a target nucleus at rest in the laboratory coordinate system, the energy E_n (MeV) of a neutron of mass, m_n, emitted at an angle θ to the direction of the incident deuteron in a (d,n) reaction is given by

$$E_n = \left[\frac{b + \sqrt{b^2 + 4c}}{2}\right]^2 \quad \text{where} \quad b = \frac{2\sqrt{m_n\, m_d\, E_d}\cos\theta}{M_R + M_n}$$

and $c = \dfrac{(M_R - m_d)E_d + QM_R}{M_R + m_n}$. M_R is the mass of the residual nucleus in the (d, n) reaction, and Q is the energy released in the reaction in MeV. The reaction is energetically possible for positive values of c only.

The program, which was written in "Atlas Autocode", first of all tests whether the reaction is possible, and if it is, the energies of the neutrons emitted at various angles θ for a selection of deuteron energies, E_d, are computed. The flight times per metre flight path of the neutrons are evaluated from the expression $T = \dfrac{72.28D}{\sqrt{E_n}}$ ns/m for D = 1 m. The computer program is as follows:

```
begin
integer m,n,p,l,q
read(m,n,p,l,q)
begin
real x,y,B,b,c,d,h,E
real array F(1:m), Q(1:p), S(1:m,1:p)
integer i,j,k
read(y,x,B)
cycle k=1,1,p
read(Q(k))
repeat
cycle j=1,1,m
read(F(j))
repeat
d=1/(B+y)
cycle i=1,1,n
read(E)
h=2*sqrt(y*x*E)*d
cycle k=1,1,p
c=((B-x)*E+B*Q(k))*d
cycle j=1,1,m
if c<0 then S(j,k)=0
if c<0 then ->10
b=h*cos(F(j))
b=(b+sqrt(b↑2+4c))/2
S(j,k)=b↑2
10:repeat
repeat
newline
caption Incident ≠ energy ≠=≠
print(E,1,3)
caption ≠ Mev.
newline
caption Energy ≠ level; spaces(3)
cycle k=1,1,p
print(Q(1)-Q(k),2,3)
space
repeat
cycle j=1,1,m
newline
caption Angle ≠
print((180(j-1)/l)+q,3,0)
spaces(5)
cycle k=1,1,p
print(S(j,k),2,3)
space
repeat
repeat
newline
```

```
newline
caption Flight ≠ times ≠ for ≠ 1 ≠ metre ≠ flight ≠ path.
newline
caption Incident ≠ energy ≠ = ≠
print(E,1,3)
caption ≠ Mev.
newline
caption Energy ≠ level; spaces(3)
cycle k=1,1,p
print(Q(1)-Q(k),2,3)
space
repeat
cycle j=1,1,m
newline
caption Angle ≠
print((180(j-1)/1)+q,3,0)
spaces(5)
cycle k=1,1,p
if S(j,k)=0 then ->20
print(72.28/sqrt(S(j,k)),3,2)
space\\\\
->30
20: caption ABSURD ≠
30: repeat
repeat
newline
newline
repeat
newline
end
end of program
```

In order to carry out the calculations the computer requires the following data in the order:-

The numbers of angles, deuteron energies and Q-values:

The value of 1 required to determine the interval 180/1 between successive angles and the value of q which gives the initial angle:

The masses of the neutron, deuteron and the residual nucleus:

The Q-values:

The angles:

The deuteron energies.

As an example, the printout of the computer for the energies and flight times of the neutrons emitted in the B10(d,n)C11 reaction is shown below.

Incident energy = 0.600 Mev.

Energy level	0.000	2.000	4.320	4.810	6.350	6.490	6.900	7.500
Angle 0	6.857	4.953	2.722	2.245	0.714	0.569	0.118	0.000
Angle 30	6.791	4.896	2.679	2.206	0.691	0.549	0.107	0.000
Angle 60	6.612	4.744	2.566	2.103	0.632	0.495	0.081	0.000
Angle 90	6.376	4.544	2.419	1.970	0.559	0.431	0.055	0.000
Angle 120	6.148	4.352	2.280	1.845	0.494	0.375	0.037	0.000
Angle 150	5.987	4.217	2.184	1.759	0.452	0.338	0.028	0.000
Angle 180	5.92	4.169	2.149	1.728	0.438	0.326	0.026	0.000

Flight times for 1 metre flight path.

Incident energy = 0.600 Mev.

Energy level	0.000	2.000	4.320	4.810	6.350	6.490	6.900	7.500
Angle 0	27.60	32.48	43.81	48.24	85.52	95.79	210.06	ABSURD
Angle 30	27.74	32.67	44.16	48.66	86.93	97.58	220.66	ABSURD
Angle 60	28.11	33.19	45.12	49.84	90.92	102.69	253.35	ABSURD
Angle 90	28.62	33.91	46.48	51.50	96.67	110.13	307.69	ABSURD
Angle 120	29.15	34.65	47.87	53.21	102.79	118.10	373.67	ABSURD
Angle 150	29.54	35.20	48.91	54.50	107.50	124.28	429.04	ABSURD
Angle 180	29.68	35.40	49.30	54.98	109.28	126.61	450.68	ABSURD

APPENDIX II.

The Computer Program for Calculating Sum Line Shapes.

The computer program for calculating the sum line shape due to the simultaneous detection in a NaI(Tℓ) crystal of two γ-rays in cascade from the line shapes of the individual γ-rays is given below. First of all the line shapes presented to the computer for the γ-rays γ(1) and γ(2) are normalized so that the ratio of the numbers of counts in the photopeaks of γ-rays γ(1) and γ(2) is f(1):f(2), where f(i) is the photopeak detection efficiency of γ-ray γ(i). The sum line shape $N(k',s) = \sum_{i=1}^{256} N(i,1)\, N(j,2)$ where $j = k' - i$, is then computed using the normalised distributions N(i,1) and N(j,2) for the individual γ-rays of the cascade. The printout of the computer gives the sum line shape displaced by a few channels due to the effect of the energy threshold of the multichannel pulse height analyser and it is necessary to correct for this displacement by observation. The program in "Atlas Autocode" is as follows:

```
begin
integer i,n,j,m,k,l,q
real a,b,x,y
integer array A(1:256), B(1:256), C(1:512)
i=1
10:read(A(i))
if A(i)=-1 then ->20
i=i+1
->10
20: n=i
A(n)=0
j=1
30:read(B(j))
if B(j)=-1 then ->40
j=j+1
->30
40:m=j
B(m)=0
read(a)
cycle i=1,1,n
A(i)=int(a*A(i))
repeat
read(b)
cycle j=1,1,m
B(j)=int(b*B(j))
repeat
cycle k=1,1,m+n
C(k)=0
repeat
cycle i=1,1,n
cycle j=1,1,m
k=i+j
C(k)=(A(i)*B(j)+C(k))
repeat
repeat
read(x,y)
newline
newline
caption Summing ⊭ spectra ⊭ of ⊭ gamma-rays ⊭ with ⊭ energies ⊭
print(x,2,2)
caption ⊭ and ⊭
print(y,2,2)
caption ⊭ Mev.
newline
newline
read(q)
cycle l=1,1,32
cycle k=(1+(l-1)*16),1,16*l
print((C(k)/q),5,0)
space
if k>m+n then ->50
repeat
newline
newline
repeat
newline
50: end of program
```

The computer requires the following data in the order:-

The line shapes for the γ- rays terminated by -1:

The normalizing factors;
The energies of the γ- rays:
The power of 10 by which the sum line shape is multiplied.

APPENDIX III

The Computer Program for Calculating the Cascade Line Shapes.

First of all the sum line shapes due to all pairs of γ-rays emitted in the cascade are computed using the program given in Appendix II. The sum line shapes are adjusted by renumbering the channels so that the channel number of a sum peak is the same as the channel number of the photopeak of an individual γ-ray of the sum energy. After the programmer has carried out the necessary adjustments on all of the sum line shapes, the sum line shapes and the line shapes for the individual γ-rays are presented to the computer. The line shapes are then normalized so that the number of counts in the photopeak of the line shape for an individual γ-ray $\gamma(k)$ is $N_o \frac{\omega}{4\pi} f(k) \left[1 - \frac{\omega}{4\pi} \sum_{i \neq k} f(i)\right]$ and the number of counts in the sum peak of the pair of γ-rays $\gamma(k)$ and $\gamma(\ell)$ is $N_o \left(\frac{\omega}{4\pi}\right)^2 f(\ell) f(k)$. N_o is an arbitrary constant chosen to be 10^5 in the present case. The contents of the j-th channel of all the component line shapes for the cascade are added together to give the contents of the j-th channel of the cascade line shape. The program is given below.

```
begin
integer z,f,s,p,h
read(z,f)
begin
array c(1:z,1:f), e(1:z), E(1:f)
real d

cycle p=1,1,f
read(d)
cycle s=1,1,z
read(c(s,p))
if c(s,p)=-1 then ->10
c(s,p)=d*c(s,p)
repeat
->11
10:h=s
cycle s=h,1,z
c(s,p)=0
repeat
11:repeat


cycle s=1,1,z
e(s)=0
cycle p=1,1,f
e(s)=e(s)+c(s,p)
repeat
repeat


newline
newline
caption Cascade¢of¢
cycle p=1,1,f
read(E(p))
print(E(p),1,2)
repeat
caption ¢MeV¢gamma-rays
newline
newline
cycle h=1,1,12
newline
cycle s=(h-1)*10+1,1,h*10
if s>z then ->40
print(e(s),4,0)
spaces(2)
repeat
repeat
40:end
end of program
```

The computer requires the following data in the order:-

The numbers of channels and line shapes:

The normalizing factor for the first line shape:

The first line shape terminated by -1:

The normalizing factor for the second line shape:

The second line shape terminated by -1;

ETC.

The energies of the γ- rays.

REFERENCES

(1) Ajzenberg-Selove and Lauritsen: Rev. Mod. Phys. 27, 77 (1955). Nucl. Phys. 11, 1 (1959).

(2) Ajzenberg-Selove and Lauritsen: Energy Levels of Light Nuclei, Nuclear Data Sheets - National Academy of Sciences and National Research Council (U.S.A.) (1962).

(3) Bromley, Nagatani, Northcliffe, Ollerhead and Quinton: Proceedings of the Rutherford Jubilee International Conference (Ed. Birks), 597 (1961).

(4) Kjellman, Nilsson and Schwarz: Proc. Ruth. Jub. Int. Conf., 605 (1961). Ark. Fys. 21, 169 (1962).

(5) Hinds and Middleton: Proc. Phys. Soc., 75, 754 (1960).
Weger and Hall : Phys. Rev. 119, 1654 (1960).

(6) Armitage and Meads : Nucl. Phys. 33, 494 (1962).

(7) Vlasov, Kaplinin, Ogloblin and Chuev: Zh. eksper. teor. Fiz. 39, 1618 (1960) (Translation, Soviet Phys. - JETP (U.S.A.) 12, 1129.)

(8) Taylor, Barros, Forsyth, Jaffe and Ramavataram: Proc. Phys. Soc. 75, 772 (1960).
Gorodetzky, Gallmann and Rebmeister: Phys. Rev. 137, B1466 (1965).

(9) Pellegrini: Nucl. Phys. 24, 372 (1961).
Armitage and Meads: Nucl. Phys. 33, 494 (1962).
Baldeweg, Bredel, Guratzsch, Klabes, Kühn and Stiller: Nucl. Phys. 64, 55 (1965).

(10) Bonner and Brubaker: Phys. Rev. 50, 308 (1936).

(11) Staub and Stephens : Phys. Rev. 55, 131 (1939).

(12) Powell: Proc. Phys. Soc., A181, 344 (1943).

(13) Whitehead and Mandeville: Phys. Rev. 77, 732 (1950).

(14) Ajzenberg: Phys. Rev. 82, 43 (1951).

(15) Pruit, Swartz and Hanna: Phys. Rev. 92, 1456 (1953).

(16) Dyer and Bird: Aust. J. Phys. 6, 45 (1953).

(17) Reid: Proc. Phys. Soc. 67A, 466 (1954).

REFERENCES (Contd.)

(18) Genin: C.R. Acad. Sci. (Paris), 246, 1028 (1958).

(19) Karadeniz: Unpublished (c. 1956), see however Galloway, Thesis, Edinburgh University Library, (1959).

(20) Hjalmar and Slätis: Arkiv. for Fysik 18, 193 (1960).

(21) Coombe and Walker : Proc. Phys. Soc. 80, 1218 (1962).

(22) Green, Scanlon and Wilmott: Proc. Phys. Soc. 68A, 386 (1955).

(23) Shpetnyi: Zh. eksper. teor. Fiz. 32, 423 (1957). (Translation, Soviet Phys. - JETP (U.S.A.) 5, 357.

(24) Juna, Horvath and Konecny: Czech. J. Phys. B10, 715 (1960).

(25) Garg, Gale and Calvert: Nucl. Phys. 37, 319 (1962).

(26) Morrison, Ferguson and Evans: Proc. Ruth. Jub. Int. Conf., 575 (1961).

(27) Riley, Braben and Neilson: Nucl. Phys. 47, 150 (1963).

(28) Siemssen, Cosack and Felst: Nucl. Phys. 69, 209 (1965).

(29) Good: Nucl. Instr. and Meth. 6, 323 (1960).

(30) Neilson, Dawson and Johnson: Rev. Sci. Inst., 30, 963 (1959).

(31) Shafroth and Hanna: Phys. Rev. 95, 86 (1954).

(32) Meyerhof and Chase: Phys. Rev. 111, 1348 (1958).

(33) Galloway and Sillitto: Proc. Roy. Soc. Edinb., A65, 247 (1961).

(34) Bradford: Thesis, Edinburgh University Library (1962).

(35) Sprenkel and Daughtry: Phys. Rev. 124, 854 (1961).

(36) Ramussen, Hornyak and Lauritsen: Phys. Rev. 76, 581 (1949).

(37) Singh: Phys. Rev. 114, 871 (1959).

(38) Hornyak, Ludemann and Roush: Nucl. Phys. 50, 424 (1964).

(39) Warburton, Alburger and Wilkinson: Phys. Rev. 132, 776 (1963).

(40) Segel, Singh, Hanna and Grace: Private communication, (To be published) (1966).

REFERENCES (Contd.)

(41) Galloway: Thesis, Edinburgh University Library (1959).

(42) Garg: Nucl. Instr. and Meth. 6, 72 (1959-60).

(43) Green and Bell: Nucl. Instr. and Meth. 3, 127 (1958).

(44) Garg: Nucl. Instr. and Meth. 6, 187 (1959-60).

(45) Owen: Nucleonics 17, 92 (1959).

(46) Batchelor, Gilboy, Purnell and Towle: Nucl. Instr. and Meth. 8, 146 (1960).

(47) Kahn: Phys. Rev. 90, 503 (1953).

(48) Neiler and Good: Fast Neutron Physics Part I, (Ed. Marion and Fowler, Interscience Publishers)(1960).

(49) Neilson, Sample and Warren: Fast Neutron Physics, Part II, (1963).

(50) Mullard Technical Handbook: Operating notes for Photomultiplier Tubes (1960).

(51) Stump and Talley: Rev. Sci. Inst. 25, 1132 (1954).

(52) Flagge and Harris: Rev. Sci. Inst. 26, 619 (1955).

(53) Hendrick: Rev. Sci. Inst. 27, 241 (1956).

(54) Kane: Rev. Sci. Inst. 28, 583 (1957).

(55) Penman: Rev. Sci. Inst. 30, 745 (1959).

(56) Barna: Nucl. Instr. and Meth. 24, 247 (1963).

(57) Vingiani and Monaro: Nucl. Instr. and Meth. 14, 138 (1961).

(58) Jarczyk, Knoepfel, Lang, Müller and Wölfli: Nucl. Instr. and Meth. 17, 310 (1962).

(59) Weitkamp: Nucl. Instr. and Meth. 23, 13 (1963).

(60) Miller and Snow: Nucleonics 19, 174 (1961).

(61) Nordhagen: Nucl. Instr. and Meth. 12, 291 (1961).

(62) Batchelor, Gilboy, Parker and Towle: Nucl. Instr. and Meth. 13, 70 (1961).

REFERENCES (Contd.)

(63) Bayman: Thesis, Edinburgh University Library (1954).

(64) Maydan and Vass: Proc. Phys. Soc. 86, 817 (1965).

(65) Kurath: Phys. Rev. 101, 216 (1956);
Phys. Rev. 106, 975 (1957).

(66) Inglis: Rev. Mod. Phys. 25, 390 (1953).

(67) Cohen and Kurath: Nucl. Phys. 73, 1 (1965).

(68) Freeman: Nucl. Phys. 37, 215 (1962).

(69) Roush, Jaffe, Figuera and Hornyak: Nucl. Phys. 67, 577 (1965).